NTNU

Norwegian University of
Science and Technology

A signal analysis toolbox for power system identification in Smart Grids

Sjur Føyen
Mads-Emil Bratland Kvammen

Master of Energy and Environmental Engineering
Submission date: June 2018
Supervisor: Olav B Fosso, IEL
Co-supervisor: Jalal Khodaparast, IEL

Norwegian University of Science and Technology
Department of Electric Power Engineering

Abstract

This thesis delves into the two fields of signal analysis and small-signal stability of power systems. Due to the extensive deployment of PMUs in today's Smart Grid, new possibilities arise to assess the small-signal stability by measurement based techniques. The benefits of this approach are many, the most compelling being that the power system has become too complex to be accurately modelled with a component-based approach. A whole range of methods are available for the purpose of signal analysis in power systems, all with various assumptions, strengths and weaknesses. Insight into the analysis methods and the measurement data in itself is important for choosing the appropriate techniques for a given signal. The methods described in this thesis are: **Prony's method**, **Robust Recursive Least Squares** (**RRLS**) and the FFT based **Welch's method**. Prony's method is known as a ringdown (post-disturbance transient) analyzer, while the two latter are known as ambient analyzers.

To improve estimation robustness and accuracy, pre-filtering is implemented with the **Empirical Mode Decomposition** (**EMD**). This technique works as a *non-linear* and *non-stationary* band-pass filter, effectively extracting the desired frequency spectrum in the electro-mechanical range. This is validated using Welch's method, which reveals negligible change in the power spectral density of the investigated frequency range.

Both Prony's method and RRLS assume an underlying parametric model, and require specifying a model order. This issue is transformed into a benefit, extracting the consistent information from multiple analyses with varying model order. **Clustering** is used as *post-processing intelligence* to identify the dominant modes of the estimation. The third technique, Welch's method, is used for validation purposes.

The methods and data are contextualized; subsequently, the techniques are described with relevant theory, and thoroughly tested for both simulated and real-world data. The estimation from ringdown data is compared to the estimation from ambient data, which in real-time scenario often is the only option for evaluation. The three analyzers contribute to mutual validation of the modal content, improving the credibility of the estimates. For simulated data, the measurement based estimation is also evaluated against eigenvalue inspection of the linearized power system model.

This thesis is based in part on a conference paper to be published at SPEEDAM 2018. This article describes theory of Prony's method, as well as the EMD and Clustering technique. Since then, the thesis has evolved in scope and depth.

The results from detailed testing show that the investigated combination of methods performs well on real-world PMU-measurements. Prony's method identifies the modes of ringdown data and the RRLS method identifies the modal content in the ambient data. The damping ratio is in general slightly underestimated in the ambient data compared to ringdown data. However, both give a good indication of the modal content.

A comprehensive toolbox of the methods mentioned above has been indigenously created (in Python) as a part of thesis work; the toolbox utilizes weaknesses of some methods, e.g. the model order selection problem in Prony's method and RRLS, as input to other methods, such as the clustering technique. The result is an autonomous algorithm, taking care of each sub-method's deficiency.

Sammendrag

Denne masteroppgaven går i dybden i feltene signalanalyse og transiente stabilitet i elektriske kraftsystemer. Takket være den utstrakte etableringen av Phasor Measurement Units (PMUs) i dagens Smart Grid, åpnes det for nye muligheter til å analysere den transiente stabiliteten med målebaserte metoder. Det er mange fordeler med denne tilnærmingen - og dens betydning øker grunnet et kraftsystem som blir for komplekst for komponentbaserte metoder. Det finnes et vidt spekter av metoder for signalanalyse i elektriske kraftsystemer, som alle har forskjellige antakelser, styrker og svakheter. Innsikt i flere metoder, og målingenes opphav, er viktig for å velge de riktige teknikkene for et gitt signal. Metodene som er beskrevet i denne oppgaven er som følger: **Prony's metode**, **Robust Recursive Least Squares** (**RRLS**), på norsk Robust Rekursiv Minstekvadraters Løsning, og FFT-baserte **Welch's metode**. Prony's metode er kjent som en ringdown-analyse, altså en metode som analyserer det transiente forløpet etter en forstyrrelse, mens Welch's metode og RRLS kategoriseres som ambient-analyse.

For å forbedre nøyaktigheten og robustheten til metodene, er prefiltrering implementert med **Empirical Mode Decomposition** (EMD). Denne teknikken fungerer som et ulineært, ikke-stasjonært båndpassfilter, som effektivt henter ut det ønskede frekvensspekteret, som her ligger i det elektromekaniske området fra 0.2-2 Hz. EMD-filteret er validert med Welch's metode, som viser at filteret gjør neglisjerbare endringer på det ønskede frekvensspekteret.

Både Prony's metode og RRLS antar en underliggende, parametrisk modell, som betyr at en bruker må spesifisere ordenen til modellen. Dette - som vanligvis er sett på som et problem - brukes til estimeringens fordel, ved å ta vare på kun den informasjonen som holder seg relativt konstant for flere estimat med varierende orden. **Clustering** brukes som en *post-filtreringsalgoritme* for å identifisere estimatets dominerende modi. Den tredje teknikken, Welch's metode, er brukt for valideringsformål.

Metodene og målingene er satt i kontekst; deretter er teknikkene beskrevet med relevant teori, og testet for både simulerte og ekte data. Estimat fra ringdowns er sammenliknet med estimat fra ambient data, som ofte er den eneste valideringsmåten for virkelige målinger. De tre analysemetodene bidrar til felles validering av modalinnholdet, som forbedrer påliteligheten til estimatene. For simulerte data er målingene - i tillegg til de ovennevnte - vurdert mot egenverdianalyse fra lineariseringen av den simulerte modellen.

Denne oppgaven er delvis basert på en konferanseartikkel som skal publiseres på SPEEDAM 2018. Artikkelen beskriver teorien bak Prony's metode, i tillegg til EMD og Clustering. Siden den ble levert, har oppgaven utviklet seg i både omfang og dybde.

Resultatene fra den detaljerte testingen viser at den beskrevne kombinasjonen av metoder klarer seg bra på virkelige PMU målinger. Prony's metode identifiserer modiene i ringdown data, og RRLS identifiserer modiene i ambient data. Dempingsfaktoren er som regel litt underestimert i ambient data sammenliknet med ringdown data. Allikevel gir begge en god indikasjon på modalinnholdet i signalet.

En omfattende verktøykasse for signalanalyseteknikker har blitt laget (i Python) som del av masteroppgaven.

Acknowledgements

We, the authors, would like to mark our gratitude to our supervisor Prof. dr.ing. Olav Bjarte Fosso, for introducing us to the adventurous life of academic research. He has displayed unique abilities to inspire motivation and confidence; providing directions to promising topics, and believing in the choices we make. In addition to being a role model as a researcher, Olav has a skill for planting ideas that we first understand the full impact of months later. Throughout the past year we have particularly enjoyed his many anecdotes, at times enlightening the topic at hand, and always brightening the mood. We would also like to thank our co-supervisor Postdoctoral Researcher Dr. Jalal Khodaparast, for continuous support and encouragement. His enthusiasm to share his experience has been of great value to the foundation of our work. We are really excited about our trip with him to Amalfi.

To Associate Professor Vijay Venu Vadlamudi we owe our inspiration to never stop the pursuit for intuitive knowledge. We have countless times found ourselves wondering if Vijay would approve of this explanation, or that rationale - especially if "fundamentals" were involved. We will always remember the many moments and discussions with him since we first met him in our second year. We are forever grateful for his suggestions, greatly enhancing the narrative presentation of our thesis.

Relating the wealth of theoretical knowledge to real situations would have been impossible without the PMU measurements provided by Statnett. We owe our gratitude to Prof. Kjetil Uhlen and Postdoctoral Researcher Dr. Dinh Thuc Duong for sharing their extensive experience with analysis of PMU data.

Last, but not the least, we thank our flatmate and friend (Sjur's girlfriend) Marte for suffering the long evenings of theoretical discussion, and still taking her time to proofread the thesis.

Sjur Føyen
Mads-Emil B. Kvammen

Contents

1 Introduction **1**

2 Theory **4**

2.1 Context of applied methods and measurement data 4

2.2 Parametric Modelling 6

2.3 Original Prony 7

2.4 Prony filter 11

2.5 Robust Recursive Least Square 12

2.6 Welch's method for frequency estimation 15

2.7 Empirical Mode Decomposition as band-pass filter 16

2.8 Clustering as post-processing intelligence 18

2.9 Additional concepts 21

2.9.1 Signal to noise ratio 21

2.9.2 Aliasing 21

3 Remarks on implementation **23**

3.1 Proposed method for ringdown analysis 24

3.2 Proposed method for ambient analysis 24

3.3 Simulation study 26

3.3.1 Ringdown analysis 29

4 Testing and validation on simulated data **31**

4.1 Case 1 - Line outage and reconnection 31

4.1.1 Constant load test 31

4.1.2 Variable load - Ringdown analysis 33

4.1.3 Variable load - Ambient analysis prior to ringdown 36

4.1.4 Variable load - Ambient analysis after ringdown 40

4.2 Case 2 - Line outage and disconnection 44

4.2.1 Variable load - Ringdown analysis 45

4.2.2 Variable load - Ambient analysis prior to ringdown 48
4.2.3 Variable load - Ambient analysis after ringdown 48
4.3 Case 3 - Analysis of voltage angle for line disconnection 51
4.3.1 Variable load - Ringdown analysis 51
4.3.2 Variable load - Ambient analysis prior to ringdown 53
4.3.3 Variable load - Ambient analysis after ringdown 56

5 Testing and validation on PMU data **61**
5.1 Case 1 - 10 Hz 61
5.1.1 Linear portion of ringdown signal 62
5.1.2 Including non-linear portion in linear ringdown analysis 63
5.1.3 Ambient data prior to ringdown 64
5.1.4 Ambient data after ringdown 67
5.2 Case 2 70
5.2.1 Ringdown analysis 71
5.2.2 Ambient data prior to ringdown 73
5.2.3 Ambient data after ringdown 76

6 Concluding remarks and further work **79**

A Appendix - Paper to be published **84**

B Appendix - Poster for SPEEDAM 2018 **93**

List of Figures

2.1 Ambient and ringdown data from the Nordic grid 5
2.2 Classification of methods 6
2.3 Demonstration of Prony Analysis 8
2.4 Demonstration of moving timewindow estimation in RRLS 12
2.5 Welch power spectrum of a measured signal 16

2.6 Decomposing ringdown PMU-data into IMFs . . . 17
2.7 Decomposing ambient PMU-data into IMFs . . . 17
2.8 Example decomposition for different model orders . . . 19
2.9 Clustering of noisy, synthetic signal . . . 20
2.10 Aliased high frequency signal . . . 22
3.1 Decomposing ringdown PMU-data into IMFs . . . 24
3.2 Downsampling . . . 24
3.3 Cluster identification using PA_O . . . 24
3.4 Decomposing ambient PMU-data into IMFs . . . 25
3.5 Clustering of results in each timestep, k . . . 25
3.6 Illustration of mode-tracking in ambient data . . . 25
3.7 Variation of the forgetting factor . . . 26
3.8 Kundur Two Area System . . . 27
3.9 50 seconds of ambient data . . . 28
3.10 Change in modal components with change in system loading . . . 28
3.11 Comparing measured signal for same fault with and without load variation . . . 29
3.12 Comparing measured signal for same fault with and without load variation . . . 30
4.1 Simulation data from PF in case 1 . . . 31
4.2 Cluster plot from both estimations . . . 32
4.3 Comparing reconstructed signal to original signal without offset . . . 33
4.4 IMF plots from EMD-filter . . . 34
4.5 Cluster plot from both estimations on ringdown signal . . . 34
4.6 Comparing reconstructed signal to post EMD-filtered signal . . . 35
4.7 Part of the ambient data analyzed . . . 36
4.8 IMF plots from EMD-filter in line 9-10 . . . 37
4.9 IMF plots from EMD-filter in line 5-6 . . . 37
4.10 Cluster plot from both estimations in ambient signal . . . 38
4.11 Mode-tracking of identified modes . . . 38

4.12 Mode-tracking of most critical mode 39
4.13 Mode-tracking of damping ratio for mode in Figure 4.12 39
4.14 Welch's power spectrum of measured signal 40
4.15 Mode-tracking of identified modes 41
4.16 Mode estimation results from line 5-6 41
4.17 Mode-tracking of damping on modes in Figure 4.15a and 4.16b 42
4.18 Welch's power spectrum of measured signal 43
4.19 Welch's power spectrum of measured signal in line 5-6 prior to EMD-filtering . . 43
4.20 Simulation data from PF in case 2 45
4.21 IMF plots from EMD-filter results on line 9-10 46
4.22 IMF plots from EMD-filter results on line 5-6 46
4.23 Cluster plot from both estimations on ringdown signal 47
4.24 Comparing reconstructed signal to post EMD-filtered signal 48
4.25 Mode-tracking of identified modes 49
4.26 Damping of modes in Figure 4.25 49
4.27 Welch power spectrum of measured signal 50
4.28 Welch power spectrum of measured signal in line 5-6 prior to EMD-filtering . . . 50
4.29 Simulation data from PF in case 3 51
4.30 IMF plots from EMD-filter 52
4.31 Cluster plot from both estimations on ringdown signal 52
4.32 Comparing reconstructed signal to post EMD-filtered signal 53
4.33 IMF plots from EMD-filter results on line 9-10 utilizing IMF 4-9 54
4.34 IMF plots from EMD-filter results on line 5-6 utilizing IMF 3-8 54
4.35 Mode-tracking of identified modes 55
4.36 Mode-tracking of damping on inter-area mode in Figure 4.35 55
4.37 Welch power spectrum of measured signal 56
4.38 IMF plots from EMD-filter results on line 9-10 utilizing IMF 4-9 57
4.39 IMF plots from EMD-filter results on line 5-6 utilizing IMF 3-6 57

4.40 Mode-tracking of identified modes . . . 58

4.41 Damping of modes in Figure 4.40 . . . 58

4.42 Welch's power spectrum of measured signal . . . 59

5.1 Measurements from a large disturbance in the Nordic Grid, with ringdown portion expanded. . . . 61

5.2 Cluster plots of ringdown signal . . . 62

5.3 Reconstruction of modes, in this case one decaying sine wave . . . 63

5.4 Cluster plots of non-linear ringdown signal . . . 63

5.5 Reconstruction of transient behaviour including nonlinear portion . . . 64

5.6 IMF plot of EMD result, extracting IMF 1-5 . . . 65

5.7 Comparison of Welch's power spectra of measured signal with varying IMF composition . . . 65

5.8 Mode-tracking of identified modes in PMU signal . . . 66

5.9 Mode-tracking of identified modes in PMU signal . . . 66

5.10 Damping ratio of the two most critical modes . . . 67

5.11 IMF plot of EMD result, extracting IMF 1-6 . . . 68

5.12 Comparison of Welch's power spectrum in measured signal with and without EMD-filtering . . . 68

5.13 Tracking of frequency of estimated modes . . . 69

5.14 Damping of 0.96 Hz mode . . . 69

5.15 Clustering result after convergence . . . 69

5.16 Measurements from a disturbance in the Nordic Grid, with ringdown portion expanded. . . . 71

5.17 Cluster plot of ringdown signal . . . 71

5.18 Reconstruction of modes, in this case one decaying sine wave . . . 72

5.19 IMF plot of EMD result, extracting IMF 4-7 . . . 73

5.20 Welch's power spectra of measured signal . . . 73

5.21 Mode-tracking of identified modes in PMU signal . . . 74

5.22 Clustering result after convergence . . . 75

5.23 IMF plot of EMD result, extracting IMF 4-8 . . . 76

5.24 Welch's power spectra of measured signal 76
5.25 Mode-tracking of identified modes in PMU signal 77
5.26 Clustering result after convergence 77

List of Tables

3.1 Modes identified by PF for base case 28
3.2 Modes identified by PF with one line between buses 8 and 9 disconnected 29
4.1 Consistent modes for multiple model orders in constant load test 32
4.2 Modes identified by PF during ringdown in case 1 33
4.3 Consistent modes for multiple model orders in ringdown variable load test . . . 35
4.4 Modes identified by PF in ambient data prior to ringdown in case 1 36
4.5 Modal information at end of ambient data prior to fault 38
4.6 Modes identified by PF in ambient data after ringdown in case 1 40
4.7 Modal information at end of ambient data post fault 42
4.8 Modes identified by PF during ringdown in case 2 45
4.9 Consistent modes for multiple model orders in ringdown variable load test . . . 47
4.10 Modes identified by PF in ambient data after ringdown in case 2 48
4.11 Modal information at end of ambient data post fault 50
4.12 Consistent modes for multiple model orders in ringdown variable load test . . . 52
4.13 Modal information at the end of ambient data prior to fault 55
4.14 Modal information at end of ambient data post fault 58
5.1 Ringdown: dominant mode(s) 62
5.2 Ringdown: dominant mode(s) 63
5.3 Modes identified prior to ringdown 66
5.4 Modes identified after ringdown 70
5.5 Ringdown: dominant mode(s) 72
5.6 Modes identified prior to ringdown 75
5.7 Modes identified after ringdown 78

List of Equations

2.1 Example differential equation for a time-continuous LTI system 6

2.2 Approximation of derivative with finite differences 7

2.3 Example difference equation for a discrete LTI system 7

2.4 General difference equation 7

2.5 Estimate of the observed data, consisting of N equally spaced samples 8

2.6 Linear prediction model for N > 2p and N-p number of difference equations . . . 9

2.7 Least-squares approximation 9

2.8 Characteristic polynomial function of the system 10

2.9 The factorized characteristic polynomial function of the system 10

2.10 Scaling of poles 10

2.11 Calculating frequency 10

2.12 Estimate on exponential form 11

2.13 Rewriting estimates where C are the signal residues 11

2.14 All measurement values as a linear combination of roots and residues 11

2.15 Main principle of RRLS 12

2.16 Estimating next sample in RRLS 13

2.17 Calculate the estimation error 13

2.18 Updating $\hat{\boldsymbol{\alpha}}$ 14

2.19 Calculating $\boldsymbol{L}[k]$ 14

2.20 Calculating $\boldsymbol{P}[k]$ 14

2.21 Calculating the lossfunction $\rho[\epsilon]$ 15

2.22 Calculating σ 15

2.23 Calculating the derivative of the lossfunction $\rho^{'}[\epsilon]$ 15

2.24 Calculating the double derivative of the lossfunction $\rho^{''}[\epsilon]$ 15

2.25 Signal-to-noise ratio. 21

3.1 Component-based approximation 26

3.2 Calculate eigenvalues from system matrix $\boldsymbol{A}$ 27

1 Introduction

Signal analysis is a general tool used in a variety of fields. Digitally recorded music, heart monitoring and identification of brain activity are just some of the possible applications. Common for all is that insight into the investigated signal is required, so that applied methods can be refined to the signal content.

In this thesis, signal analysis is used as a tool to identify slowly oscillating electro-mechanical modes from measurements in the power system. A simple analogy will be used to get the reader in the right mindset:

Picture the power system as a multiple tandem bicycle, and each cyclist a generator. The bicycle has to run at a certain speed, and everyone contributes to keeping this exact speed. Suddenly, one cyclist falls off, and consequently the speed drops. The remaining cyclists will need to work harder to speed up again, yet as they all push harder, the bicycle speed goes too high. Subsequently, they all relax a bit, and as the speed reduces, suddenly they go too slow. This process repeats until they finally stabilize around the desired speed, that is, the swing motion damps out, provided that the bicycle system is stable. The alternative scenario is that each cyclist moves further and further away from the equilibrium speed, eventually falling off one by one.

As any analogy, it is not completely descriptive of the dynamics and complexity of what it tries to explain. However, it tells the most important - this thesis is about swing motions, sine waves and damping. In power systems, these swings appear continuously in everyday operation. As small disturbances happen from second to second, the generators (as well as other rotating mass) strive to maintain stability. This is the field of small-signal stability. If left untreated, the oscillations can prove fatal, thus they should be identified with certainty and accuracy. In worst-case scenario, breakups similar to that in the western North American power system on August 6^{th} 1996 may occur [1]. During the breakup, cascading events left 7.5 million people without power in a period up to 6 hours.

However, operators today are good at keeping the system well within the stability limits. The challenge is mainly to operate the grid efficiently in an economic sense, and keep investment costs as low as possible by reducing the necessary margins for maintaining stability. Increased awareness and real-time monitoring of system damping is a key factor for full utilization of the existing grid, and a decisive step towards the Smart Grid. Including small-signal stability for determining line flow limits, gives a more accurate estimation of the optimal power flow, as described in [2].

Phasor Measurement Unit (PMU) is a relatively new tool for high-resolution measurements, and provides better opportunities for monitoring small-signal stability. For this purpose, measurements are generally classified as either ringdown data, ambient data or probing data. A wide variety of signal analysis methods exists for each data type. This thesis does not pursue probing data, but focuses on three different methods suited for analysis of ringdown and ambient data, as well as pre- and post-processing techniques.

The objectives for analyzing these data are manifold, and not all are discovered yet. A well-known issue is to estimate damping ratio of inter-area oscillations, which are considered to be the most difficult electro-mechanical oscillations to control. Damping ratio is a term widely used as a stability criterion in small-signal oscillations. It is a dimensionless measure which describes the rate of decay in oscillatory modes. In power systems, the damping ratio of a mode is considered to be satisfactory if it is above 5 % [3, p. 194].

Another objective is to monitor system changes through the identified modal content. For this purpose, mode-tracking is defined as monitoring of the constantly changing modal content in the power system. It is either used for comparison of ambient and ringdown data, or just as an approach for supervision of change between timesteps in ambient data.

The thesis has three main parts: theory, implementation and testing.

- The theory is split into several parts, and most are dedicated to one particular technique. The techniques described in detail are: Prony Original, Robust Recursive Least Squares, Welch's method, Empirical Mode Decomposition and Clustering. Additionally, some sections will describe important aspects of signal processing in general. All sections include a self-contained intuitive description, and some are followed by a walk-through of the theoretical foundation for the given topic.
- Implementation presents a more practical approach to the theoretical methods. Here, the techniques will be illustrated with figures and important choice of parameters highlighted.
- The testing is divided into two sections. The first incorporates a simulated power system model, and analyses of its time-domain "measurements". The second encompasses analyses of real-world PMU measurements from the Nordic Grid. The multitude of test-cases are to illustrate different aspects of the algorithms.

For the reader with little experience with signal analysis in power systems, the intuitive sections - along with skimming of the testing sections - will provide a first impression of the field. The proceeding walk-through will facilitate thorough understanding of the seemingly complex theoretical foundation.

The method chosen for extracting modal information from ringdown data, is Prony's method. This models the signal as a sum of damped, complex exponentials - or equivalently - decaying sinusoidals. The goal is to determine the frequency, damping, phase and amplitude of these components [4]. This method has been by far the most used and researched ringdown analyzer in power systems. Also, the authors have had a look at the subspace method ESPRIT (Estimation of Signal Parameters via Rotational Invariance Techniques) [5]. ESPRIT has not been extensively used for power system purposes, and although perhaps a potential candidate, it is not pursued in this thesis.

For extracting modal information in ambient data, a recursive method is used: the Robust Recursive Least Squares (RRLS) method. With a Newton-Raphson type approach, gradually improving the estimation accuracy, frequency and damping is estimated in each timestep [6].

Applied methods are not yet perfected and are thus subject to continued investigations in order to find improvements. The main contributions in this thesis relate to the:

1. application of Empirical Mode Decomposition (EMD) as a pre-processing filter technique

2. post-processing of the results by the use of machine learning, improving the performance and robustness of applied methods

In addition to applied identification methods, Welch's method is implemented as a validation technique of the results.

All methods described in this thesis are programmed by the authors in Python, based on the described theory. The exception is the core part of Empirical Mode Decomposition, Welch's method and the clustering method applied, all of which are open source code. However, these are redefined to form seamless and well-functioning algorithms.

It is emphasized that this thesis has a heuristic approach to the mode identification problem. Some of the applied techniques lack thorough mathematical justification, due to the complex features of measured signals. Rather, the methods are presented with focus on validation by testing and observation. Thus, one should keep in mind that the results are subject to the particular tested cases (although those shown here only represent a fraction), and extrapolation of traits and characteristics is not necessarily valid. Further testing, particularly on real-world PMU measurements, should be undertaken for exploring and solving more issues and traits with the applied methods.

Shortly after this thesis is delivered, the conference article in appendix A, which is a result of research presented here, will be made available in the IEEE-database. The paper presents two Prony variations, with EMD as pre-filter and clustering as post-processing intelligence. Ever since the paper was delivered, the thesis has evolved into a more comprehensive study of measurement based small-signal analysis. Note that the authors altered the theoretical notation in the thesis, to highlight the similarities of RRLS and Prony. The poster in appendix B gives a motivational introduction to the concepts in the paper, as well as providing the context. The poster will be presented at the conference SPEEDAM 2018 in Amalfi, June 2018.

2 Theory

2.1 Context of applied methods and measurement data

Signal analysis is applicable in many fields, and knowledge related to a method in itself holds academic value. Yet in each application the measurements have their distinct features, and practical use awaits the understanding of how this *data should be approached. Will the assumptions of a certain method hold true? Which behaviour is expected, and which is observed from the measurements? To know the data and available methods is essential for choosing the appropriate signal analysis toolbox.*

Phasor Measurement Units provide high resolution, time-stamped data of voltages and currents in large power systems. For small-signal stability purposes these data are generally classified as either ambient, ringdown or probing data. The following will clarify the differences between them.

Ambient: normal operating state. In a large power system, currents, voltages and power flows (amongst others variables) vary as a consequence of millions of customers turning their electric equipment ON and OFF. Aggregated, these changes are assumed to behave like continuous small-amplitude, random disturbances. The system response to these variations is described as ambient data, and contains distorted information of the system's oscillatory behavior. The characteristics of ambient data are certainly an area of research interest, as the complexity of the dynamics is high and the justification for the current assumption is thin.

Ringdown (transient): damped, oscillatory behaviour following a disturbance, such as line tripping or production outage. These disturbances happen from time to time, and causes motions much greater (larger amplitude) than the small switching that produces ambient data. Ringdown portions typically contain much richer information than ambient data, and are much easier to evaluate by visual inspection. However, disturbances do not happen often, and the resulting ringdowns are not always suitable for the relevant methods. Installed equipment can be used to induce ringdowns for analysis purposes, e.g. the Chief Joseph 1400 MW braking resistor in Washington [7].

Probing: insertion of known input fluctuations, e.g. pseudo-noise. For ambient conditions, the fluctuations are considered to be *hidden*, or *unknown*, which means they cannot be used for improving the power system modelling. Probing signals can be used to evaluate how known inputs affect the system response, and dedicated methods estimate observable modes better than can be extracted from ambient data.

In Figure 2.1, both ambient and ringdown data are shown for a short time-period. The measurements originate from a PMU in the Nordic grid, a generation outage occurring at 42 seconds.

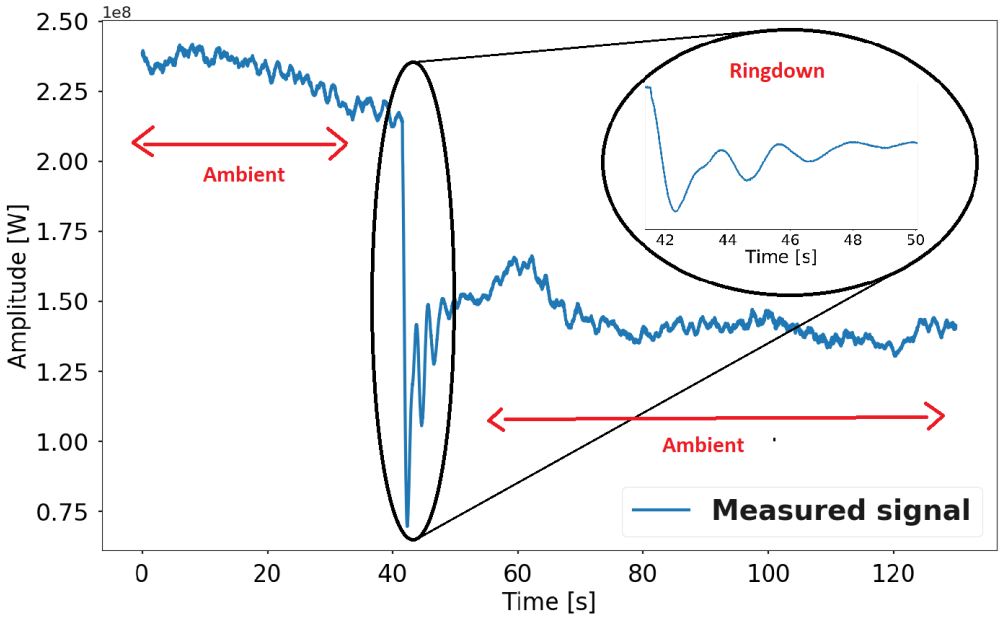

Figure 2.1: Ambient and ringdown data from the Nordic grid

This thesis will focus on ambient and ringdown conditions. Probing conditions are certainly of interest, but relevant data is not available in the Nordic grid. The reader is referred to [7] for an introduction to probing methods. For ringdown and ambient conditions, a wide range of analysis techniques exists. In addition to most methods being confined to one of the aforementioned data types, they can be classified by the following criteria:

- *Linear/Non-linear:* Linear methods, like Prony analysis, assume the response to originate from a linear model. Do not confuse this with a linear graph like $y = ax + b$; although related, it is the linearity of the governing differential equations that is referred to. The power system is highly non-linear, and not all measurements should be analyzed with linear methods. Yet often the power system behaviour is linear, and these linear characteristics are of importance to operating personnel.

- *Parametric/Non-parametric:* Parametric methods assume a parametric model for the oscillating behaviour. In this approach lies *a priori* knowledge of the data - the signal is assumed to behave in a particular way. These methods in practice try to fit the signal to the model, and if the assumption is flawed, so is the result. Contrarily, non-parametric methods do not fit the signal to a model, and the methods are related to the signal only. The few assumptions are often related to the periodical behaviour of the signal, e.g. for Fourier based methods. Non-parametric methods are generally considered more robust for estimating frequency content, yet do not perform modal decomposition, and are usually not suitable for estimating damping coefficients.

- *Recursive/Non-recursive (block-processing):* Non-Recursive, or Block-Processing methods utilize a single time window for analysis. These methods have clear purpose in off-line applications, e.g. first evaluating the start and end of a ringdown signal, and then applying a ringdown analyzer on this window. These methods can also be used for real-time applications, by sliding the window as new data is streamed to the algorithm. Recursive methods perform online analysis perhaps more elegantly, by utilizing information from the previous time-steps to update the current, facilitating faster processing and better robustness.

In Figure 2.2, the classification is illustrated. This is a reduced version of the tree made in [8].

The methods explained in this paper are in bold.

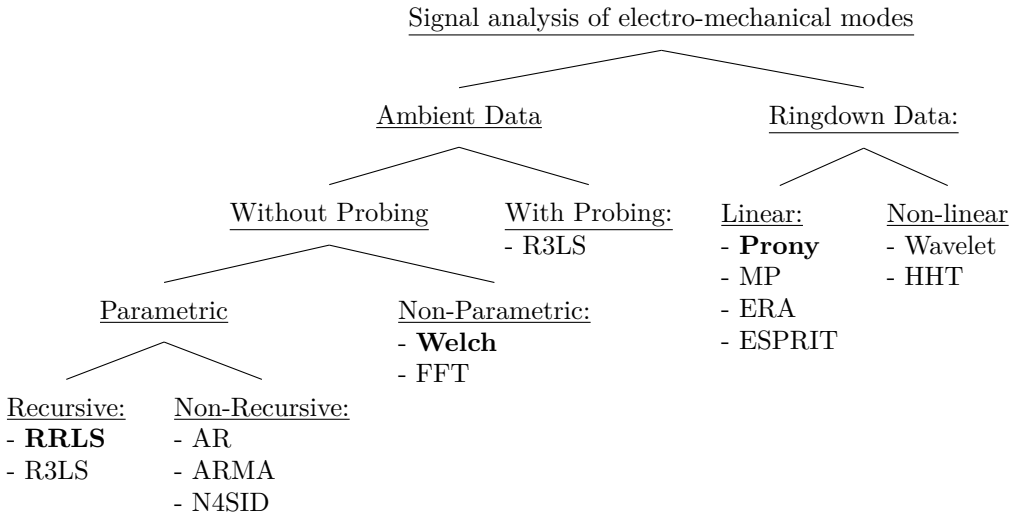

Figure 2.2: Classification of methods

The thesis centers on two parametric methods, Prony and Robust Recursive Least Squares (RRLS). Welch's method is primarily used for validation purposes, and is not investigated in detail. Prony and RRLS have different purposes, but the similarities in their parametric models are noteworthy. Hence, the following chapter will describe the modelling of power systems for small-signal stability, from a measurement based perspective.

2.2 Parametric Modelling

Parametric modelling bears strong resemblance to component-based small-signal analysis, where the dynamics are linearized around an operating point. For the measurement based parametric approach, the signal is assumed to behave linear. These similarities become evident through inspection of the theoretic foundation.

As such, the starting point is to model the power system as Linear and Time-Invariant (LTI). The Time-Invariant part is related to the system, not the measured signal, yet allows for extracting "permanent" knowledge from the measurements; if the initial state and input are the same, no matter at what time they are applied, the output waveform will always be the same [9]. The Linear part, as mentioned in section 2.1, applies to the governing differential equations. The concepts of LTI systems are mathematically described in [10], yet fathoming the full impact of these concepts comes after practical experience, rather than through mere vigorous study of the mathematics. An example of a time-continuous LTI model is given in equation (2.1).

$$c_2\frac{\delta^2 y(t)}{\delta t^2} + c_1\frac{\delta y(t)}{\delta t} = d_2\frac{\delta^2 x(t)}{\delta t^2} + d_1\frac{\delta x(t)}{\delta t} + d_0 x(t) \tag{2.1}$$

where $y(t)$ = response (output), $x(t)$ = excitation (input) and c, d = constant coefficients.

It must be stressed that this model does not describe the whole system. As a PMU only captures the observable modes in its location, the results are confined to a small part of the complete system small-signal dynamics. Observability is defined as the possibility to observe the ith modal variable in the kth state variable [11]. In this thesis, observability of modal components are investigated for power-flow measurements in the power system.

The system described in (2.1) represents a time-continuous model. However, the measurement values are obtained as samples at discrete time points. Thus, the model must be described with finite differences, that is, with discrete equations. This conversion is of course not necessary if the physical phenomena actually is discrete. However, as many models are time-continuous, the following theory serves as a connection between the time-continuous model, and the sinusoidal information obtained through the discrete analysis methods.

$$\begin{gathered} y(t) = y[n] \\ \frac{\delta^p y(t)}{\delta t^p} = \frac{\nabla^p y[n]}{h^p} + O(h) \\ \text{where O(h) is leading error of order h and} \\ \frac{\nabla^p y[n]}{h^p} \propto y[n] - y[n-1] - ... - y[n-p] \end{gathered} \tag{2.2}$$

where (2.2) shows the relationship between derivatives and backward finite differences [12]. Rewriting (2.1) as an approximated discrete system yields:

$$a_0 y[n] + a_1 y[n-1] + a_2 y[n-2] = b_0 x[n] + b_1 x[n-1] + b_2 x[n-2] \tag{2.3}$$

where a and b are coefficients different from - but related to - c and d in (2.1).

Rearranging, and generalizing to p previous values for y, and q previous values for x gives the general difference equation shown in (2.4).

$$y[n] = -\sum_{i=1}^{p} a_i y[n-i] + \sum_{i=0}^{q} b_i x[n-i] \tag{2.4}$$

The estimation of a_i and b_i is the desired information for deriving the modal decomposition of the signal. Equation (2.4) lays the foundation for Prony Analysis (including Prony Filter as described in appendix A) for ringdown data, as well as RRLS for ambient data. Note that p is the AR (Auto-Regressive) model order, which is directly related to the number of estimated modes. q is the MA (Moving-Average) order, and is not pursued here.

2.3 Original Prony

Prony Original (PA_O) dates back to the 18th century, discovered by count Gaspard de Prony [13]. Its use was not fully uncovered before the arrival of the digital computer, as several of the

involved processes are computationally demanding. The pioneering work by Hauer *et al.* [4] applied the method to power system ringdown measurements in 1990. Since then the method has matured, and is used extensively by power system operators and researchers, although some challenges persist to date.

Prony analysis is still limited to ringdown measurements, and has for a long time been classified as a block-processing method. However, Zhou *et al.* [14] utilized the similarities between two neighbouring blocks to formulate a recursive Prony algorithm. A recursive solution is more beneficial to ambient methods than for ringdown analyzers, and in this thesis, Prony's method is described in non-recursive form. It is used to perform modal decomposition on a damped, oscillating signal. In other words, the signal is approximated to a sum of damped sinusoidals:

$$\hat{y}(t) = \sum_{i=1}^{N} A_i e^{\sigma_i t} \cos(2\pi f_i t + \phi_i) \tag{2.5}$$

Where:

$$\begin{aligned} A_i &= \text{Amplitude of the } i^{th} \text{ component} \\ \sigma_i &= \text{Damping coefficient of the } i^{th} \text{ component} \\ \phi_i &= \text{Phase of the } i^{th} \text{ component} \\ f_i &= \text{Frequency of the } i^{th} \text{ component} \\ N &= \text{Total number of damped exponentials} \end{aligned}$$

The user is left to specify the model order p, which roughly results in $p/2$ estimated sinusoidals (or modes) depending on odd or even choice of p.

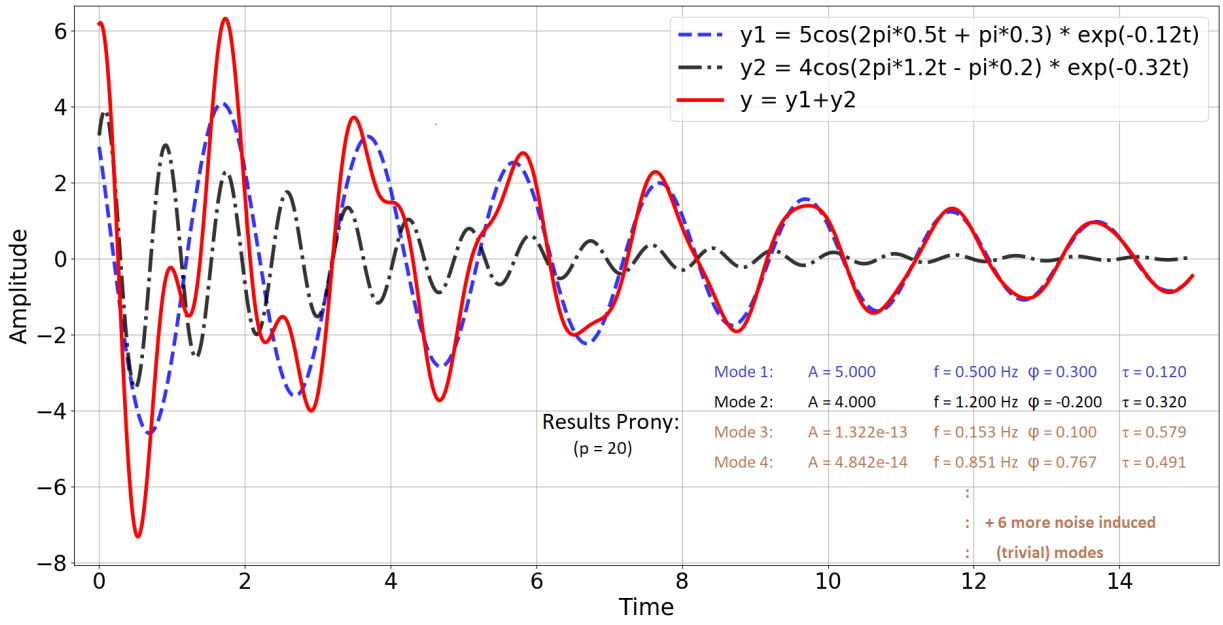

Figure 2.3: Demonstration of Prony Analysis

The method is demonstrated in Figure 2.3. This describes the method from a user's perspective, i.e. the typical input/output from a Prony program. A signal y is given to the algorithm,

suspected to have observable, sinusoidal features. In this case this certainly holds true; it is a summation of two pure sine functions of time. A model order is also required, here $p = 20$ is passed to the algorithm. Prony will then return the best fit of $p/2$ sine waves to the signal. Consider the results in Figure 2.3: the two sine waves are more or less exactly identified. The remaining 8 modes have a completely negligible amplitude, and can be discarded with little need for intelligent post-processing.
Typically, the method is extremely precise for synthetic signal with clear, sinusoidal features. Determining the model order and which of the resulting modes that can be assumed to be responsible for the signal behaviour, are trivial tasks for such signals. However, when the signal is distorted by noise, unknown inputs and/or non-linearities, they must be addressed properly. This concept is pursued further in section 2.8.

Theoretical walk-trough

The following theory is based on a proceeding specialization project work and the paper shown in appendix A.

Equation 2.5 should be view as the end result of PA_O; the amplitude, phase, frequency and damping of the sinusoidal components. However, back tracing is not a suitable presentation of the theory; instead, remember the general difference equation in 2.4. PA_O assumes zero input to the system which eliminates the b_i-terms, and the resulting difference equation represents a Linear Prediction Model (LPM). Having N number of samples, and choosing a model order p, the LPM can be extended to (2.6) by stating that the difference equation should be satisfied for the previous $(N - p)$ measurements:

$$-\underbrace{\begin{bmatrix} y[N-1] \\ y[N-2] \\ \vdots \\ \hat{y}[p] \end{bmatrix}}_{=\boldsymbol{\Psi}} = \underbrace{\begin{bmatrix} y[N-2] & y[N-3] & \cdots & y[N-p-1] \\ y[N-3] & y[N-4] & \cdots & y[N-p-2] \\ \vdots & \vdots & \ddots & \vdots \\ y[p-1] & y[p-2] & \cdots & y[0] \end{bmatrix}}_{=\mathbf{A}} \cdot \underbrace{\begin{bmatrix} a_1 \\ \vdots \\ a_p \end{bmatrix}}_{=\boldsymbol{\alpha}} \tag{2.6}$$

The reader is encouraged to verify equation (2.6), as this gives valuable insight in the use of measurements, as well as implementation concepts related to indexing. This is an over-determined system for $N > 2p$, with $(N - p)$ rows and p columns. For solving this system, the linear least-square approximation method is used, yielding an estimation of $\boldsymbol{\alpha}$ that will describe a model close to the measured values. This method is intuitively described in [15, Ch. 4.3], but the mathematical representation in compact form is given below for completeness.

$$\hat{\boldsymbol{\alpha}} = (\mathbf{A}^T\mathbf{A})^{-1}\mathbf{A}^T\boldsymbol{\Psi} \tag{2.7}$$

where:

$\mathbf{A}$ = difference equation matrix from eq. 2.6
$\mathbf{A}^T$ = transpose of $\mathbf{A}$
$\mathbf{\Psi}$ = measurement vector from eq. (2.6)
$\hat{\boldsymbol{\alpha}}$ = a-coefficient vector

The next step is to connect these predictor coefficients to the modal decomposition. This is done through the Z-transform. It is shown in [16] that they form the characteristic equation in (2.8):

$$1 + a_1 z^{-1} + \ldots + a_p z^{-p} = 0 \tag{2.8}$$

The polynomial is factorized in equation (2.9) in order to obtain the roots of the polynomial (e.g. by using the freely available numpy.roots in python).

$$(z^{-1} + \zeta_1)(z^{-1} + \zeta_2) \ldots (z^{-1} + \zeta_p) = 0 \tag{2.9}$$

These roots are closely linked to the eigenvalues, λ, of the modal decomposition in the following manner:

$$\lambda_n = f_{samp} \ln \zeta_n \tag{2.10}$$

where f_{samp} is the sampling frequency of the input signal and ζ_n is the corresponding polynomial root. The resulting eigenvalues appear in complex conjugate pairs, for all but the strictly real and non-oscillatory modes. From the eigenvalues, the frequencies f and damping ratios η are found.

$$f_n = \frac{|Im(\lambda_n)|}{2 \cdot \pi} \qquad \eta_n = \frac{Re(\lambda_n)}{|\lambda_n|} \tag{2.11}$$

For relating (2.5) to the identified modes, it must be written in complex form. Using Euler's Formula on the cosine term results in equation (2.12).

$$\begin{aligned}\hat{y}(t) &= \sum_{i=1}^{N} A_i e^{\sigma_i t}\left(\frac{e^{j2\pi f_i t}e^{j\phi_i}}{2} + \frac{e^{-j2\pi f_i t}e^{-j\phi_i}}{2}\right) \\ &= \sum_{i=1}^{N} \frac{1}{2} A_i e^{\pm j\phi_i} e^{\lambda_i t}\end{aligned} \tag{2.12}$$

where the eigenvalue is: $\lambda_i = \sigma_i \pm j2\pi f_i$

The amplitude and phase of the modal components are estimated by another least-squares approximation. Extending equation (2.13) to all measurement values, results in equation (2.14), as stated in [17] with $\boldsymbol{C}$ as the residual.

$$y[k] = \sum_{i=1}^{p} C_i \zeta_i^k, \quad k = 0, 1, ..., N-1 \tag{2.13}$$
$$\text{where } C_i = \frac{1}{2} A_i e^{\pm j\phi_i}$$

$$\begin{bmatrix} y[0] \\ y[1] \\ \vdots \\ y[N-1] \end{bmatrix} = \begin{bmatrix} \zeta_1^0 & \cdots & \zeta_p^0 \\ \zeta_1^1 & \cdots & \zeta_p^1 \\ \vdots & \ddots & \vdots \\ \zeta_1^{N-1} & \cdots & \zeta_P^{N-1} \end{bmatrix} \cdot \underbrace{\begin{bmatrix} C_1 \\ C_2 \\ \vdots \\ C_p \end{bmatrix}}_{=\mathbf{C}} \tag{2.14}$$

where the i*th* amplitude and phase are identified as the absolute value and angle of C_i, respectively.

2.4 Prony filter

In this Prony variation, the perspective is slightly different although the starting and finishing points are the same. The main difference between PA_O and Prony Filter (PA_F) is that the former assumes all input to be zero - eliminating the b_i-terms from the difference equation. In PA_F on the other hand, all input is zero *except* $x[0]$ which is equal to 1, and the system is modeled as a transfer function from an input pulse to output response. This difference does however not change the fact that both methods perform similarly, as discovered in the paper shown in appendix A. The reader is referred to work done in the appended paper for further insight into similarities/differences between the two methods, including detailed testing.

2.5 Robust Recursive Least Square

Robust Recursive Least Square (RRLS) was first proposed for speech analysis in 1995 by Kovačević, Milosavljević and Veinović [18] as an improvement to conventional recursive least square methods. Although introduced in 1995, its beneficial aspects were first identified in power system implementation by Zhou *et al.* [6] in 2007. The method is of similar character as the recursive least square method given in detail in [19, ch.7.4], although without the robustness of a loss-function defined in RRLS.

Unlike PA_O, RRLS is a recursive method, estimating eigenvalues in the signal from a stream of input measurements. RRLS iterates along a timewindow defined by the model order, p. In each step, p measured values are used to estimate the next before moving the timewindow as seen in Figure 2.4. In an iterative approach such as this, convergence is not certain for the first parts of the measured data. For this reason, it can not be used as a dedicated ringdown analyzer, yet the accuracy is reported in [6] to improve if ringdowns are included in the time window or data stream.

In a continuous stream of data, the recursive method can add the latest measurement to the estimation while forgetting the earliest measurement, all the while requiring fixed storage and calculation time in each iteration. The main principle of RRLS is demonstrated with the following equation:

$$Modal\ content[k] = Modal\ content[k-1] + weighting\ factor * prediction\ error \tag{2.15}$$

This is demonstrated in Figure 2.4.

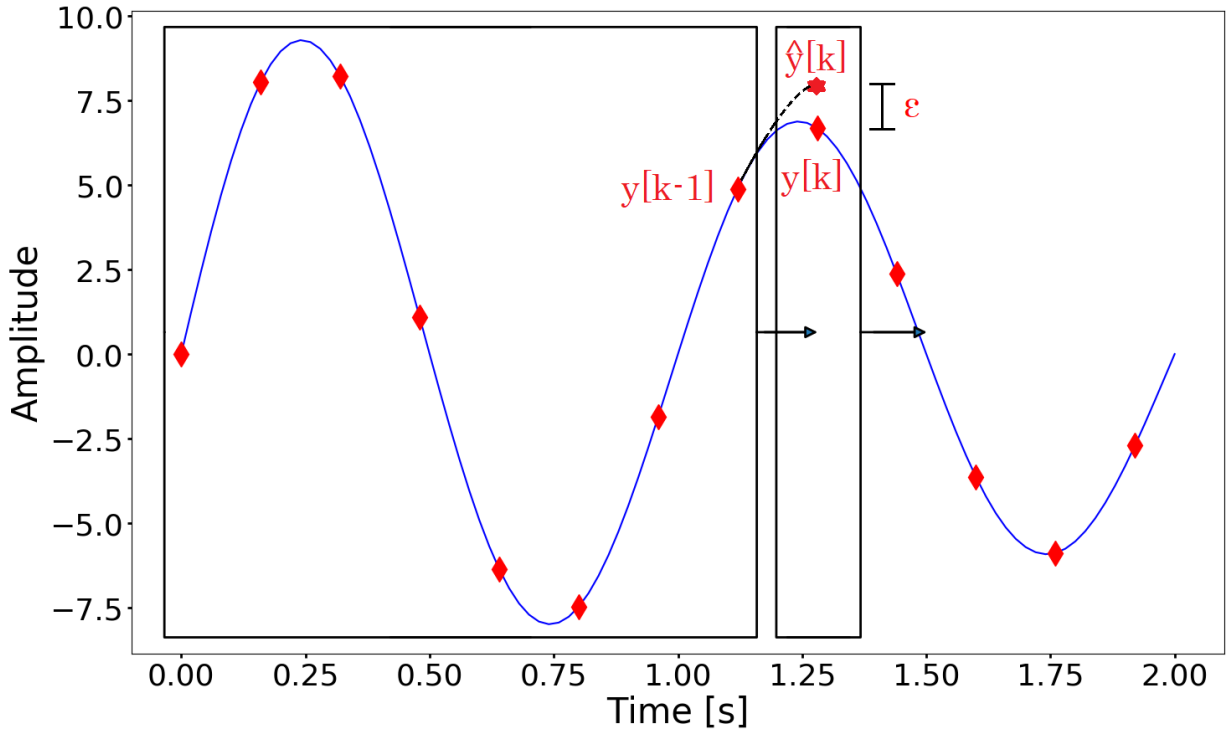

Figure 2.4: Demonstration of moving timewindow estimation in RRLS

From the eigenvalues calculated for each new input measurement, frequency and damping of modal components in the signal can be found. Small signal stability can be assessed by monitoring changes in frequency and damping found in each timestep. Understanding this principle should be sufficient for using the method. The main purpose of delving into the following theory, is to see how the weighting factor is determined, and how this is related to an important parameter called the forgetting factor, μ. To understand *why* the weighting factor is calculated as it is, the reader is referred to [18].

Theoretical walk-through

Similar to PA_O, RRLS assumes a parametric model, with zero input to the system in the general difference equation shown in (2.4). This is known as AR (Auto-Regressive) modelling, and like PA_O, the b_i-terms are eliminated to form the Linear Prediction Model. However, in this recursive version, the equation system in 2.6 is not formed. The LPM is used for its most obvious purpose; to predict the next sample, based on $\mathbf{\Psi}$ and α. This is shown in equation (2.16) with model order p.

$$\begin{aligned}\hat{y}\Big[k|\hat{\boldsymbol{\alpha}}[k-1]\Big] &= -a_1[k-1]y[k-1] - a_2[k-1]y[k-2] - \ldots - a_p[k-1]y[k-p] \\ &= \Big[-y[k-1],\ldots,-y[k-p]\Big]\cdot\Big[a_1[k-1],\ldots,a_p[k-1]\Big]^T \\ &= \boldsymbol{\psi}^T[k]\cdot\hat{\boldsymbol{\alpha}}[k-1] \end{aligned} \tag{2.16}$$

$$\begin{aligned}\boldsymbol{\psi}[k] &= \Big[-y[k-1],\ldots,-y[k-p]\Big]^T \\ \hat{\boldsymbol{\alpha}}[k-1] &= \Big[a_1[k-1],\ldots,a_p[k-1]\Big]^T\end{aligned}$$

where k is the next value and must be greater than p, i.e. it needs p values for the initial prediction. In a data stream, k corresponds to the newest sample.

Equation (2.17) through (2.20) are characterized as the core part of the RRLS algorithm derived in [18]. This is done with a Newthon-Raphson-type approach for the least-squares problem, using IMML to avoid matrix inversion and thus reducing computational burden between timesteps. Explaining the full mathematical derivation would be too lengthy, and only the practical consequences will be presented. First the $\hat{\boldsymbol{\alpha}}$-estimate for the current timestep is updated as shown in (2.18), by use of the estimation error ϵ calculated in (2.17).

$$\epsilon\Big[k|\hat{\boldsymbol{\alpha}}[k-1]\Big] = y[k] - \hat{y}\Big[k|\hat{\boldsymbol{\alpha}}[k-1]\Big] \tag{2.17}$$

$$\hat{\boldsymbol{\alpha}}[k] = \hat{\boldsymbol{\alpha}}[k-1] + \boldsymbol{L}[k] \cdot \rho^{'}\left[\epsilon\left[k|\hat{\boldsymbol{\alpha}}[k-1]\right]\right] \tag{2.18}$$

$\hat{\boldsymbol{\alpha}}$ is related to the frequencies and damping coefficients, similar to PA_O:

- the general difference equation gives the characteristic polynomial given in (2.8), which is defined in each timestep
- the eigenvalues, and thus frequency and damping, can be found from the roots of $\hat{\boldsymbol{\alpha}}$ as shown in (2.9), (2.10) and (2.11)

In equation (2.18) (elaborated in [18]), $\boldsymbol{L}[k]$ is a p x 1 intermediate vector, used to simplify the notation. It is calculated using equation (2.19).

$$\boldsymbol{L}[k] = \frac{\boldsymbol{P}[k-1] \cdot \boldsymbol{\psi}[k]}{\mu[k] + \rho^{''}\left[\epsilon\left[k|\hat{\boldsymbol{\alpha}}[k-1]\right]\right] \cdot \boldsymbol{\psi}^T[k] \cdot \boldsymbol{P}[k-1] \cdot \boldsymbol{\psi}[k]} \tag{2.19}$$

$\mu[k]$ is the forgetting factor of the current timestep, providing an exponential weighting of past errors. This is implemented so that the importance of previous estimation decreases with increasing distance from the current timestep. $\boldsymbol{P}(k)$ is a p x p state matrix updated in each timestep using (2.20). It is used as a function to ensure continuity in the estimation, remembering the calculations from the previous timestep when estimating the next. Instead of introducing the current timestep as a function of all previous timesteps, $\boldsymbol{P}(k)$ is written as a function of only the previous timestep with the forgetting factor in addition to the latest estimation update as given in [19, ch.7.4]. The result is a recursive method, taking into account all previous estimations through the latest. Equation (2.20) is found using IMML on the exponential weighted sample spectral matrix given in [19, p. 756].

$$\boldsymbol{P}[k] = \frac{\boldsymbol{P}[k-1] - \boldsymbol{L}[k] \cdot \boldsymbol{\psi}^T[k] \cdot \boldsymbol{P}[k-1] \cdot \rho^{''}\left[\epsilon\left[k|\hat{\boldsymbol{\alpha}}[k-1]\right]\right]}{\mu[k]} \tag{2.20}$$

$\rho^{'}[\epsilon]$ and $\rho^{''}[\epsilon]$ are the first and second derivatives of the "hard" defined loss-function $\rho[\epsilon]$ defined in (2.21). The loss-function is the robustness part of the method, weighing robustness and efficiency. σ is the standard deviation of ϵ, defined in (2.22).

$$\rho[\epsilon] = \begin{cases} \frac{1}{2}\epsilon^2 & \text{if } |\epsilon| \leq 3\sigma \\ \frac{3}{2}\sigma^2 & \text{if } |\epsilon| > 3\sigma \end{cases} \tag{2.21}$$

$$\sigma = \frac{median\Big(\Big|\boldsymbol{E} - median(\boldsymbol{E})\Big|\Big)}{0,6745} \tag{2.22}$$

where $\boldsymbol{E}$ in (2.22) is a vector containing all calculated values of ϵ including the latest timestep k.

Equation (2.21) gives the derivatives shown in (2.23) and (2.24).

$$\rho^{'}[\epsilon] = \begin{cases} \epsilon & \text{if } |\epsilon| \leq 3\sigma \\ 0 & \text{if } |\epsilon| > 3\sigma \end{cases} \tag{2.23}$$

$$\rho^{''}[\epsilon] = \begin{cases} 1 & \text{if } |\epsilon| \leq 3\sigma \\ 0 & \text{if } |\epsilon| > 3\sigma \end{cases} \tag{2.24}$$

Each timestep is dependent on $\hat{\boldsymbol{\alpha}}$ and $\boldsymbol{P}$ from the previous timestep, in addition to all previous values of ϵ. Ones all of these values are updated, k can be increased by 1 and the process can be repeated from (2.16).

2.6 Welch's method for frequency estimation

As discussed in section 2.1, the appropriate approach to analyze PMU data is with a toolbox of methods. Prony and RRLS are parametric methods, and although with some differences, they both assume an underlying parametric model. As an additional verification, a non-parametric method gives a different perspective of the measured signal. In 1967, Welch [20] proposed a Fast Fourier Transform (FFT) based, non-parametric method for estimation of power spectra, today known as Welch's method. By transforming block segments of the time domain signal to the frequency domain and estimating the periodogram, it can visualize the power spectral density

of the signal by averaging the periodograms calculated in each segment of time. The resulting power spectral density of a measured signal is shown in Figure 2.5, where the estimated power spectral density gives a clear indication that there is a mode with a frequency around 0.485 Hz present. The power spectral density is given in [Watt/Hz].

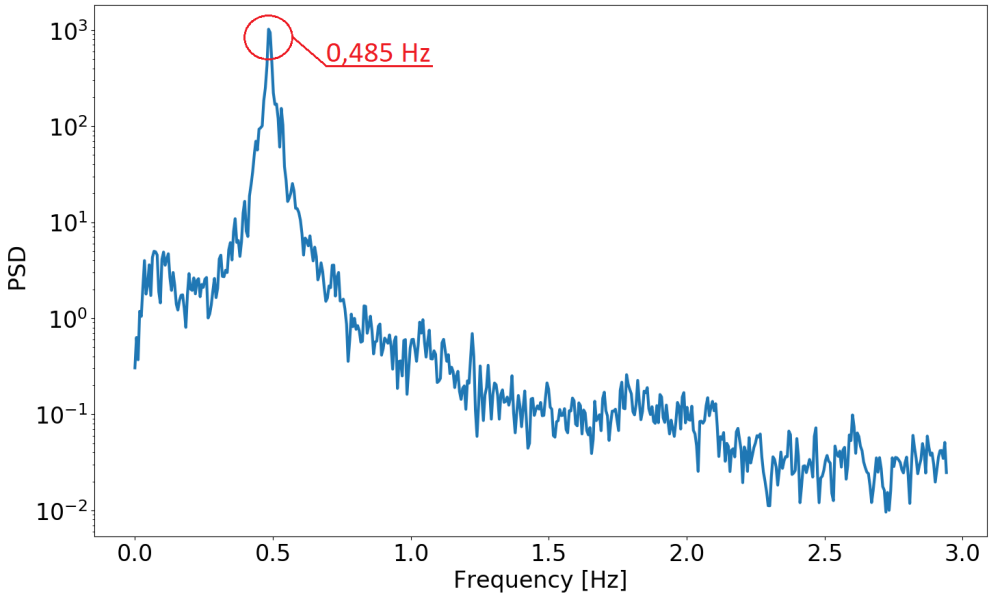

Figure 2.5: Welch power spectrum of a measured signal

As this method is used as a simple validation, its theory is not discussed in detail in this thesis. A basic overview of its concepts is provided, while in-depth fundamentals can be found in [20]. The black-box algorithm used for testing is the "welch"-method from the open source `Python` library `SciPy` [21].

2.7 Empirical Mode Decomposition as band-pass filter

All methods implemented in this thesis require pre-treating of the input signal, either to remove high frequency noise, signal trend or both. For PA, a variety of solutions to improve its robustness under noisy conditions are proposed. Kumaresan and Feng [22] proposed two different pre-filtering methods to improve PA, one based on a predefined FIR filter and another defining the pre-filter iteratively from the measured data. Pre-filtering using the Empirical Mode Decomposition is also proposed in [23]. For the RRLS method, a weighted adaptive algorithm has been proposed for detrending [6].

In this thesis, Empirical Mode Decomposition (EMD) is used as a band pass filter, removing high frequency noise and signal trend. EMD is a method for non-linear, non-stationary signal processing that decomposes the signal into a set of Intrinsic Mode Functions (IMFs) [24] as seen in Figure 2.6 and 2.7. An IMF is an oscillatory mode function where the mean value of its upper and lower envelope is zero. The described oscillatory mode may be of non-linear behaviour and thus contains variable frequency. An example of this is IMF 3 in Figure 2.6, which has a clearly fluctuating frequency.

The IMFs are extracted one at a time - starting with the highest frequency - and contain information on a modal component in the signal. Figure 2.6 shows the decomposition of PMU-data from a ringdown into IMFs. Even though the signal looks quite smooth, the high frequency

noise is present. By selecting the IMFs with an average frequency in the desired range, one may rebuild the denoised signal.

Figure 2.7 shows a longer timewindow of ambient data. The presence of high frequency noise is greater compared to the ringdown signal. In addition, due to an increase in time span, the low frequency modes of the last IMFs must be treated before application of an ambient analyzer.

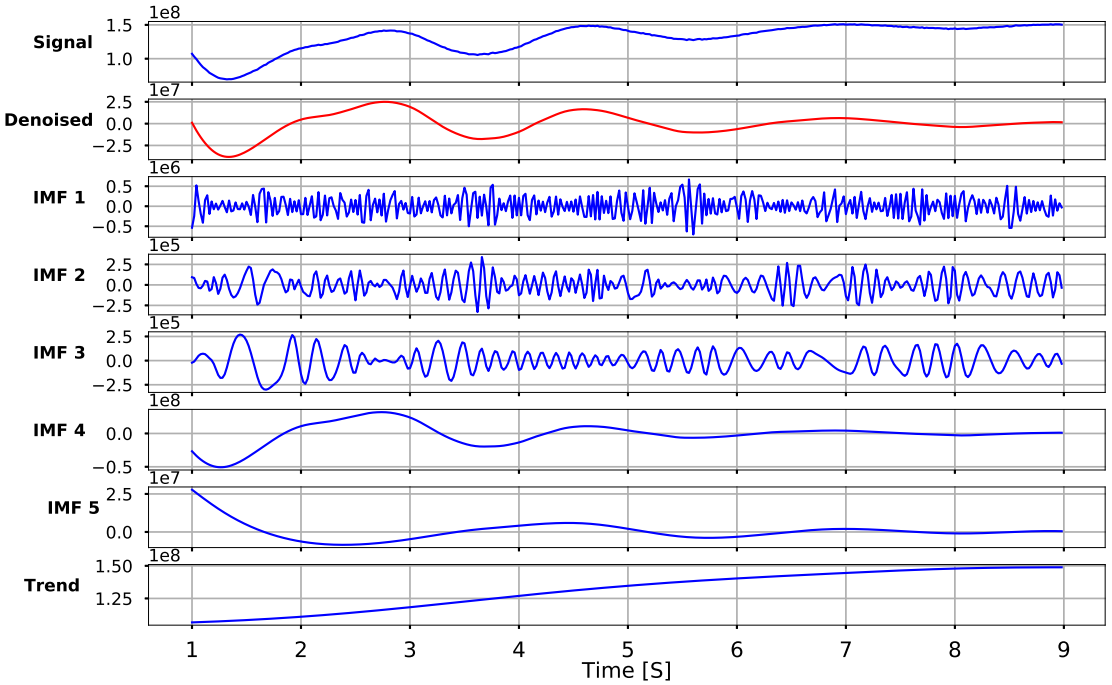

Figure 2.6: Decomposing ringdown PMU-data into IMFs

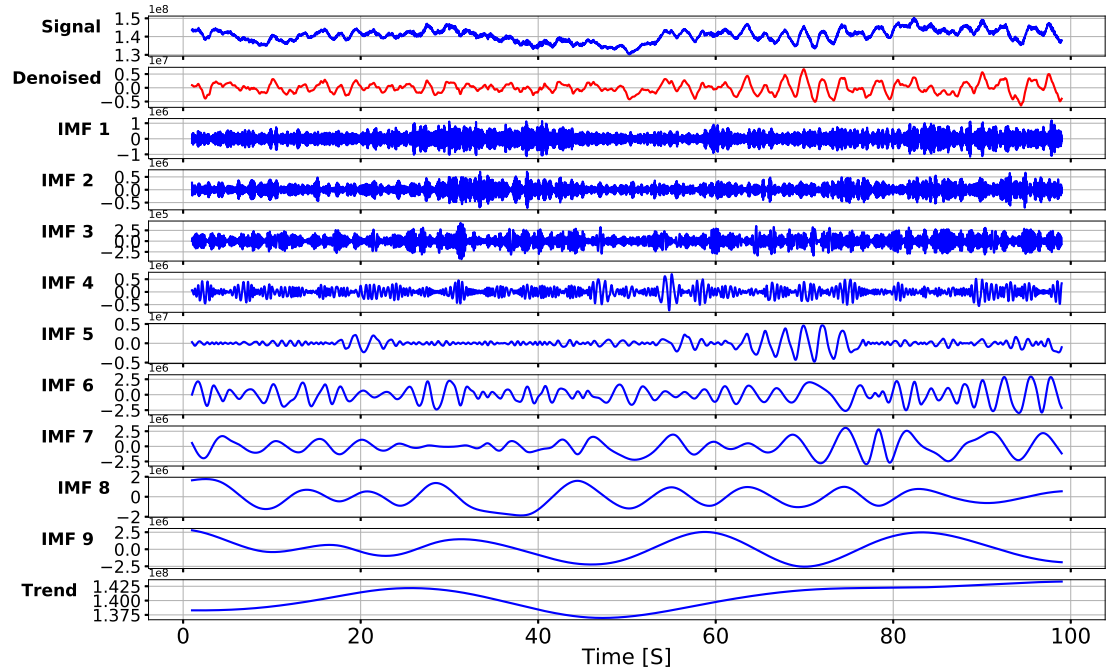

Figure 2.7: Decomposing ambient PMU-data into IMFs

Theoretical walk-through

To separate the IMFs using the EMD technique, there are certain conditions that must be met. Each IMF must have a mean value of zero, and a number of extremas that equals the number of zero-crossings (or at most differs by one). The stepwise process to identify IMFs in a measured signal $y(t)$ is:

1. Start with signal y(t) as input
2. Identify extremas
3. Calculate the upper and lower envelope of the signal (e_{up}, e_{down})
4. Find the mean value ($m(t)$) of the upper and lower envelope
5. Extract the difference from the signal: $d(t) = y(t)$ - $m(t)$
6. Repeat steps 2-5 with $d(t)$ as input, until it satisfies the conditions of an IMF
7. Set $d(t)$ as an IMF, and subtract it from the input signal. Repeat the process with the residue $r(t)$ as input signal ($r(t) = y(t)$ - $d(t)$)
8. Continue until there are no more extrema present in signal

The EMD output extracts modal components starting with the highest frequency and ending with the residual "trend" of the signal. The hierarchy in the decomposed modes gives the EMD characteristics similar to those of a dyadic filter bank [25]. The average frequency of each IMF gives a rough criterion for choosing which IMF to include in the filtered signal. By merging the IMFs with an average frequency in the electro-mechanical range (oscillating frequency from 0.2 to 2 Hz), the high frequency components and the signal trend (given by the residual) is excluded, and a filter has been implemented. Examples of high frequency components that must be removed are torsional modes typically occurring in the range of 10-46 Hz and measurement noise.

In this thesis, the EMD implemented is based on the work by Deshpande [26].

One challenge when using the EMD is that modes with closely spaced frequencies may be mixed together. This makes the basic version of EMD more challenging for identification of electro-mechanical modes unless special strategies are used for intermittent or closely-spaced tones as described by Fosso and Molinas [27]. For high frequency filtering on the other hand, its characteristics are well suited, as it elegantly extracts high frequency components without altering the remaining signal components.

Implementing the EMD for online purposes on ambient data is a challenge. The EMD algorithm's timeconsumption increases with signal length, due to an increase in the number of extrema. In addition, the more slowly varying modes that were incorporated in the signal trend for the shorter timewindows are decomposed into additional IMFs. For these reasons, a recursive implementation of the EMD-technique is certainly of interest.

2.8 Clustering as post-processing intelligence

All linear, parametric methods have particular concerns that must be addressed. Each one has its particularities, yet most have the following in common:
- Defining model order(s)[1]

[1]Some models require several model orders to be specified, e.g. ARMA (2, both for poles and zeroes)

- Selecting resulting modes
- Validity and robustness of the model for given signal

In this thesis, these concerns are addressed by running the relevant parametric method in a range of model orders. It is hypothesized that the *true modes* and their shapes will remain close to constant. *True modes* are those that are responsible for actual linear behaviour in the system. Subsequently, the *trivial modes* (identified by their frequency, damping and amplitude) will change significantly. *Trivial modes* are those that fit the noise and non-linear behaviour. For ringdown analysis, the purpose of the method is to separate the true from the trivial modes, without excluding those that are less observable. For ambient, online analysis, this method offers the possibility of automatic tracing of changes in the modal content in the power system. Furthermore, if no clusters are found, this is an indicator that the signal is not suitable for the analysis method.

Other solutions to this challenge are not as of yet well documented, and are subject to investigation. For PA, singular value decomposition is commonly used to identify an ideal model order. This is a sound approach for pure, sinusoidal signals, yet is not ideal when the signal is distorted by noise, inputs or non-linearities. A different approach is validation through a non-parametric method - Welch's being the most used - which investigates the power of a signal for different frequencies. In doing so, the dominant modal components is identified by their frequency, and their remaining modal information extracted from the parametric decomposition.

Figure 2.8 shows the modal decomposition of a noisy signal for two different model orders. This signal actually contains three different modal components, with frequencies of 0.28 Hz, 0.75 Hz and 1.5 Hz. The objective is to separate these from the trivial modes.

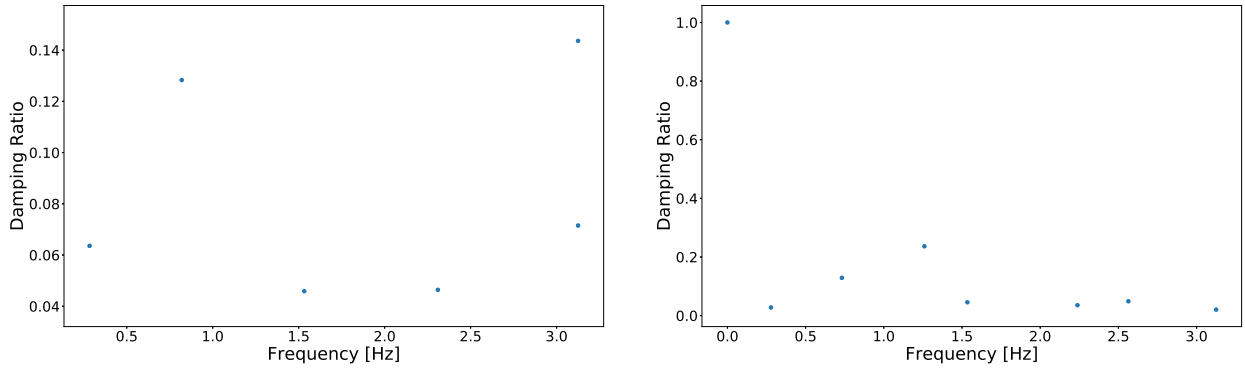

(a) $p = 10$ **(b)** $p = 14$

Figure 2.8: Example decomposition for different model orders

For ringdown analysis using PA, the frequency, damping, amplitude and phase are available for identification of true modes. For clustering purposes, a three-dimensional data-input improves predictability, and frequency, damping and amplitude are given as input. For ambient analysis using the RRLS method, only the frequency and damping are available, resulting in two-dimensional clustering.

By utilizing the modal decomposition in a range of model orders, a base for clustering is achieved. Figure 2.9 shows the three-dimensional clustering of multiple model orders from the same case as in Figure 2.8. It can be noted that all true modes are identified among the trivial noise.

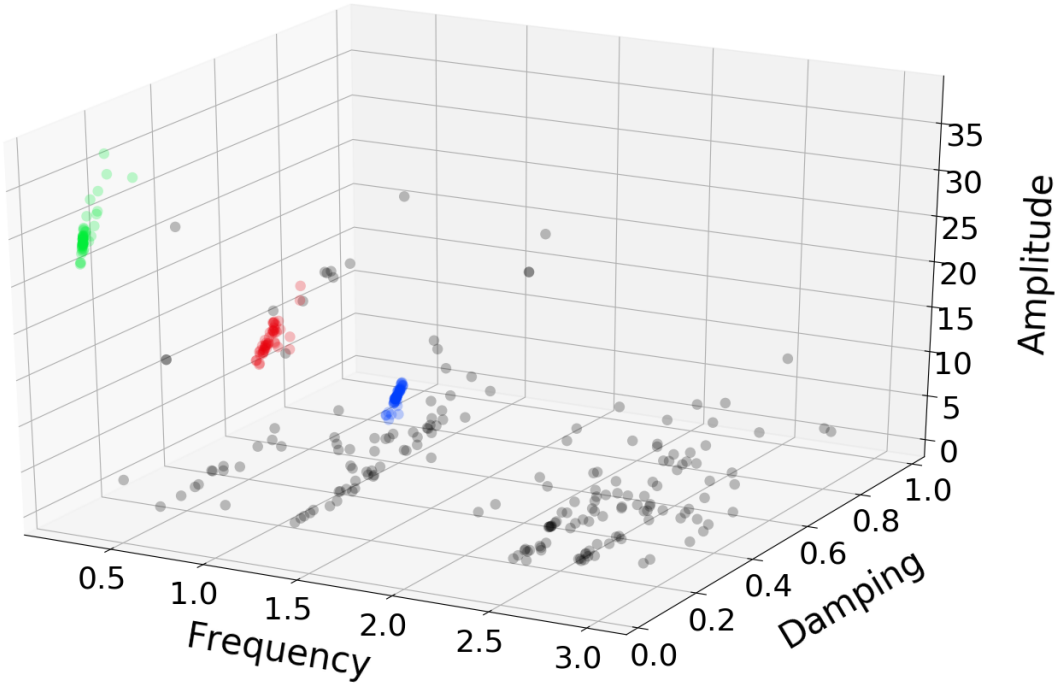

Figure 2.9: Clustering of noisy, synthetic signal

Theoretical walk-through

The range of model orders selected differs between the methods. For PA, a lower limit of $p = 10$ and an upper limit of $p = N/2$ is chosen for the model order range to ensure a good basis for clustering. The lower limit is defined as 10 to mitigate simulations where the number of observable modes is larger than the model order. For RRLS, a predefined range of model orders is selected, giving predictability of the computational burden. A lower limit of $p = 20$ and an upper limit of $p = 39$ are chosen. A "hard" limit is possible, due to the small difference between the higher model orders.

The clustering method used in this thesis is a density-based algorithm named "Density-based spatial clustering of applications with noise" (DBSCAN). This method was first proposed by Ester *et al.* [28], to make clustering more versatile. Density-based algorithms are not limited to finding spherical clusters of a predefined size. It can on the other hand, by considering the density of an area, find clusters of arbitrary shapes. It works as an unsupervised learning mechanism, labelling data in clusters and assigning the rest as noise [29].

The DBSCAN algorithm depends on two input parameters: epsilon (ϵ) and minimum cluster size (minClu). It labels each datapoint into three categories: either it is a core point, a border point or noise. By first assuming that none of the input-data belongs to a cluster, DBSCAN chooses one of the unassigned objects as a starting point. From this point each object within a distance of ϵ is considered as a neighbour. If the point is found to be a core point [28], it finds all objects in its area using ϵ and minClu. All these objects are then assigned to the same cluster. If it is not considered as a core object, and is not present in another cluster, it is labelled as noise. The clustering is completed once every object is either assigned to a cluster or labelled as noise.

As previously stated, the input data from PA to DBSCAN is three-dimensional. Frequency,

damping and amplitude of all identified modes from all model order simulations of PA are utilized. RRLS on the other hand uses only frequency and damping. For weighting purposes, the algorithm is altered so that only a small deviation in frequency is allowed. For amplitude and damping, some deviation is accepted in each cluster. Combined with the choice of ϵ, this defines the degree variation accepted.

2.9 Additional concepts

Concepts introduced in this section are based on a proceeding specialization project.

2.9.1 Signal to noise ratio

To determine the quality of the rebuilt signal in ringdown analysis, signal-to-noise ratio (SNR) is used [17]. SNR is calculated in decibels using the root-sum-of-squares of the error and the measured value. This value is an indicator of the ratio between signal and noise power. If the ratio is greater than 1 (0 dB), it indicates more signal than noise in the estimate. SNR implicitly assumes that noise and signal are uncorrelated and come from different sources [30].

$$SNR = -20 \log_{10} \left(\frac{\sqrt{\sum_{i=1}^{N} (\hat{y}[i] - y[i])^2}}{\sqrt{\sum_{i=1}^{N} (y[i])^2}} \right) \tag{2.25}$$

Where:

$$\begin{aligned} SNR &= \text{the signal-to-noise ratio in decibels} \\ \hat{y}[i] &= \text{the } i^{th} \text{ estimated amplitude} \\ y[i] &= \text{the } i^{th} \text{ measured amplitude} \end{aligned}$$

2.9.2 Aliasing

A high sampling frequency when applying least square techniques, results in bad approximation of low-frequency modes in addition to a high computational burden. For instance, PA struggles with identification of electro-mechanical modes when the number of samples per cycle is too high [17]. For online ambient analysis, a high sampling frequency would increase the computational burden, making it less practical to implement. Reducing the number of samples to an appropriate level is necessary.

A common problem when reducing the number of samples in a measured impulse response, is that valuable information regarding the signal is lost. According to the Nyquist-Shannon sampling theorem [31], the sampling frequency needed when digitising an analogue signal must be twice that of the highest frequency in the signal. This frequency is commonly called the Nyquist frequency [32, p. 269].

Say that the sampling frequency of a composite signal containing multiple modes is reduced so that the sampling frequency is below twice that of the highest frequency in the composite signal.

The mode with that frequency would not be possible to replicate with its original frequency since information is lost. An alias of that original mode will instead be made within the new frequency range. This means that a high frequency mode will be seen as a low frequency version of itself as observed in figure 2.10. This phenomenon is known as aliasing [33, p. 130]. In fact, any frequency outside the sampling range will alias to a frequency within. An unfortunate result is that the estimate can yield additional frequencies in the range of interest. When the aliasing occurs, the high frequency component in the signal will be folded back over the low frequency components, thus modifying them as described in [34].

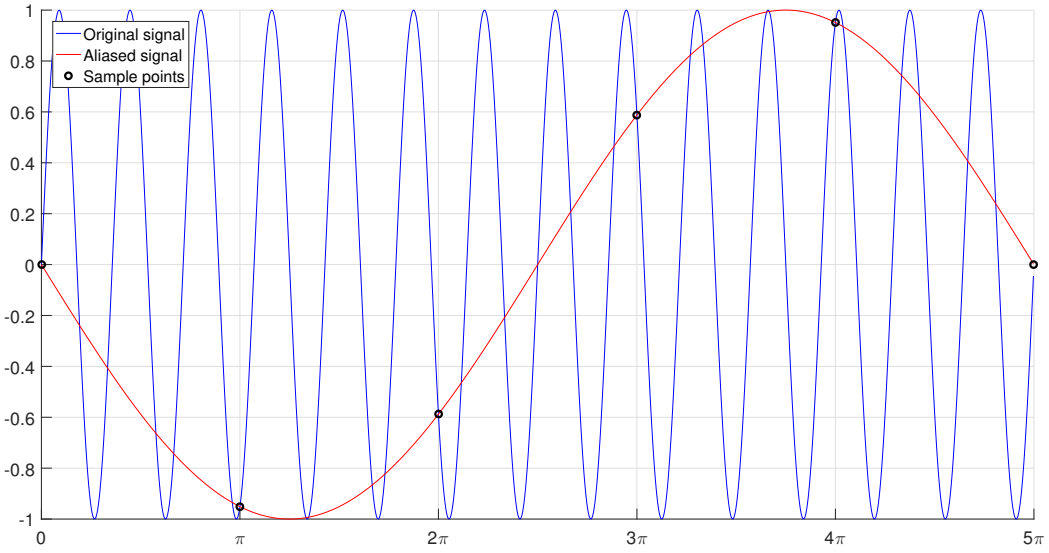

Figure 2.10: Aliased high frequency signal

To avoid this problem, the input signal should be pre-filtered so that all frequencies above the range of interest are removed. This is known as anti-aliasing, and is accommodated by EMD in this thesis.

3 Remarks on implementation

The modes of interest in this thesis lie in the electro-mechanical range. In accordance with the Nyquist-Shannon sampling theorem discussed in section 2.9.2, the sampling frequency must be at least 4 Hz to contain information of the modes at 2 Hz. In this thesis the sampling frequency is set to 6 Hz, well above the minimum limit, to avoid loss of modal information. For data sampled at higher frequencies, approximately 6 Hz is achieved through downsampling. The sampling theorem applies to the high frequency noise as well. When the sampling frequency is below twice the noise frequency, information is lost and signal aliasing occurs as previously illustrated. To assure that this problem is handled, the signal is filtered for high frequency noise by using the EMD-technique, without altering the components in the electromechanical range.

For higher model orders, many of the modes found by PA have insignificant amplitudes, or very high damping ratios. These are discarded before feeding the clustering algorithm, as they do not influence the signal dynamics. Choosing a hard limit on mode amplitude (1/30 relative to the highest amplitude), and excluding modes with damping ratio above 50%, is a brute way of post-filtering the results. A more sophisticated evaluation method is presented by Zhou, Pierre and Trudnowski [35]. However, the hard limit is sufficient for this method, with the purpose of removing the obvious trivial modes. The clustering algorithm is responsible for classifying the rest. For the RRLS-method, amplitude is not a logical parameter, thus excluding the same option for a brute amplitude post-filter. However, both methods find complex conjugate pairs of modes due to the properties of the prediction model and characteristic equation. For analysis, only the positive modal component is taken into account. In PA_O each complex modal pair has an equal amplitude contribution. This is handled before removing the negative component.

To identify the true modes in the signal, clustering is proposed for both methods as a type of post-processing intelligence. Although the implementation is slightly different, the principle for clustering is the same in both methods.

For explanatory purposes, timestep is defined in this thesis as a single measurement at a given time. As seen in Figure 2.2, there are numerous methods for analysis of power system measurements. Considering that no method is perfect for all measurement types, the term timewindow is defined in this thesis as a part of a measured signal which is under investigation. Figure 2.1 shows how a measured signal is divided into three sections of interest. The first and last section contain ambient data, where a timewindow is defined as a smaller part used for analysis and prediction of the following timestep. Sliding this timewindow along the entire section of ambient data results in a continuous evaluation of modal content. The shorter part in the middle shows a ringdown, where all measurements are used in one analysis; the timewindow is then defined as the entire section.

In this thesis, reconstruction is used as a term for recreating the signal based on identified modal components.

3.1 Proposed method for ringdown analysis

- Pre-Filtering using EMD
  - Identify signal IMFs
  - Extract IMFs in the electro-mechanical range
  - Rebuild signal without high frequency noise and signal trend
- Downsample signal to 6 Hz
- Define range of model orders to be investigated
- Do PA_O for all p orders in defined range:
  - Build LPM in (2.6)
  - Estimate $\boldsymbol{\alpha}$ using least-squares
  - Find roots of characteristic polynomial in (2.8)
  - Calculate eigenvalues from roots with (2.10)
  - Establish equation system shown in (2.14)
  - Solve the equation system for residual $\mathbf{C}$
  - Calculate frequency and damping from each eigenvalue
  - Calculate amplitude and phase from each residual
  - Post-filter the insignificant modes
- Cluster the remaining modes

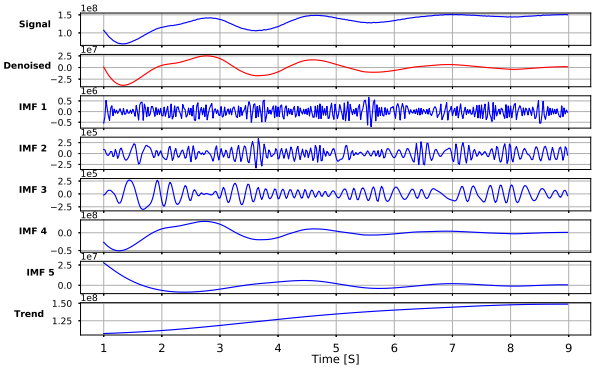

Figure 3.1: Decomposing ringdown PMU-data into IMFs

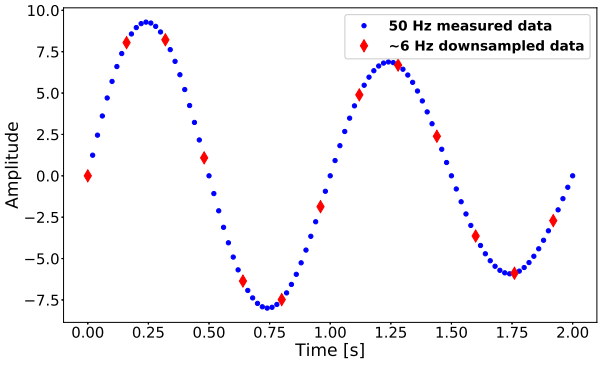

Figure 3.2: Downsampling

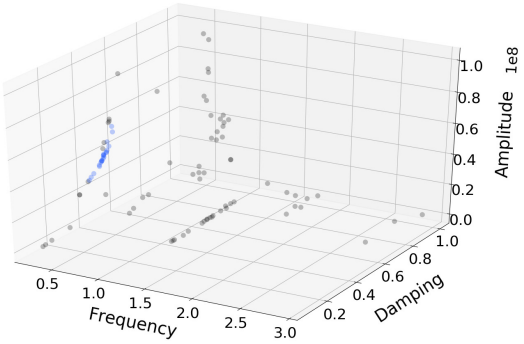

Figure 3.3: Cluster identification using PA_O

3.2 Proposed method for ambient analysis

In this thesis, the input data given is of a predefined size. This allows for an offline pre-filtering method using the EMD-method. For further work, this method should be extended to an online implementation, which combined with the already online RRLS and clustering would give a complete method for mode-tracking. Here, the entire signals is filtered with the EMD. RRLS and clustering run in timewindows of the filtered signal, simulating an online implementation where timesteps are provided one at a time.

The RRLS-method requires an initial guess of two parameters, $\boldsymbol{P}$ and $\hat{\boldsymbol{\alpha}}$ in addition to the forgetting factor μ. The selection affects the time it takes for the method to converge. By testing, it was discovered that $\boldsymbol{P}$ converged with values in the matrix around 10^{-2} for normalized

input data. The initial guess for $\boldsymbol{P}$ was then set to 10^{-2} times $\boldsymbol{I}$, where $\boldsymbol{I}$ is the identity matrix with dimensions p x p. $\hat{\boldsymbol{\alpha}}$ is on the other hand defined for cold start, where all values in the p x 1 vector are set to zero. Lastly, the forgetting factor, μ, is initially set to 0.9 in the first 5 % of the measured signal, allowing fast convergence before it is gradually increased to 0.999 after 15 % as illustrated in Figure 3.7. This factor is a compromise between variance and bias. As documented in [18], μ is recommended to be set in the range of 0.95 to 0.99. Zhou, Pierre, Trudnowski and Guttromson found in [6] that for abrupt changes in the system, μ should be set low so that the bias decreases and convergence is reached faster. For normal operating, μ should be restored to 0.999 to reduce the variance. In this thesis, the implemented method is tested for ambient data only, without abrupt changes, thus setting μ closer to 1 and keeping almost all previous estimations in memory.

- Pre-Filtering using EMD
  - Identify signal IMFs
  - Extract IMFs in the electro-mechanical range
  - Rebuild signal without high frequency noise and signal trend
- Downsample signal to 6 Hz
- Define range of model orders, p (20 to 39 in this thesis)
- Set initial values for $\boldsymbol{P}$, $\hat{\boldsymbol{\alpha}}$ and μ.
- Do RRLS and clustering in each timestep, k:
  - Simulations for all model orders in the defined range are conducted in each timestep, using values from the same model order in the previous timestep
  - Calculate the amplitude estimate of current timestep using equation (2.16)
  - Calculate the estimation-error in equation (2.17)
  - Update $\hat{\boldsymbol{\alpha}}$ for each model order in equation (2.18)
  - Cluster the results from all model orders in the current timestep, extracting the identified modes
- Plot identified modes from each timestep as a function of time to identify changes in the modal components.

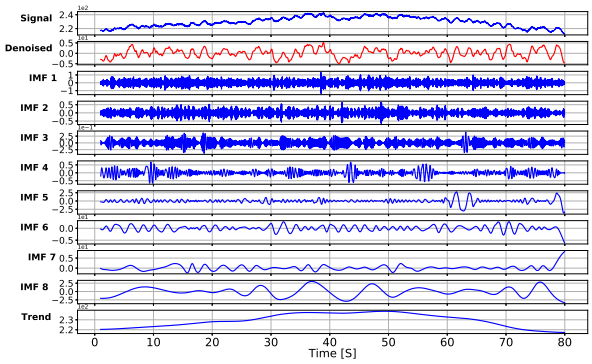

Figure 3.4: Decomposing ambient PMU-data into IMFs

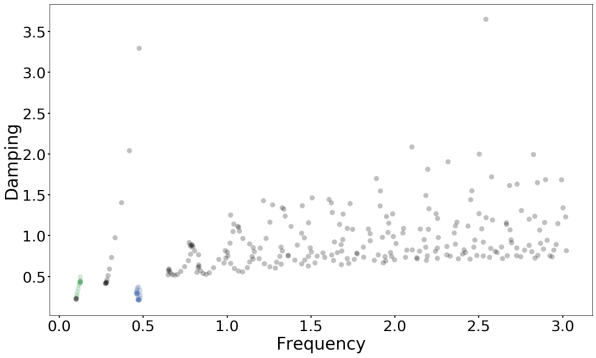

Figure 3.5: Clustering of results in each timestep, k

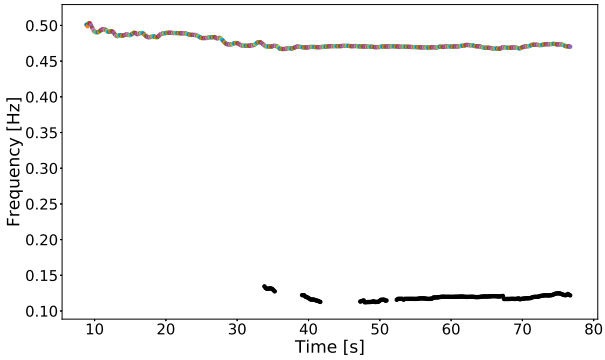

Figure 3.6: Illustration of mode-tracking in ambient data

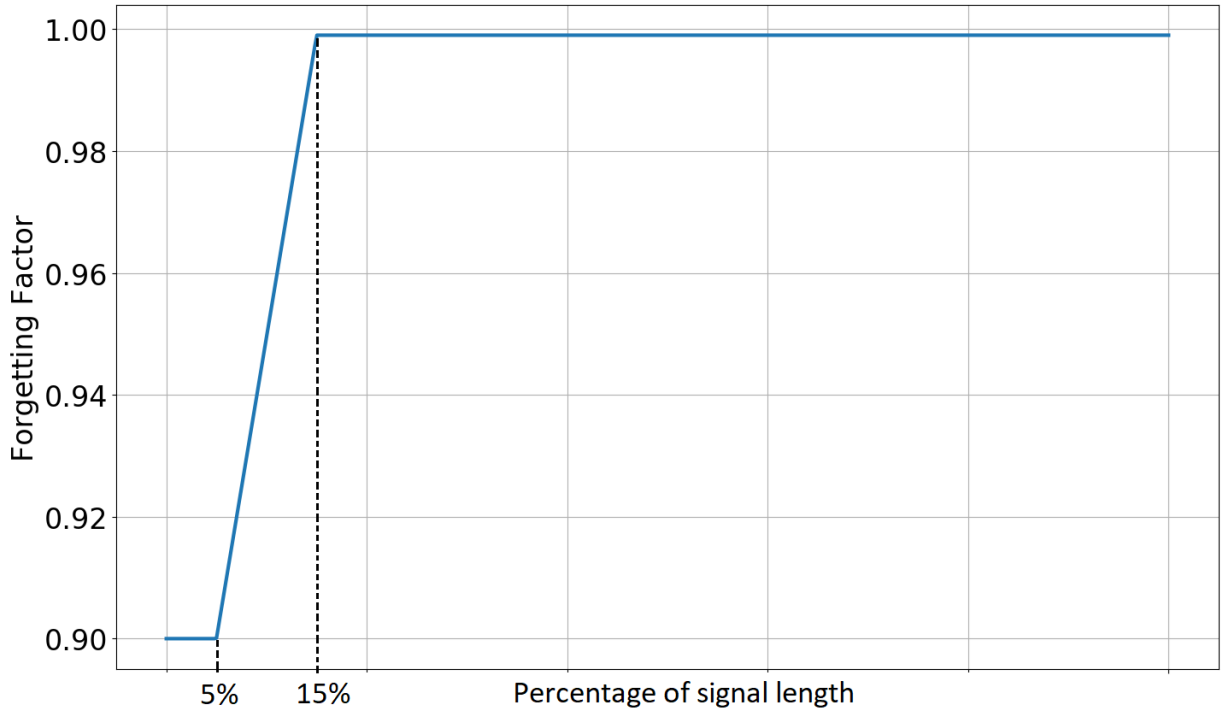

Figure 3.7: Variation of the forgetting factor

3.3 Simulation study

In this thesis, the methods are verified using `DIgSILENT's` power system modelling tool `PowerFactory` (PF). In contrast to the measurement based methods discussed so far, PF relies on a component-based approach to estimate system eigenvalues.

By linearizing the power system around an operating point, the assumption is that its motions can be described by a set of ordinary differential equations [36] as shown in equation (3.1).

$$\begin{aligned} \dot{\boldsymbol{x}}(t) &= \boldsymbol{A}\boldsymbol{x}(t) + \boldsymbol{B_L}\boldsymbol{q}(t) + \boldsymbol{B_E}\boldsymbol{u_E}(t) \\ \boldsymbol{y}(t) &= \boldsymbol{C}\boldsymbol{x}(t) + \boldsymbol{D_L}\boldsymbol{q}(t) + \boldsymbol{D_E}\boldsymbol{u_E}(t) \end{aligned} \tag{3.1}$$

where $\boldsymbol{x}$ contains all states of the system, $\boldsymbol{A}$ is the system-matrix describing all aspects of the system related to its states, $\boldsymbol{q}$ is a random vector added as noise to perturb the system, while $\boldsymbol{u_E}$ is the system input vector. $\boldsymbol{y}$ is on the other hand the system output.

The $\boldsymbol{A}$-matrix contains information of the entire linearized system, where all eigenvalues, λ, in the stationary case can be found using (3.2). It is emphasized that the $\boldsymbol{A}$-matrix in a component-based approach is not the same as the $\boldsymbol{A}$-matrix seen in the measurement based approach in section 2.3. While the measurement based $\boldsymbol{A}$-matrix only contains measurement information which leads to the identification of excited modes, the component-based $\boldsymbol{A}$-matrix contains the modal information of all modes in the model.

$$det(\boldsymbol{A} - \lambda_i \boldsymbol{I}) = 0 \tag{3.2}$$

The power system model used is the *Kundur Two Area Model* [37, p. 813] as shown in Figure 3.8. The model is a two area, eleven bus system with four generators and two loads.

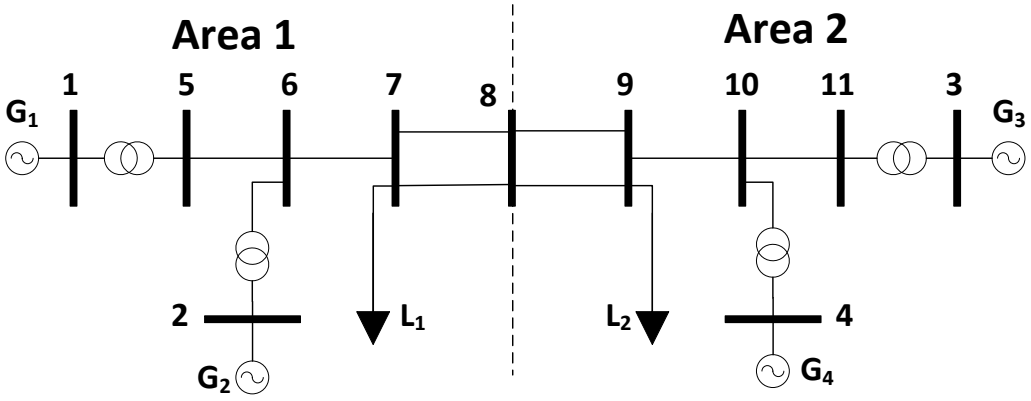

Figure 3.8: Kundur Two Area System

Ambient data is added to the model to increase the similarity with the real world power system. Using dynamic loads to simulate ambient data revealed power measurements similar to those seen in the power grid. As far as the authors of this thesis are concerned, the general assumption is that dynamic loads can be modelled using white Gaussian noise. This has been, and will continue to be an area of research as the validity of the assumption is not yet proven.

The ambient data generated in this thesis is a combination of both fast and slowly varying noise. The former is created by adding small amplitude noise in each timestep with zero mean and finite variance in the given timewindow similar to white Gaussian noise. The noise simulates 50 Hz changes in the power system, and is a combination of measurement noise, small load changes, etc. The latter is larger, slowly-varying load changes. These are simulated as three step-changes occurring repeatedly in periods defined by frequencies in the electro-mechanical range. Concretely, the changes occur in steps defined by the three frequencies 0.2 Hz, 0.8 Hz and 1.3 Hz with variable magnitude. As the load vary randomly and the data streams investigated in PF are no longer than 20 minutes, the load changes may or may not not have a zero mean. The combination of fast and slowly varying load changes result in a system response similar to that which can be seen in a real power system.

The ambient data is added to the base real power demand of 967 MW and 1767 MW at loads L_1 and L_2 respectively. Figure 3.9 shows the varying power transfer in the lines between buses 9 and 10, and buses 5 and 6. With a constant load in the system, the power transfer would also be constant in these time-windows.

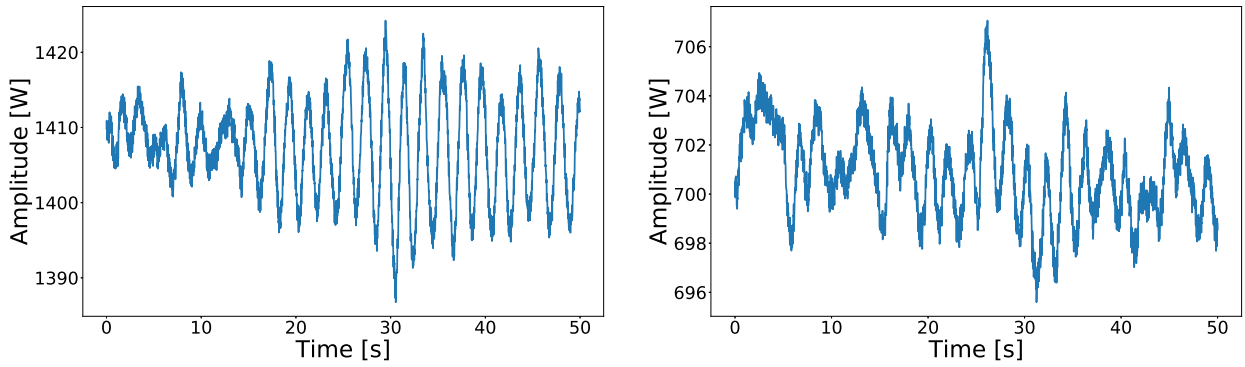

(a) Line 9-10 **(b)** Line 5-6

Figure 3.9: 50 seconds of ambient data

Using the built-in modal analysis tool in PF, the frequency and damping of the modal components present in the system are found. It must be kept in mind that it will find all modes, and not just those that are excited by a given fault. In addition, PF calculates the modal components present based on steady-state snapshot of the power system. With dynamic loads in the system, the modal components will change slightly in each time-step. This is also the case if a line is disconnected or other changes happens to the system. For the initial case, the oscillatory modes identified by PF are:

Table 3.1: Modes identified by PF for base case

Mode	Freq. [Hz]	Damp. Ratio η
1	0.470	0.028
2	0.696	0.052
3	0.976	0.102

To illustrate the changing modal components, the loads are varied in steps of 100 MW total. Figure 3.10 shows the modal components as the system loading gradually increases. It can be seen that the changes in frequency are relatively small, with the largest change being 0.025 Hz for the 0.975 Hz mode. This example is is shown with an identical increase in both loads. If the loads vary independently, it may lead to a different result. However, this still serves as an illustrative example of the problem when estimating modal components in a dynamic system.

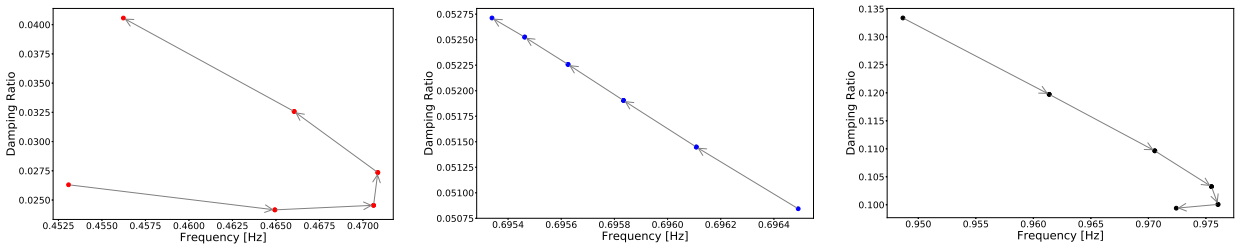

(a) 0.470 Hz mode **(b)** 0.696 Hz mode **(c)** 0.976 Hz mode

Figure 3.10: Change in modal components with change in system loading

On the other hand, if a line is disconnected, the change is more visible. From Table 3.2 the results with a loss of one of the lines between buses 8 and 9 are shown. This is one of the least drastic line outages possible, and where the system still operates within its limits. The changes

to the modal components are more significant than for the case with variable load. The most drastic change is in the 0.470 Hz mode, which has been reduced to 0.415 Hz. Inter-area modes are closely connected to the power transfer in lines between areas. A loss of line between the two areas should then result in change in the inter-area modes, thus revealing that the 0.470 Hz mode is an inter-area mode.

Table 3.2: Modes identified by PF with one line between buses 8 and 9 disconnected

Mode	Freq. [Hz]	Damp. Ratio η
1	0.415	0.017
2	0.698	0.052
3	0.992	0.111

In conclusion, it can be noted that there are many possible reasons for the modal content in the power system to change. Changes in load and line outages are just some of them. In a dynamic, ever-changing power system, this makes the modal estimation not so trivial. For analysis of ambient data, real time tracking of these changes gives an indication of power system stability.

3.3.1 Ringdown analysis

To simulate a larger fault and create a ringdown signal, the line between buses 6 and 7 is disconnected and reconnected 0.05 s later. Power flow measurements between buses 5 and 6, and buses 9 and 10, are then analyzed to identify modes.

Figure 3.11 shows the immediate system response after the fault, comparing the signal with and without variable load. Looking back at Figure 3.9, it can be noted that the ambient variations barely affect the ringdown signal in the first few seconds. The main difference between the constant and variable load plots may just be a small difference in loading, and thus a small difference in the modal content.

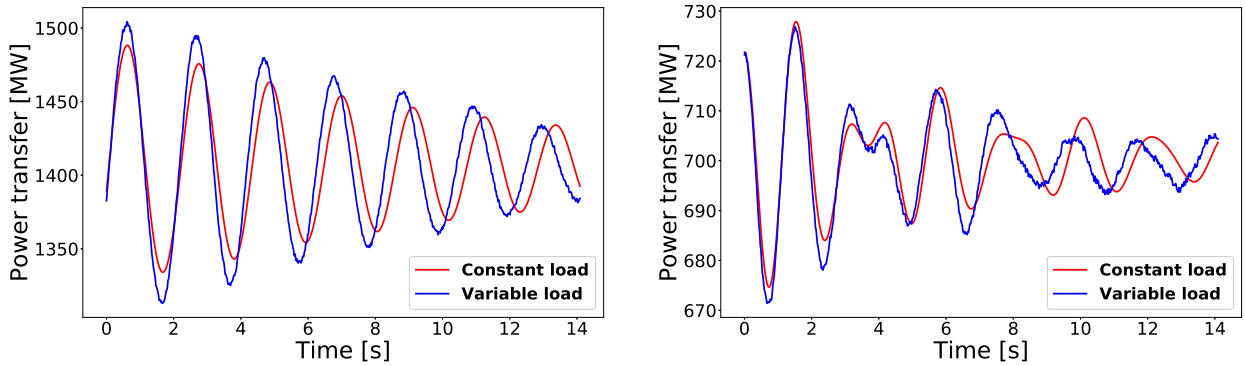

(a) Line 9-10 **(b)** Line 5-6

Figure 3.11: Comparing measured signal for same fault with and without load variation

As time passes, and the ringdown is damped out, the ambient noise becomes more present in the signal. This is clear when looking at Figure 3.11b at time after approximately eight seconds; the noise is more constant, and the signal is no longer as smooth as it was initially. Extending the signal, this trend becomes more clear as seen in Figure 3.12. Approximately 20 seconds after the fault, the signal is no longer recognizable when compared to the constant

load case. The ambient data has completely distorted the ringdown signal, with a continuous excitation of the power system, changing the signal amplitude and phase.

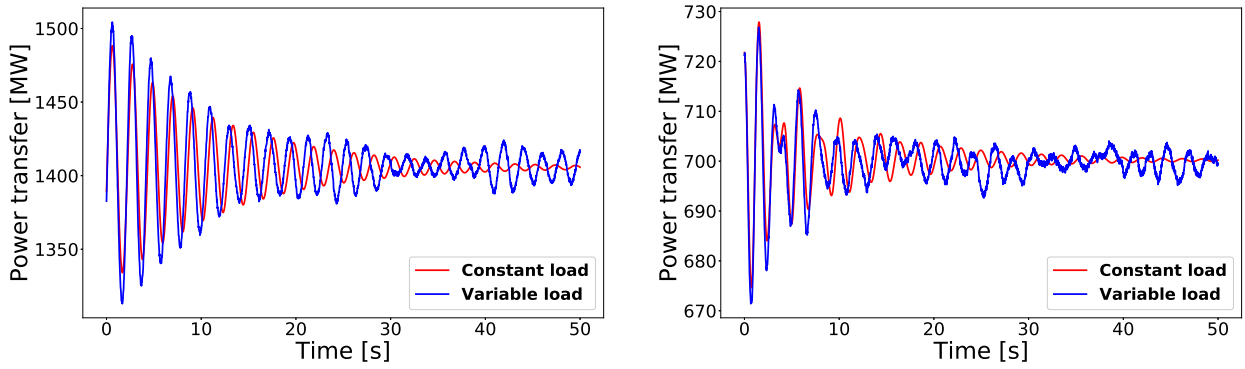

(a) Line 9-10 **(b)** Line 5-6

Figure 3.12: Comparing measured signal for same fault with and without load variation

The continuous change in the system makes the comparison of the modal estimation to the PF modes in Table 3.1 less trivial, as the modes change in each time-step. For analysis of the ringdown signal, it is clear that a short timewindow of a few seconds is needed. For analysis of the ringdown signal, the assumption is then that linear behaviour dominates this short window.

4 Testing and validation on simulated data

This section covers the testing on the Kundur Two Area model shown in section 3.3. The modal analysis tool in PF is used as a validation technique in all cases. However, this is based on a stationary and linearized version of the power system, neglecting the dynamic changes. To get a notion of how the modes vary, the modal estimation is computed at three different timesteps. The first estimation is one second prior to the fault, the next is ten seconds after the fault and the last at the very end of the measured signal.

All power system measurements in this section are from the lines between buses 5 and 6, and buses 9 and 10 in Figure 3.8. This differs from what is shown in the paper in appendix A, where the line between buses 10 and 11 is used instead of the line between buses 9 and 10. A line between buses i and j is hereby denoted simply as line i-j, where i and j are two arbitrary buses.

4.1 Case 1 - Line outage and reconnection

The first case covers the fault shown in section 3.3.1, where the line 6-7 is disconnected and reconnected within a time span of 0.05 s. Figure 4.1 shows the resulting signal, with a ringdown recorded after 600 seconds.

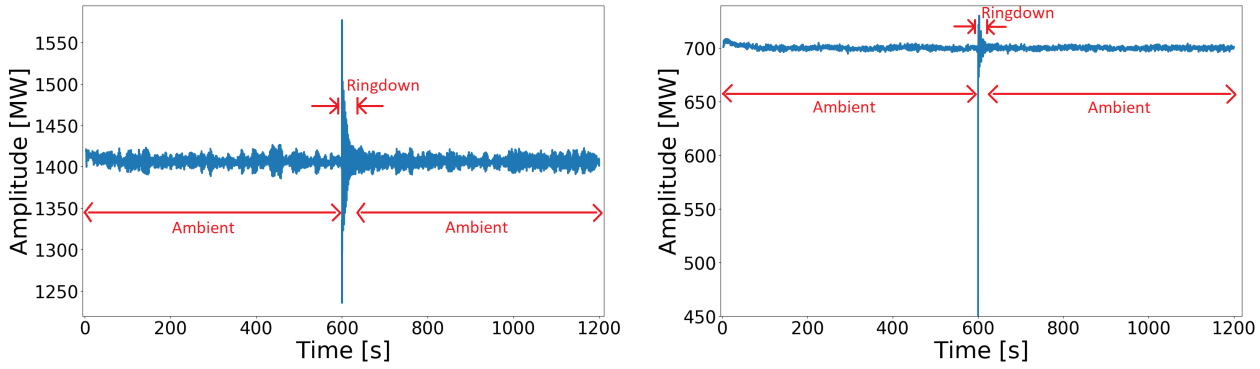

(a) Line 9-10 **(b)** Line 5-6

Figure 4.1: Simulation data from PF in case 1

4.1.1 Constant load test

To create a comparative foundation between power system changes, the results from the constant load simulation are included. The simulations are based on the constant load signal shown in Figure 3.11. As there is no ambient data in this test, the only method tested is the PA_O. The identified modal components in the constant load system are shown in Table 3.1. Without ambient data, there is no noise in the PF results. As as consequence, the EMD-filter is not tested for this signal. The first step is to remove the offset prior to Prony analysis and subsequent clustering. For this test, a timewindow of 14 seconds starting after the fault was

selected, yielding a model order range from $p = 10$ to $p = 40$. The resulting clustering for the 31 runs are shown in Figure 4.2.

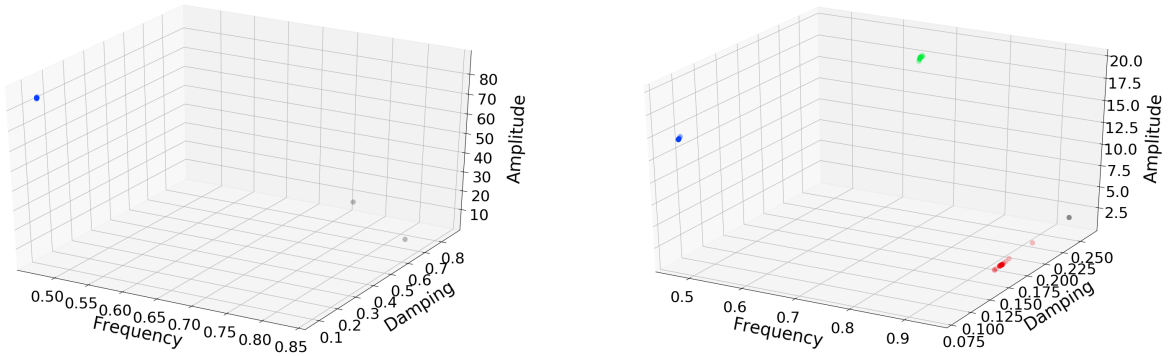

(a) Line 9-10 **(b)** Line 5-6

Figure 4.2: Cluster plot from both estimations

Clustering indicates, in addition to modes present in the system, the validity and reliability of the results through the number of occurrences in each cluster. For line 9-10, the cluster plot is shown in Figure 4.2a, where only one of the three modes from Table 3.1 is observable. With an occurrence of 31 modes in the cluster, the mode is without doubt present in the signal. Note that in the paper shown in appendix A, the measured signal in line 10-11 was used instead of line 9-10, and all three modes were successfully identified.

For line 5-6, the cluster plot in Figure 4.2b shows three different modal components. With an occurrence of 31 modes in 31 different model orders, the modal components with a frequency of 0.470 Hz and 0.696 Hz are both highly distinct. In addition, both these clusters vary little and have a large amplitude. The last cluster - with an average frequency of 0.94 Hz - has a smaller amplitude and is not as closely spaced. The number of occurrences is still 28 out of 31 possible, strongly indicating the presence of this mode in the signal. From an obervability point of view, the two modes with highest amplitude are clear and observable in the signal and thus clear in the cluster plot. The 0.94 Hz mode, are on the other hand barely observable in this line.

Table 4.1: Consistent modes for multiple model orders in constant load test

Results on line 9-10				**Results on line 5-6**			
Freq. [Hz]	η	**Amp.**	**Phase [rad]**	**Freq. [Hz]**	η	**Amp.**	**Phase [rad]**
0.470	0.028	84.65	-0.49π	0.940	0.028	1.12	0.02π
				0.470	0.028	14.60	0.59π
				0.696	0.053	19.23	0.00π

The results in Table 4.1 show that there is one distinct inter-area mode in the system. The 0.470 Hz mode oscillates between the two areas, with an approximate 180° phase shift. A comparison with the results from the component-based approach in Table 3.1, reveals an accurate match of the 0.470 Hz mode in both lines. For line 5-6, the 0.696 Hz mode marginally misses by 0.002 Hz and 0.001 on the frequency and damping ratio, respectively. However, the 0.940 Hz mode misses with 0.052 Hz. This can be a result of the low observability of this mode in the measurement compared to the other two modes.

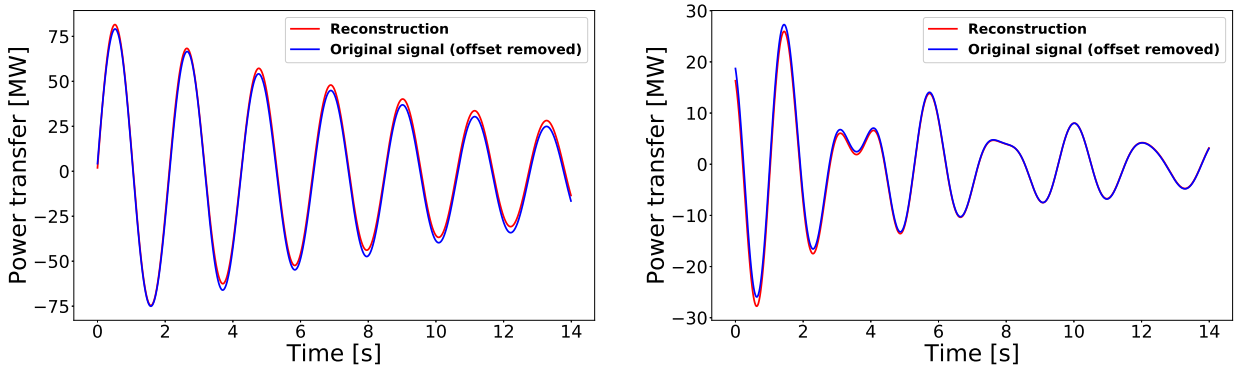

(a) Line 9-10 **(b)** Line 5-6

Figure 4.3: Comparing reconstructed signal to original signal without offset

A reconstruction of the estimated signal can be compared to the measurements if the offset is removed. This gives a good indication of estimation accuracy, as seen in Figure 4.3.

Summarized Observations

- The accuracy of the clustering technique can be measured using the number of occurrences of each mode. All but one of the identified modes occur in 31 out of 31 possible model order simulations.
- For a constant load simulation, the identified modes are clearly present with small deviation in each cluster, yielding almost perfect results.
- The fault clearly excites the inter-area mode of 0.470 Hz.
- The reconstructed oscillatory signal fits the measured signal with only small errors. The resulting signal-to-noise ratio for lines 9-10 and 5-6 are 45.1 dB and 42.9 dB, respectively.

4.1.2 Variable load - Ringdown analysis

In this section, the PA_O method is tested on the signal given in both Figure 3.11, presented as the variable load, and Figure 4.1, presented as the ringdown portion.

With a variable load, the modal content changes slightly (Table 4.2). Although a more accurate estimation of the timestep is achieved in PF, it is not representative for the entire timewindow. Thus, the modal component estimation from time-domain measurements are expected to differ slightly from the PF linearization.

Table 4.2: Modes identified by PF during ringdown in case 1

Mode	Freq. [Hz]	Damp. Ratio η
1	0.490	0.026
2	0.704	0.053
3	1.016	0.107

The first step is to filter the high-frequency noise using the EMD-filter as seen in Figure 4.4.

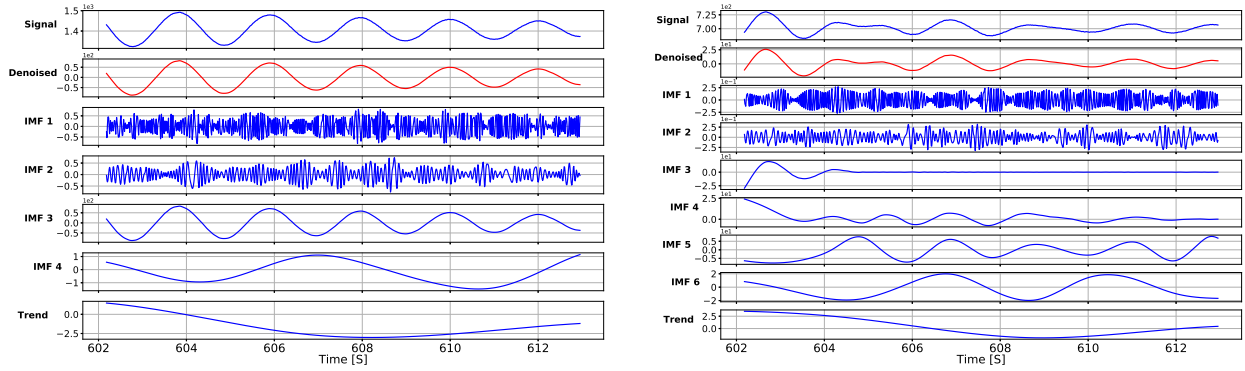

(a) Line 9-10 **(b)** Line 5-6

Figure 4.4: IMF plots from EMD-filter

By removing IMF 1 and 2 in both signals, the high frequency components are filtered out of the signal. The denoised signal in red shows the reconstructed signal without IMF 1, IMF 2 and the trend (Figure 4.4). As a result of the filtering method, the signal is significantly smoother. To deal with the known EMD-issue regarding end effects, the first and last seconds of the signal are removed.

With the first and last second of the ringdown signals removed, a reduction in the previously selected model order range is required. This process is automatic and depends on the available number of samples. The new model order range is from $p = 10$ to $p = 31$, with a maximum number of occurrences equal to 22. The resulting cluster plots are shown in Figure 4.5.

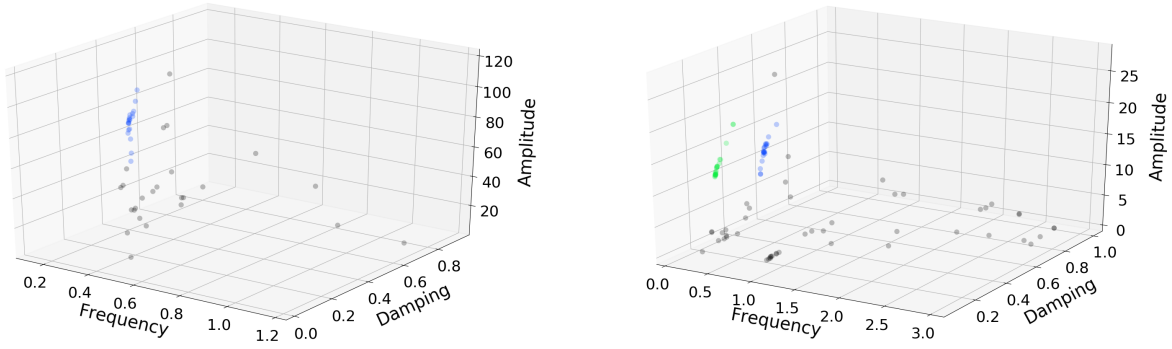

(a) Line 9-10 **(b)** Line 5-6

Figure 4.5: Cluster plot from both estimations on ringdown signal

Although the clusters in Figure 4.5 are not as closely spaced as for the constant load case in Figure 4.2, all clusters have 22 occurrences. It can be observed that there are several trivial modes present in both cluster plots, thus supporting the use of a clustering method.

Similar to the constant load case, line 9-10 has only one identified mode as seen in Figure 4.5a. For line 5-6, as seen in Figure 4.5b, only the two most observable modes from the previous case remain. This is expected, as the last mode would disappear among the ambient noise. By extracting the modal components from the cluster plot and averaging the results, modes in Table 4.3 are obtained.

Table 4.3: Consistent modes for multiple model orders in ringdown variable load test

Results on line 9-10				Results on line 5-6			
Freq. [Hz]	η	**Amp.**	**Phase [rad]**	**Freq. [Hz]**	η	**Amp.**	**Phase [rad]**
0.490	0.030	104.94	-0.65π	0.484	0.032	16.74	0.53π
				0.710	0.056	20.61	-0.16π

As expected when comparing Tables 4.3 and 4.2, the deviations are larger than for the constant load case. Regardless of this, the results give a good indication of modes present in the signal with both frequency and damping close to those identified by PF. The difference is less than the 0.470 Hz mode from section 3.3 that changed almost 0.02 Hz in frequency and 0.015 in damping with a variation in load. It can be noted that the frequency and the damping estimate in line 5-6 deviate a little more than for line 9-10. Seeing as this line is more affected by ambient variations as seen in Figure 3.12, this is as would be expected. The phase shift between the now approximately 0.49 Hz mode in the two areas is still about 180°.

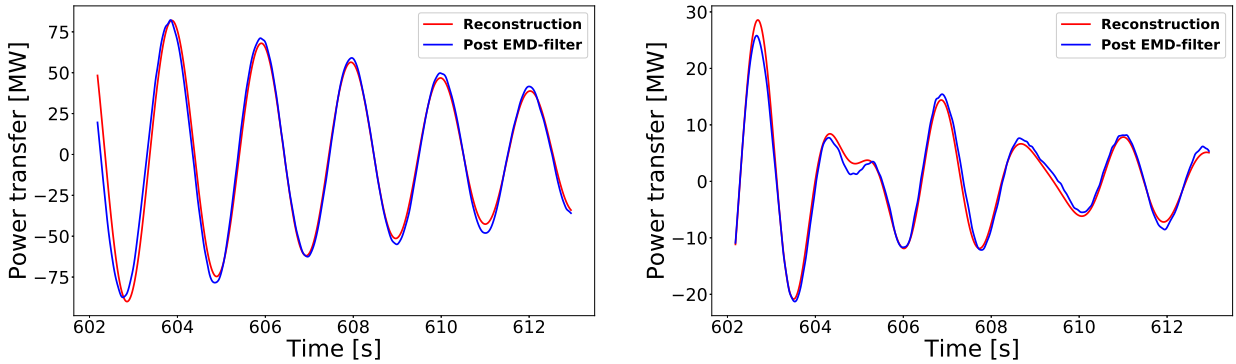

(a) Line 9-10 **(b)** Line 5-6

Figure 4.6: Comparing reconstructed signal to post EMD-filtered signal

By reconstructing the signals, taking into account the one second cut in the beginning due to EMD-filtering, the plots in Figure 4.6 are obtained. The reconstructed signal is compared to the post EMD-filtered signal. The estimation for line 9-10 post-filtered measurements in Figure 4.6a is good, even though ambient noise is included. The deviation in damping is barely noticeable, and the reconstructed signal has a signal-to-noise ratio of 31.8 dB with most of the error located early in the estimation. Line 5-6, as seen in Figure 4.6b, gives an approximation error slightly smaller than that in line 9-10. The estimated modal components are still dominating the signal, with a signal-to-noise ratio of the reconstructed signal equal to 34.6 dB.

Summarized Observations

- All the identified modal clusters contain 22 modes out of 22 possible.
- The clusters are distinct even though the conditions are noisy, supporting the hypothesis of only small variations in true modes.
- Signal reconstruction substantiates the clustered result from PA_O.

4.1.3 Variable load - Ambient analysis prior to ringdown

The next step is to analyze the ambient data prior to the ringdown. The analysis is based on the first 600 seconds shown in Figure 4.1, using the RRLS method discussed in section 3.2. The rationale is that there is continuous excitation of modes in the system due to ambient changes, making it possible to detect them. Figure 4.7 illustrates 35 seconds of ambient data from the two lines investigated.

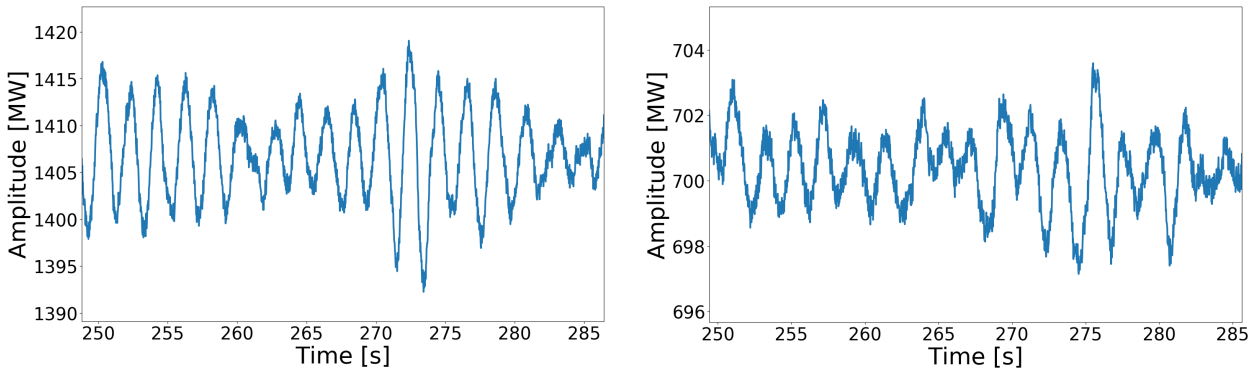

(a) Line 9-10 **(b)** Line 5-6

Figure 4.7: Part of the ambient data analyzed

It can be seen that the measurement in line 9-10 has a clear trend with small frequency variations (Figure 4.7). The measurement in line line 5-6 is not as distinct, with lower power transfer, and higher frequency and amplitude fluctuations.

Using the modal identification tool PF, modal content shown in Table 4.4 is identified one second prior to the ringdown.

Table 4.4: Modes identified by PF in ambient data prior to ringdown in case 1

Mode	Freq. [Hz]	Damp. Ratio η
1	0.485	0.025
2	0.702	0.053
3	1.009	0.110

Before modal estimation can begin, the signal must be pre-filtered as shown in Figure 4.8 and 4.9.

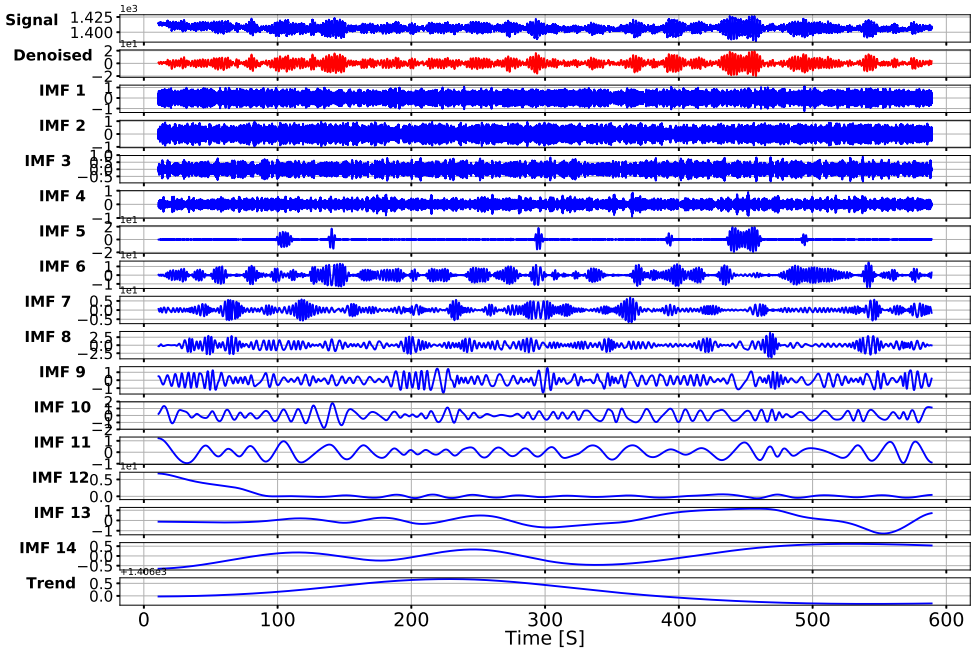

Figure 4.8: IMF plots from EMD-filter in line 9-10

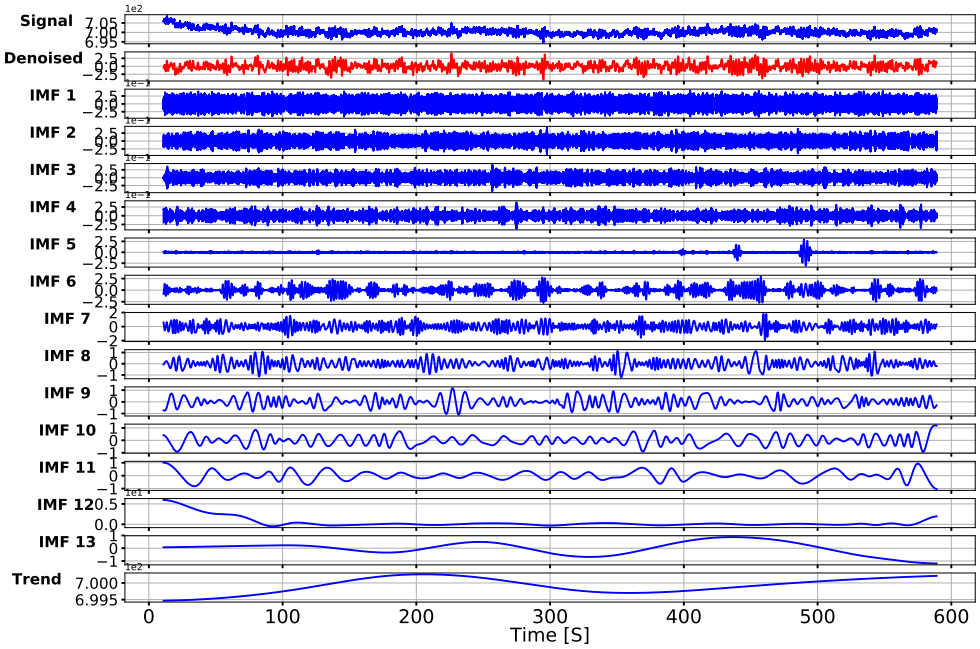

Figure 4.9: IMF plots from EMD-filter in line 5-6

Using the EMD-method, the ambient input signal is band-pass filtered, removing all IMFs with a frequency above the electro-mechanical range in addition to all IMFs with a distinct frequency less than 0.01 Hz. For both measured signals shown in Figures 4.8 and 4.9, IMF 5 through 9 were used in the denoised signal.

Feeding the described method with the filtered signal as a stream of data, clustering is done in each timestep. As an illustration, a cluster plot after convergence is shown in Figure 4.10.

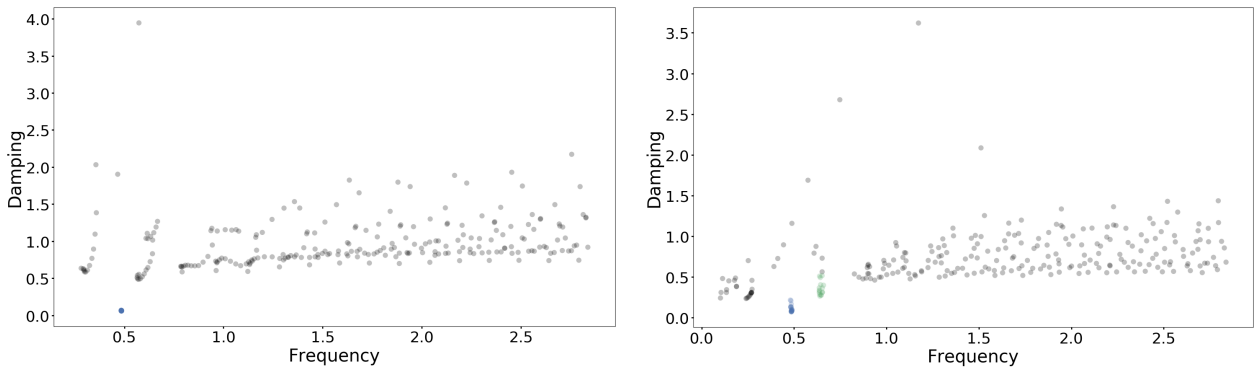

(a) Line 9-10 **(b)** Line 5-6

Figure 4.10: Cluster plot from both estimations in ambient signal

Both line measurements result in a low damped mode cluster with a frequency just below 0.5 Hz. Figure 4.10b shows, in addition to 0.5 Hz mode, a cluster that is not as compact with a modal frequency of approximately 0.6 Hz. With a lower density, higher damping and closer proximity to the remaining noise, this mode can be weighed less in the tracking of critical modes.

Extracting the identified modal components in each timestep, the automated modal tracking shown in Figure 4.11 is obtained.

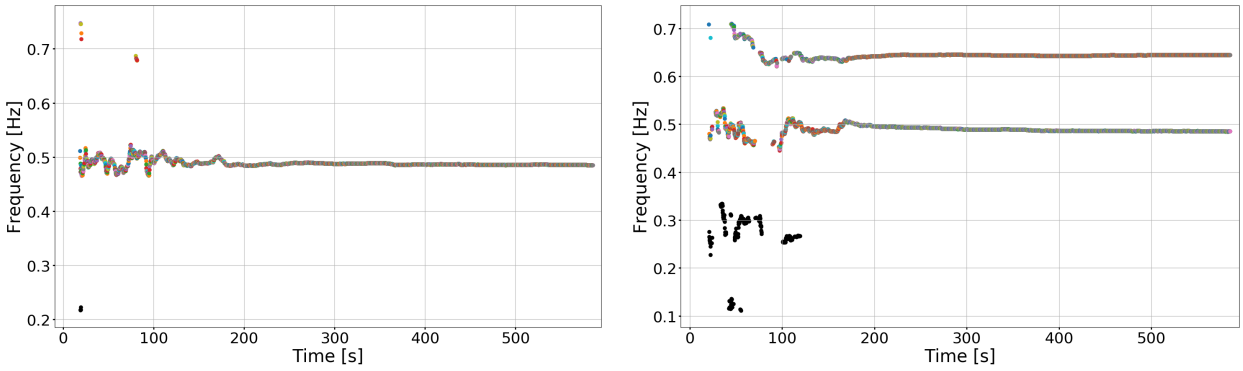

(a) Line 9-10 **(b)** Line 5-6

Figure 4.11: Mode-tracking of identified modes

Remembering that this is a Newton-Raphson-type method, it can be seen that the first 180 seconds are spent before convergence is reached. This period is defined with a high variance in the resulting frequencies along with outliers that are not present for a longer period of time. The extracted modal information at the end of estimation is shown in Table 4.5.

Table 4.5: Modal information at end of ambient data prior to fault

Results on line 9-10		**Results on line 5-6**	
Freq. [Hz]	η	**Freq. [Hz]**	η
0.485	0.02	0.485	0.035
		0.645	0.085

Comparing Tables 4.5 and 4.4 shows that estimates from both lines identify the exact frequency of the 0.485 Hz mode. For the damping ratio, line 9-10 underestimates it by 0.005, while line

5-6 estimates it to be 0.01 above its actual value. In line 5-6, an additional mode is found. This mode is closest to the 0.7 Hz mode, with some deviation in both frequency and damping. As this is not as distinct as the 0.485 Hz mode in the cluster plot and that the damping ratio is above 5 %, the 0.7 Hz mode is not pursued further. The variation in frequency and damping of the 0.485 Hz mode on both lines can be seen in Figures 4.12 and 4.13, respectively.

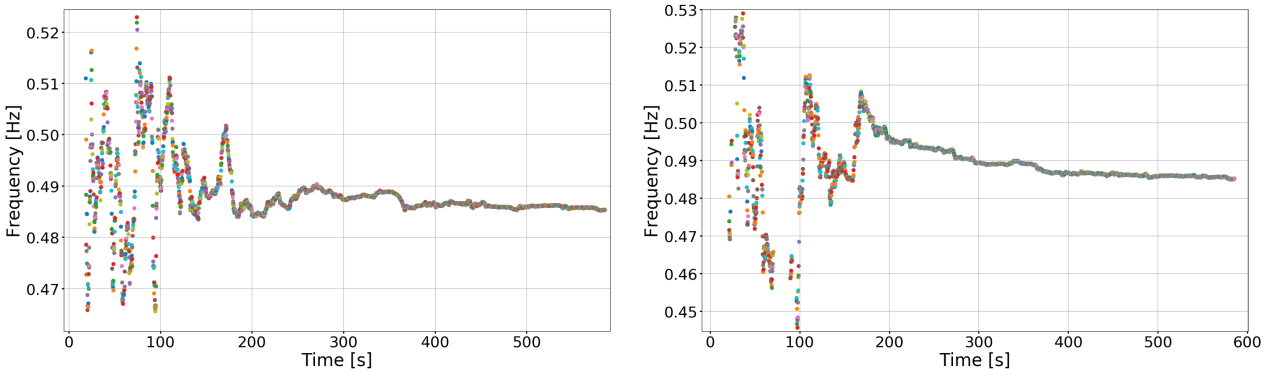

(a) Line 9-10 **(b)** Line 5-6

Figure 4.12: Mode-tracking of most critical mode

After the first 180 seconds of tuning, the forgetting factor is increased to 0.999. This decreases the variation in the estimation, and the next 200 seconds are spent with slow variations until a more constant mode is found after about 400 seconds.

It can be noted that for mode-tracking in Figure 4.13, the damping ratio is used instead of damping as shown in Figure 4.10.

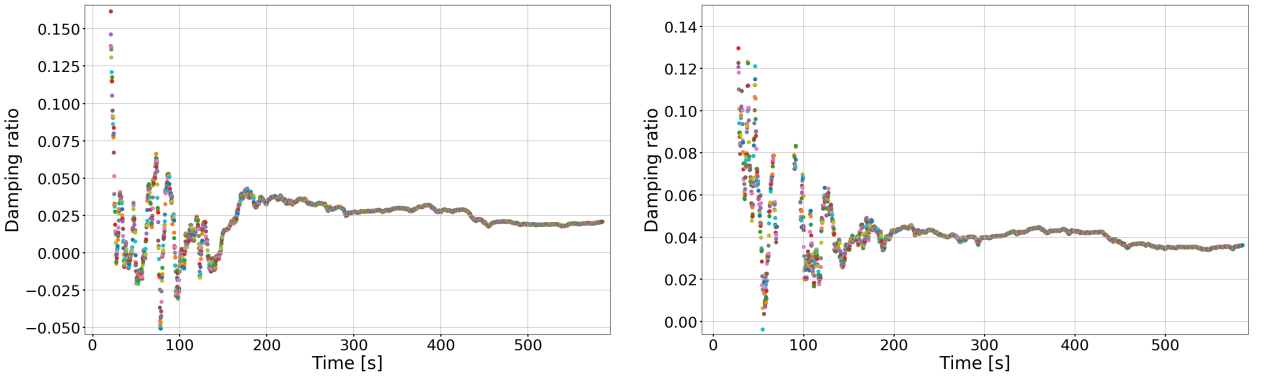

(a) Line 9-10 **(b)** Line 5-6

Figure 4.13: Mode-tracking of damping ratio for mode in Figure 4.12

As seen in Figure 4.13, the damping ratio is estimated differently in the two lines. It can however be seen that the development of each estimation shows the same tendencies, both having the same decrease in damping ratio at about 450 seconds.

As a way of verification, the ambient data is used as input to the non-parametric Welch's method. Filtering and down-sampling the data to 6 Hz before applying the method gives the detailed spectrum of low-frequency oscillation in Figure 4.14.

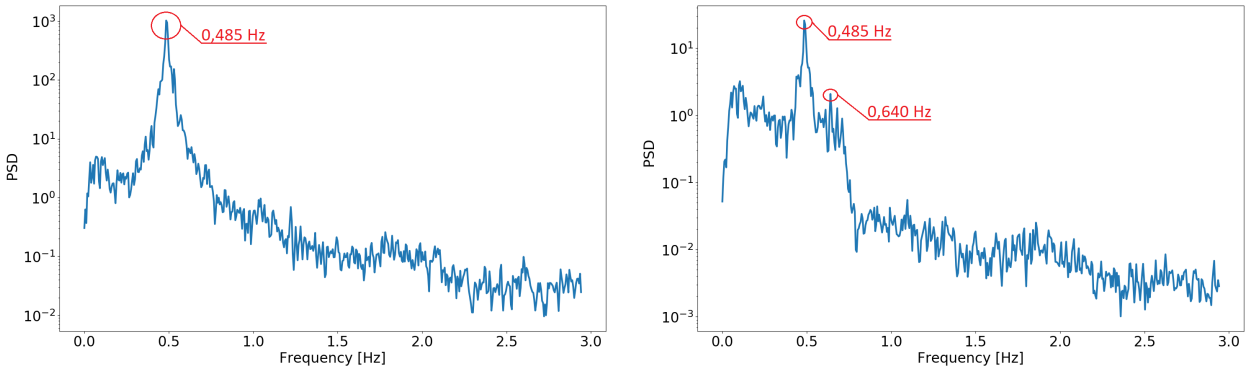

(a) Line 9-10 **(b)** Line 5-6

Figure 4.14: Welch's power spectrum of measured signal

Both lines give a clear peak of the spectral density around the 0.485 Hz mode. Line 5-6 gives some additional peaks in the area of the 0.64 Hz mode, though it is not as clear as the 0.485 Hz mode. Using 50 Hz data as input, the same conclusion is achieved.

Summarized Observations

- RRLS requires a long timewindow of data to converge when cold start is applied. To shorten this window, an initially lower forgetting factor is required. This should be increased to avoid large variations in the result.
- Clustering in an arbitrary timestep after convergence is met, shows a clear differentiation of the identified modes compared to the remaining noise.
- The mode-tracking method gives an accurate estimation of frequency compared to PF results, while there are some deviations in the damping.
- A comparison between identified modal components using RRLS and Welch's power spectrum verifies the presence of the 0.485 Hz mode.

4.1.4 Variable load - Ambient analysis after ringdown

In this case, the power system is of similar character before and after the fault. As no changes have occurred in the physical system, the identified modal components post and prior to the fault should ideally be the same. Using PF, modal components at the end of the measured signal in Figure 4.1 were identified as shown in Table 4.6.

Table 4.6: Modes identified by PF in ambient data after ringdown in case 1

Mode	Freq. [Hz]	Damp. Ratio η
1	0.486	0.025
2	0.702	0.053
3	1.010	0.109

The modes in Table 4.6 deviates only slightly from Table 4.4. The small changes originate from a different set point in the variable loads. The analysis is based on the ambient data after the ringdown as shown in Figure 4.1.

When initializing the RRLS method, one possible option is to base the starting guess on the last estimation prior to the fault. This is not always a good option, as the modal content might have changed during the fault. Applying the method using cold start, the mode-tracking results shown in Figure 4.15 were obtained.

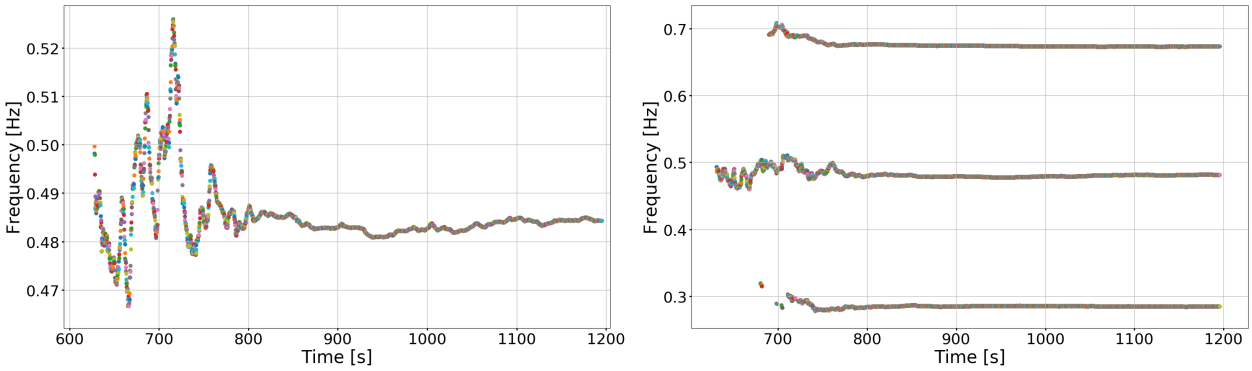

(a) Line 9-10 **(b)** Line 5-6

Figure 4.15: Mode-tracking of identified modes

Line 9-10 estimations yield, similar to the results prior to the fault, just one mode at the approximate frequency of 0.48 Hz. Line 5-6 estimations in Figure 4.15b yields, in addition to the estimated 0.48 Hz and 0.67 Hz modes found prior to the ringdown, a mode with a frequency of approximately 0.28 Hz. Note that the same mode is present initially in the mode-tracking shown in Figure 4.11b.

As the results from line 5-6 are s inconclusive, the cluster results and frequency variation of the mode believed to be the most dominant are shown in Figure 4.16.

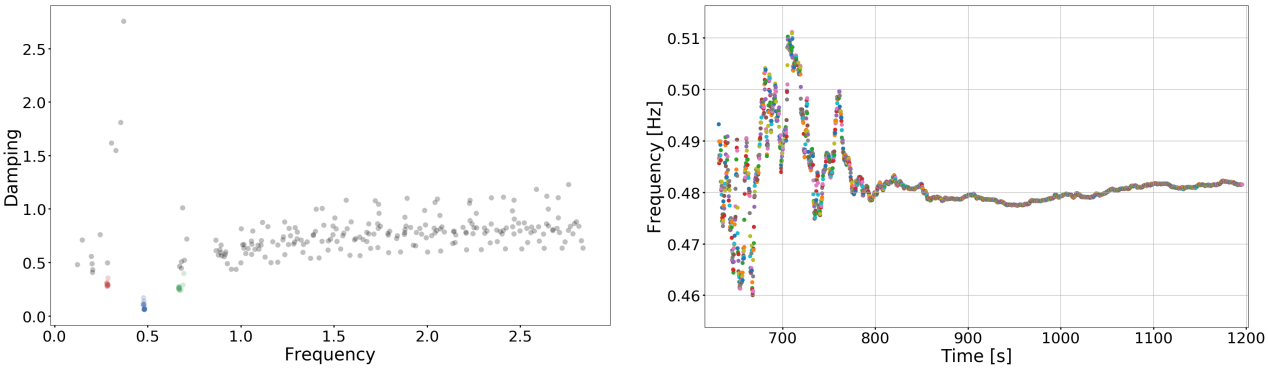

(a) Cluster plot from last timestep **(b)** Enlarging the 0.48 Hz mode

Figure 4.16: Mode estimation results from line 5-6

Looking closer at the clustering results shown from line 5-6, it can be seen that all clusters are closely spaced for the converged case in Figure 4.16a; however, the consistency differs between them. The cluster connected to the inter-area mode at 0.48 Hz contains 20 modes out of the 20 possible model orders tested. The 0.67 Hz and 0.28 Hz clusters contain only 14 and 12 modes respectively, making them less consistent and thus less reliable. This may explain why the 0.28 Hz mode was not identified prior to the ringdown.

To get a better perspective when tracking the 0.48 Hz mode in line 5-6, the results are enlarged as shown in Figure 4.16b. Comparing this with the similar results of the same mode in Figure

4.15a, the same trend can be observed. After initial variations, the frequency gradually decreases in the time period from 800 to 900 seconds, before increasing slightly towards the end of the measurements. A study of these tendencies may give insight into changes in the power system load/generator variations.

The time varying damping ratio for the approximately 0.48 Hz mode is shown in Figure 4.17. It can be observed that similar to previous tests, the damping ratio estimate is consistently smaller in line 9-10 than in line 5-6.

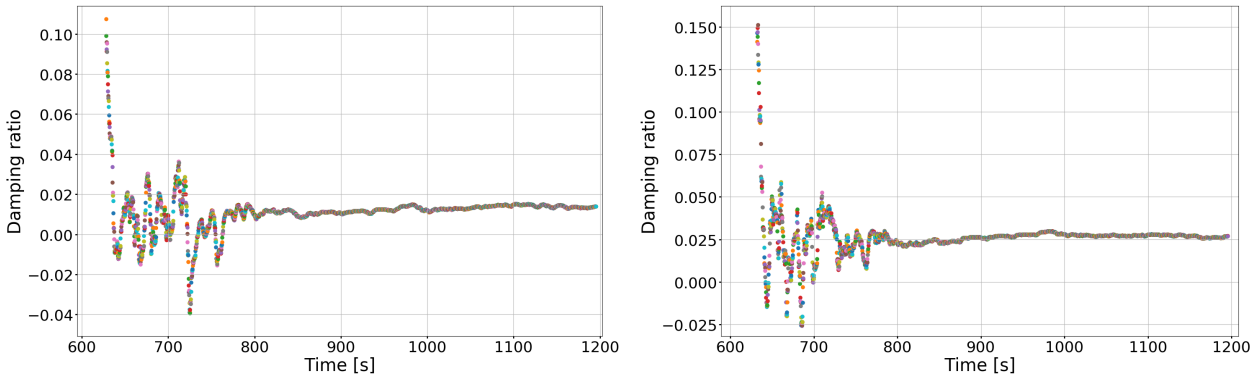

(a) Line 9-10 **(b)** Line 5-6

Figure 4.17: Mode-tracking of damping on modes in Figure 4.15a and 4.16b

The end result of mode-tracking in each line is shown in Table 4.7. Looking at the damping ratio, it is clear that the only critical mode is the 0.48 Hz. The last two modes in line 5-6 has a damping ratio above the minimum. Especially the 0.285 Hz mode, which has a damping ratio of more than 16 %. This mode is of special interest, since it was not discovered by PF and not found in the ringdown, raising question of the validity of the method used.

Table 4.7: Modal information at end of ambient data post fault

Results on line 9-10		**Results on line 5-6**	
Freq. [Hz]	η	**Freq. [Hz]**	η
0.484	0.014	0.482	0.027
		0.673	0.063
		0.285	0.162

To evaluate the results, the EMD-filtered and downsampled signal is analyzed using Welch's method. The resulting power spectrum is shown in Figure 4.18. Both lines gives a clear peak at 0.484 Hz. From Figure 4.18b it can be seen that line 5-6 has additional elevations in power for 0.3 Hz and 0.68 Hz together with some other small peaks in power density. As the identified modes in line 5-6 have frequencies identified by Welch's method, it can be concluded that the potential error is not caused by the RRLS method.

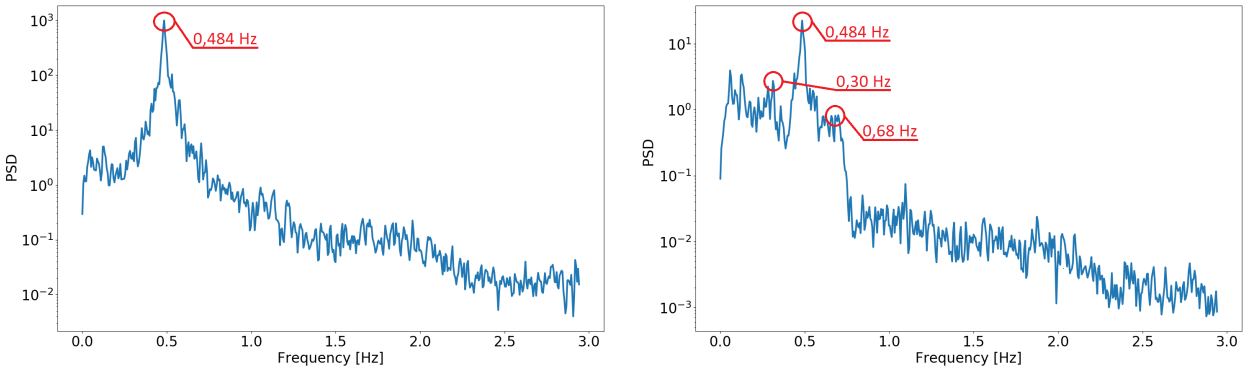

(a) Line 9-10 **(b)** Line 5-6

Figure 4.18: Welch's power spectrum of measured signal

Since the estimate of the filtered signal matches the result from Welch's method, the next source of error might be the filtering method creating additional modes. Knowing that the EMD-method has its challenges, the post-filter power spectrum of line 5-6 can be compared to the power spectrum estimated directly from the 50 Hz measurement. The spectrum shown in Figure 4.19 is the pre-filtered power spectrum, where the electro-mechanical frequency range is in focus.

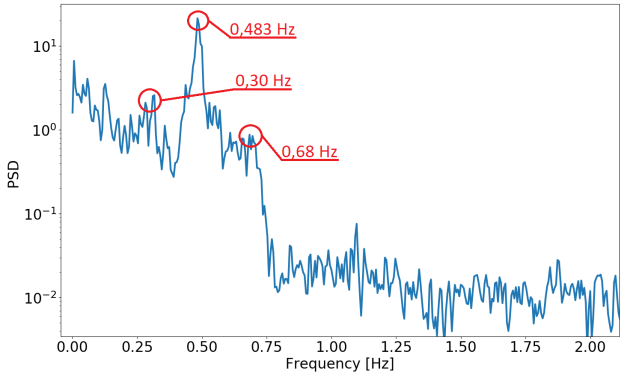

Figure 4.19: Welch's power spectrum of measured signal in line 5-6 prior to EMD-filtering

Apart from a small change of 0.001 Hz in the mode estimated to 0.484 Hz, it can be observed that there is a clear change in power spectrum density for frequencies closer to zero in the post-filtered spectrum. This shows that the EMD successfully removes low-frequency oscillations. As the pre-filtered Welch spectrum identifies the same frequencies, they appear to be present in the measured signal, thus supporting the presence of the identified modes.

Summarized Observations

- Analysis of the measurements on line 5-6 reveals an additional mode, not identified by PF. This is however a mode that is only present in 12 out of 20 different model orders, in addition to a high damping ratio of 16 %.
- The estimation of the most critical mode at approximately 0.48 Hz shows only small deviation in frequency, while damping is lower than PF in line 9-10 and a little higher than PF in line 5-6. This is consistent with the estimate prior to the ringdown.

- The power spectrum is used to validate the frequency estimation, revealing that the EMD-filtering and down-sampling left frequency in the electro-mechanical range unchanged. In addition, the effect of high-pass filtering using EMD is noticeable in the spectrum.

Case 1 summary

From theory, it is clear that both ambient and ringdown analysis methods investigated in this thesis are based on the same principles of a general difference equation and linear prediction model. Although their principles are similar, the area of application differs, yet both arrive at the same conclusion. The frequency estimation of the most critically low-damped mode (the 0.49 Hz mode), is close to perfect in all cases of ambient and ringdown analyses. The small differences may simply be a result of load variations, changing the modal components slightly.

The estimation in damping does however differs a bit more. For the ringdown analysis, estimation in both lines results in a close but slightly overestimated damping. For ambient analysis, the damping results are not as conclusive, with a trend showing that the damping is underestimated in line 9-10 and overestimated in line 5-6. However, both arrive at the same conclusion; the mode damping is below the critical limit, similar to the result of the ringdown analysis. The other two modes found in line 5-6 are not accurately estimated, with neither frequency nor damping matching PF results.

With each cluster identifying a modal component, its presence and clarity in the signal is indicated by the number of modal occurrences. A densely spaced cluster, composed of modes from each investigated model order, indicates the clear presence of a linear mode. A more spacious cluster consisting of slightly varying modes, with a number of occurrences below that of the range investigated, indicates a multitude of possibilities; either the mode is barely present in the signal, an error has occurred during filtering, the selected time-window captures non-linear parts of the signal, or the sampling frequency selected is not appropriate.

It can be argued that clusters not containing modes from all model orders are to be neglected. However, in doing so, valuable information on system behaviour in the presence of noise is discarded. Even though the identified modes are not present in all cases, they still provide information on power system behaviour and indicate quality of the measured signal.

For this case, it can be concluded that analysis of both ambient and ringdown data gives a good indication of the most critical mode in the system, while remaining modes are difficult to separate in ambient data. Ringdown analysis does however give a clearer signal, and the resulting frequency and damping estimation is in general better for all modal components.

4.2 Case 2 - Line outage and disconnection

The second case is from a test with an outage of one of the two lines between buses 8 and 9 in Figure 3.8. This case will be presented in a similar manner as case 1. The acquired measurements, including a fault after 600 seconds, are shown in Figure 4.20.

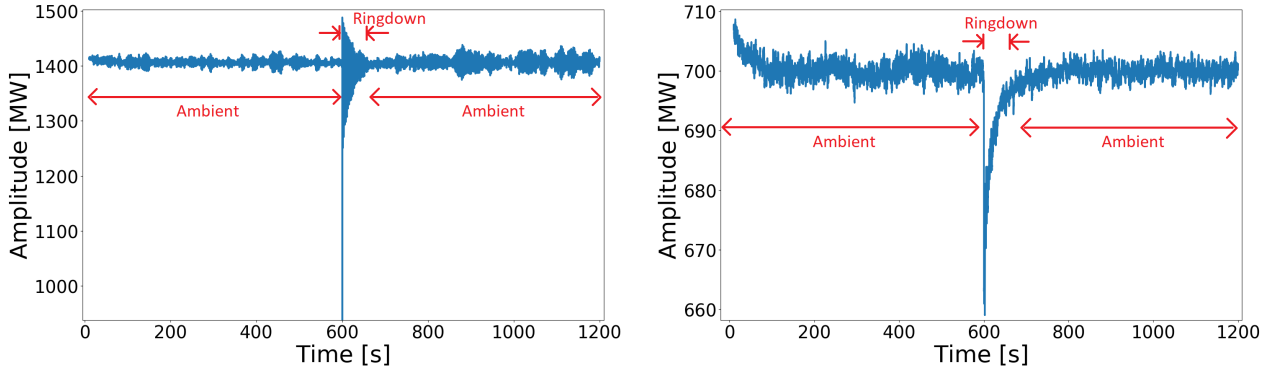

(a) Line 9-10 **(b)** Line 5-6

Figure 4.20: Simulation data from PF in case 2

From the measurement on line 5-6 shown in Figure 4.20b, it can be noted that the power transfer drops drastically at the moment of fault. Subsequently, the power transfer recovers gradually to the initial value prior to the fault. For line 9-10 in Figure 4.20a, the oscillations occur around the original operating point, which means the signal contains little low-frequency variation.

4.2.1 Variable load - Ringdown analysis

The identified modes during ringdown in the variable load test are shown in Table 4.8, where a large drop in frequency of the inter-are mode can be observed when compared to the previous case shown in Table 4.2.

Table 4.8: Modes identified by PF during ringdown in case 2

Mode	Freq. [Hz]	Damp. Ratio η
1	0.421	0.020
2	0.702	0.053
3	0.998	0.107

Figures 4.21 and 4.22 show the EMD-filtering of the ringdown signal.

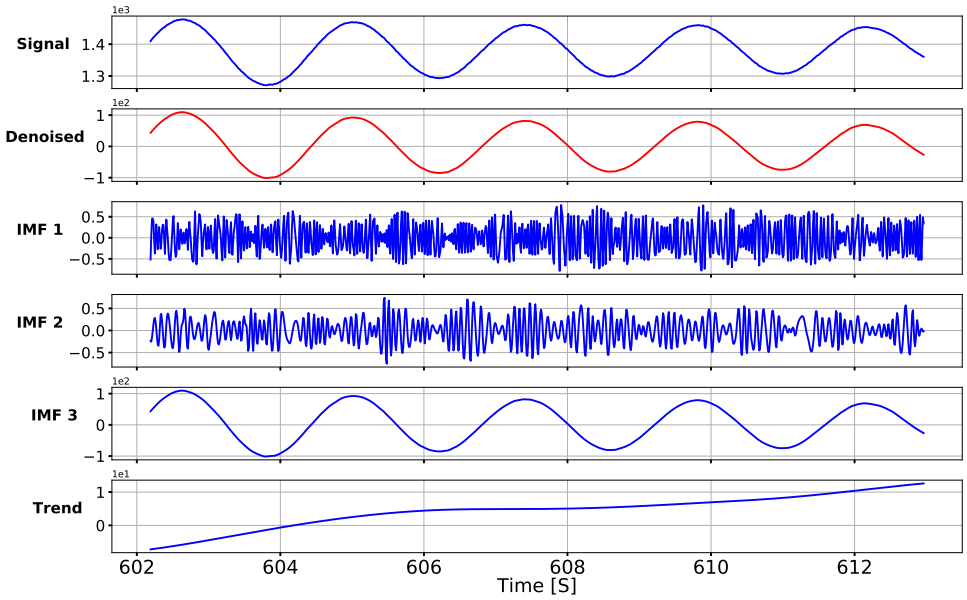

Figure 4.21: IMF plots from EMD-filter results on line 9-10

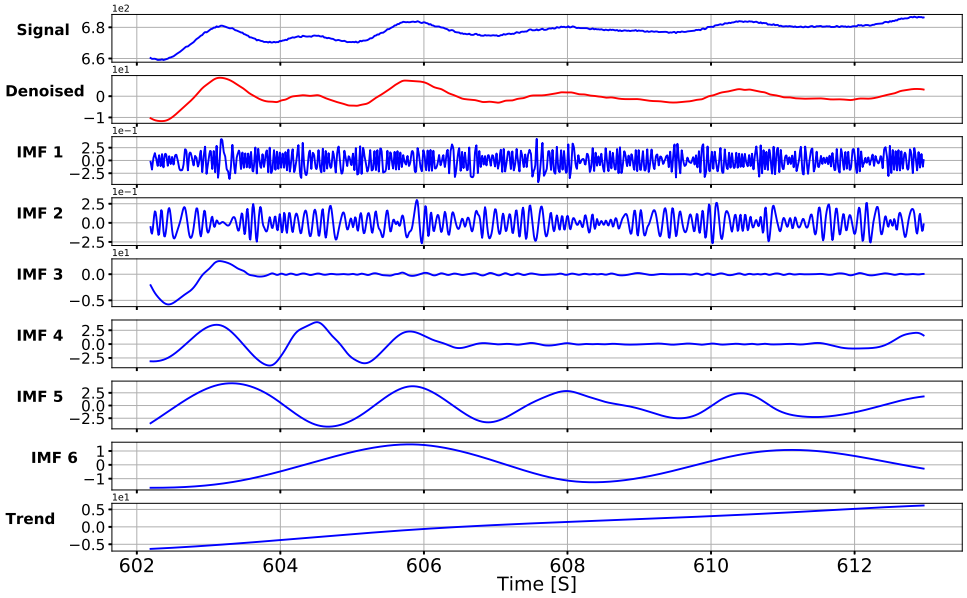

Figure 4.22: IMF plots from EMD-filter results on line 5-6

It can be noted that the EMD struggles slightly with the measurements from line 5-6 as shown in Figure 4.22. Due to the increasing power transfer, the magnitudes of oscillation and thus extrema in the signal are distorted. This makes the IMF-decomposition not as clear. Although combining IMF 3 through 6 gives results in a denoised signal without the trend, it has no clear linear tendencies needed for analysis. As seen in Figure 4.21, the signal has clear and distinct oscillations. Applying PA_O on the resulting signal illustrates the problems with the increasing power transfer during ringdown as seen from the clustering results in Figure 4.23.

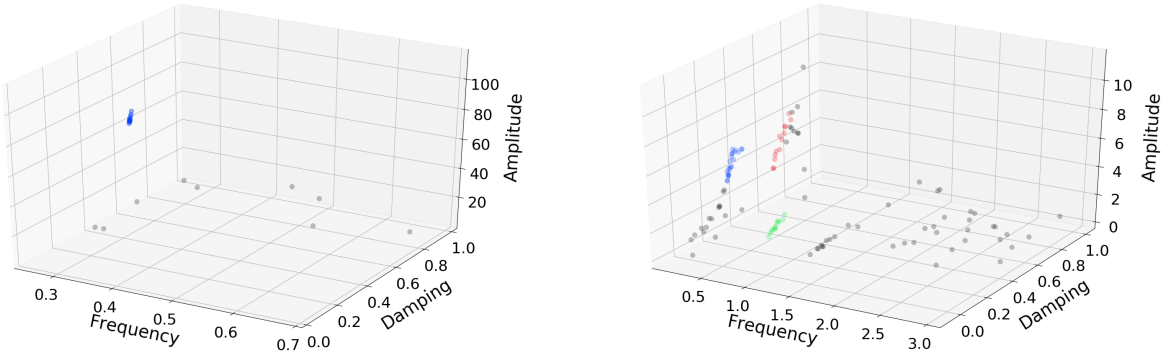

(a) Line 9-10 **(b)** Line 5-6

Figure 4.23: Cluster plot from both estimations on ringdown signal

As seen in Figure 4.23, the estimation in line 9-10 with its clear oscillatory tendencies is without a doubt conclusive. There is one mode in this signal with one dense cluster giving an average frequency of 0.418 Hz. Similarly to case 1, the cluster contains 22 out of 22 possible modes. The estimate in line 5-6 is not as conclusive with its three identified modal components, where the corresponding clusters are without a clear center. The number of modal components in each cluster is 22, 13 and 11 out of 22 for the 0.422 Hz, 0.678 Hz and 0.840 Hz, respectively. The extracted modal information of each cluster is shown in Table 4.9.

Table 4.9: Consistent modes for multiple model orders in ringdown variable load test

Results on line 9-10				**Results on line 5-6**			
Freq. [Hz]	η	**Amp.**	**Phase [rad]**	**Freq. [Hz]**	η	**Amp.**	**Phase [rad]**
0.418	0.017	112.14	-1.21π	0.840	0.032	2.15	-1.51π
				0.422	0.052	6.85	-0.19π
				0.678	0.076	9.37	-0.48π

When comparing the results in Table 4.9 to the PF estimation in Table 4.8, it is clear that line 9-10 gives a good approximation of the inter-area mode. One of the modes identified in line 5-6 has a frequency of 0.840 Hz and a damping ratio below the critical limit. Even though this mode is only present in 11 out of 22 model order estimations and has a low amplitude, it should still be considered, the problem being that it is not identified by PF. In addition to this, the damping ratio of inter-area mode is estimated well above its actual value. Lastly, it is observed that changing the timewindow of analysis has a great impact on the 0.678 Hz and 0.840 Hz modes. The 0.422 Hz mode remains clear in all tests, although still with a damping ratio estimated at approximately 5 %. The reconstructed signals are shown in Figure 4.24.

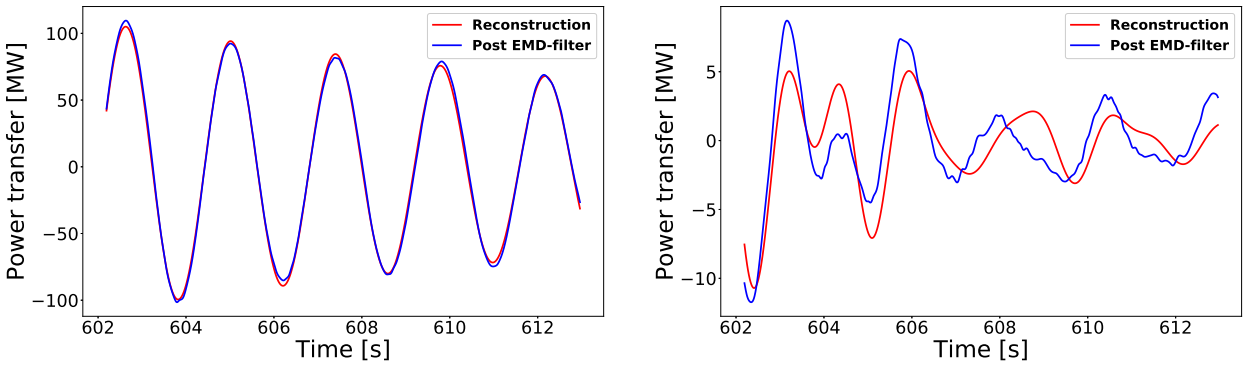

(a) Line 9-10 **(b)** Line 5-6

Figure 4.24: Comparing reconstructed signal to post EMD-filtered signal

Reconstructing the signal proves the estimation error in line 5-6, where the signal-to-noise ratio of the reconstructed signal compared with the post EMD-filtered signal is only 9.5 dB. The reconstructed signal in line 9-10 has a signal-to-noise ratio of 54.2 dB.

Summarized Observations

- Estimation of ringdown signals during an increase in power transfer yields bad approximations compared to estimations of oscillations around an operating point.
- Accuracy of estimation of ringdown signals is dependent on where in the system the measurements originate.

4.2.2 Variable load - Ambient analysis prior to ringdown

When analyzing the same ambient data for the first 600 seconds of the signal in Figure 4.20, the result is similar to that shown in section 4.1.3. These details will thus not be repeated for case 2.

4.2.3 Variable load - Ambient analysis after ringdown

The next step in testing the method is to check whether or not the ambient data after the line outage contains the same modal information as in the ringdown. Ambient data after the fault seen in Figure 4.20 is used as a basis to test the RRLS method. The resulting estimation is then compared to the identified modal components shown in Table 4.10. It can be seen that the frequency of the inter-area mode has dropped further after the ringdown to 0.414 Hz in addition to its damping decreasing to 1.7 %.

Table 4.10: Modes identified by PF in ambient data after ringdown in case 2

Mode	Freq. [Hz]	Damp. Ratio η
1	0.414	0.017
2	0.697	0.052
3	0.988	0.111

The results of the RRLS method can be seen in Figure 4.25.

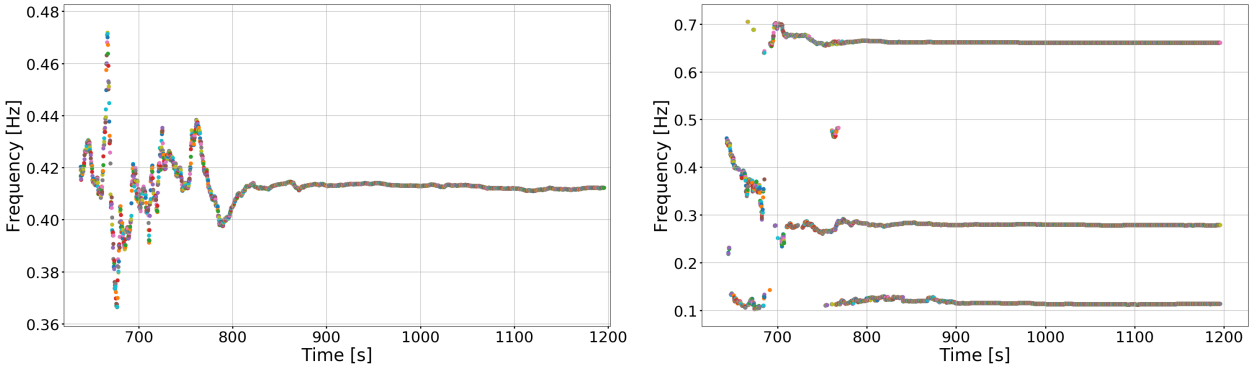

(a) Line 9-10 **(b)** Line 5-6

Figure 4.25: Mode-tracking of identified modes

Analysis of measurements in line 9-10 reveals only one mode, with a frequency after convergence of 0.412 Hz. This is close to the 0.414 Hz mode that is given by PF, where the difference can be explained simply by the fact that PF results are for a steady-state version of the dynamic system.

The results for line 5-6 differ from what is expected. The previously known inter-area mode at the frequency (from PF) of 0.414 Hz is not present. Instead, three modes are found at the frequency of 0.66 Hz, 0.28 Hz and 0.12 Hz. The results of clustering indicates that this result is not to be trusted completely. The 0.66 Hz mode is found in all of the 20 possible model orders. The last two modes of 0.28 Hz and 0.12 Hz are on the other hand barely identified in 12 and 14 instances, respectively.

Extracting the damping ratio of the 0.412 Hz mode in line 9-10 and the 0.66 Hz mode in line 5-6 gives the relation in Figure 4.26. It can be seen that the damping of both modes converge, although only the 0.412 Hz mode in line 9-10 is critically damped.

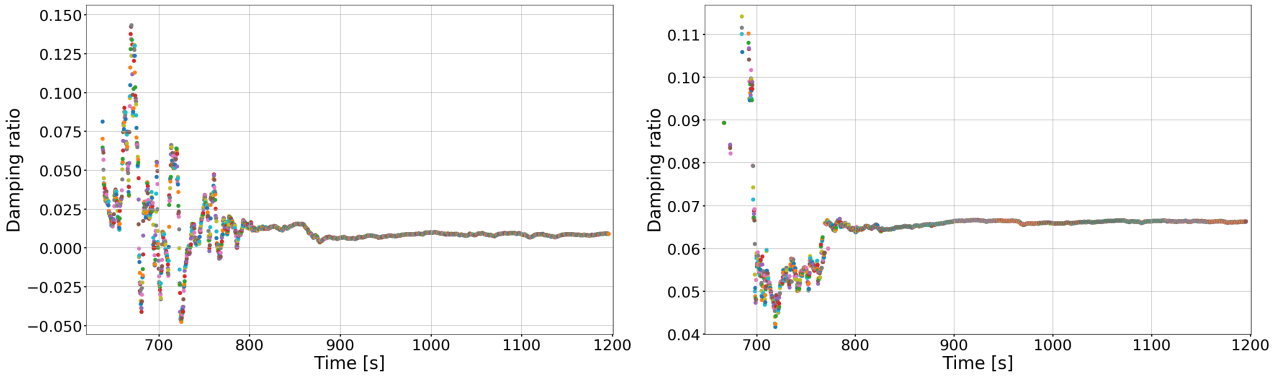

(a) 0.412 Hz mode in line 9-10 **(b)** 0.66 Hz mode in line 5-6

Figure 4.26: Damping of modes in Figure 4.25

Table 4.11 shows the estimated modal content in each signal. It can be observed that only the 0.412 Hz is critically damped and should be carefully monitored. All the modes in line 5-6 have a damping above the critical limit. What should be kept in mind is whether or not this result can be trusted. It is observed that this line is noisy, with no clear modal components that could be seen by visual inspection.

Table 4.11: Modal information at end of ambient data post fault

Results on line 9-10		Results on line 5-6	
Freq. [Hz]	η	Freq. [Hz]	η
0.412	0.009	0.66	0.067
		0.28	0.19
		0.12	0.225

To investigate the validity of the results, the signal is analyzed using Welch's method as seen in Figure 4.27. The post-filtered signal for line 9-10 give one distinct mode at 0.412 Hz, supporting the frequency found by the RRLS method. The spectrum shown in Figure 4.27 does however not indicate any clear modal components. To verify if this is a result of poor filtering, the spectrum is found for the 50 Hz pre-filtered signal as seen in Figure 4.28. Apart from the low-frequency components below 0.1 Hz, the spectrum arrives at the same conclusion that there are no clear frequencies in this signal.

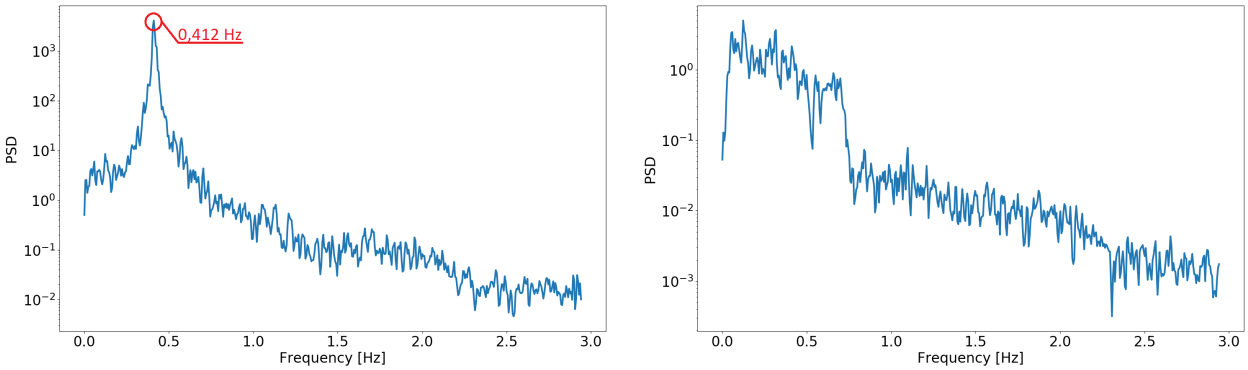

(a) Line 9-10 **(b)** Line 5-6

Figure 4.27: Welch power spectrum of measured signal

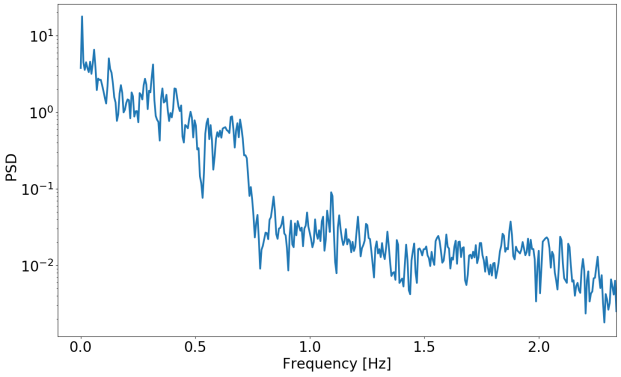

Figure 4.28: Welch power spectrum of measured signal in line 5-6 prior to EMD-filtering

Summarized Observations

- The quality of estimation is dependent of the quality of the signal which, in turn depends on where the measurement origins in the power system.
- Line 9-10 has distinct oscillatory tendencies that can easily be identified, while line 5-6 does not.

Case 2 summary

By comparing the results in line 9-10, it can be seen that the modal content changes after the fault. This results in the modal identification in ringdown analysis matching the results of ambient analysis after the fault. The ambient analysis prior to the fault does however not match, as the system topology has changed. The damping ratio in the ringdown is closer to the actual value, while the ambient analysis tends to underestimate it.

For line 5-6, it is concluded that the measurements are not good for estimation. With a signal without any distinct linear tendencies, the methods used struggle to identify modal components during and after the fault. This shows that the placement of PMUs should not be arbitrary.

4.3 Case 3 - Analysis of voltage angle for line disconnection

As discovered in the previous case, not all measurements are suitable for analysis. The power transfer in certain lines may be contaminated with noise and outliers, giving no clear linear behaviour that the methods in this thesis can utilize. To investigate other possibilities in frequency and damping estimation, the voltage angle at the connected bus terminals is investigated. The reason for choosing the voltage angle is its close relationship with active power in power system analysis. The objective of this case is to analyze the same fault as in case 2, the only difference being that the voltage angle at the connected terminal is measured instead of the active power transfer. This will render the amplitude (and phase) less indicative, although they are still used for clustering purposes.

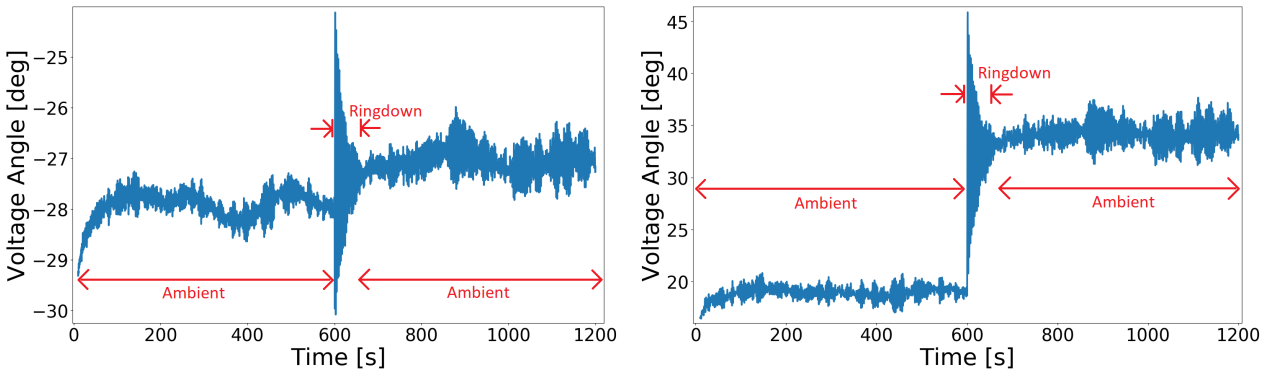

(a) Line 9-10 **(b)** Line 5-6

Figure 4.29: Simulation data from PF in case 3

4.3.1 Variable load - Ringdown analysis

The extracted voltage angles shown in Figure 4.29 display a clear ringdown for both lines. This is ascertained in the EMD-filtering results in Figure 4.30. There is barely any noise present, and both have clear linear oscillatory tendencies.

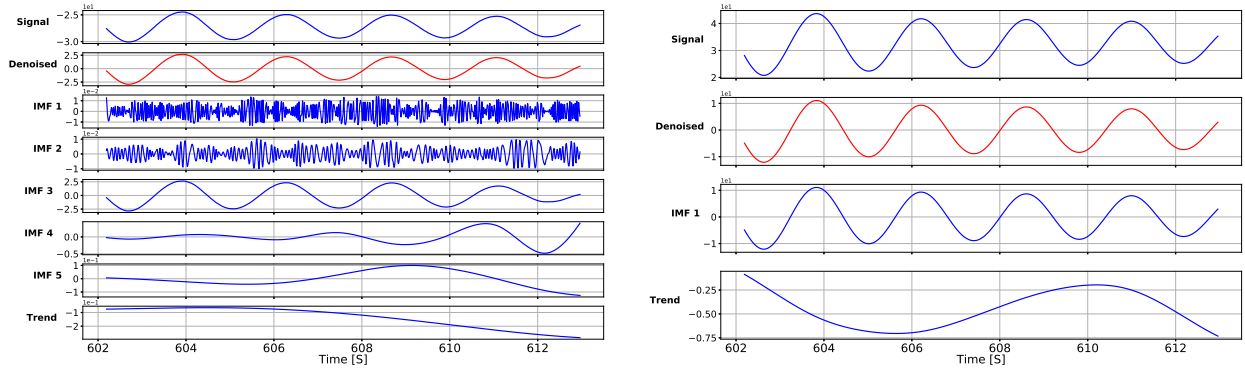

(a) Line 9-10 **(b)** Line 5-6

Figure 4.30: IMF plots from EMD-filter

Testing PA_O on this signal results in the cluster plots in Figure 4.31.

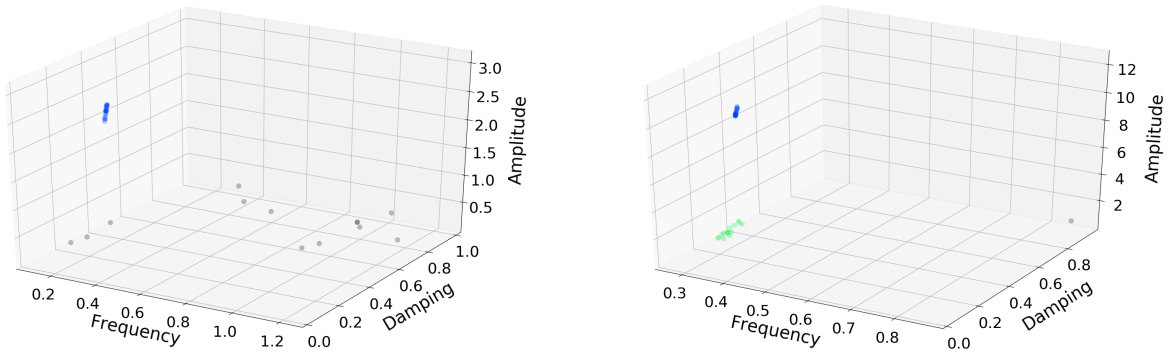

(a) Line 9-10 **(b)** Line 5-6

Figure 4.31: Cluster plot from both estimations on ringdown signal

It can be seen that for line 9-10, one cluster is identified for all 22 possible model orders, similar to the case with analysis of active power transfer. For line 5-6 there are two clusters identified, where one has a much lower amplitude and a higher damping than the other. The cluster with the highest amplitude has 22 out of 22 occurrences, while the other has only 11. The modal components estimated are shown in Table 4.12.

Table 4.12: Consistent modes for multiple model orders in ringdown variable load test

Results on line 9-10		**Results on line 5-6**	
Freq. [Hz]	η	**Freq. [Hz]**	η
0.419	0.019	0.418	0.018
		0.288	0.146

Both lines identify the inter-area mode at approximately 0.42 Hz with a damping ratio of just under 2 %. For line 5-6, a second mode is identified. This mode has a large damping ratio in addition to only being present in half of the possible model orders tested. Using the estimated modal information, the reconstructed signal reveals an almost perfect match as seen in Figure 4.32.

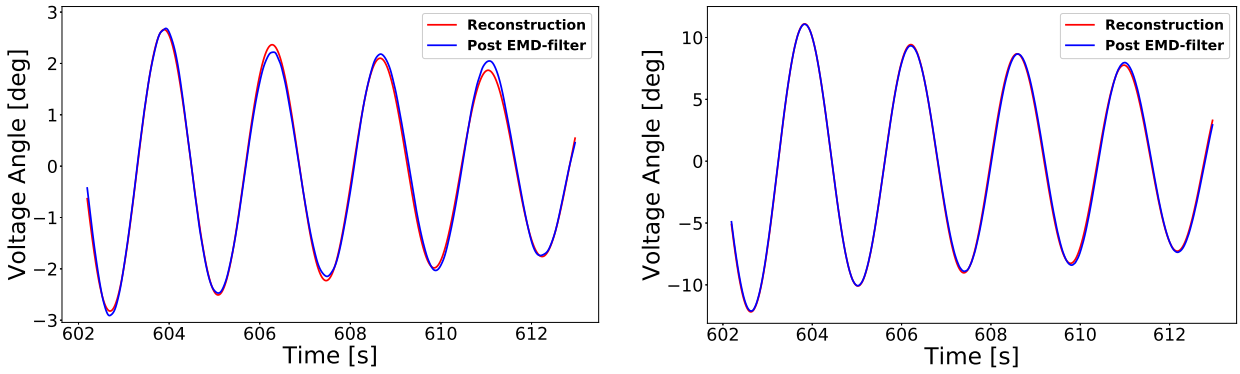

(a) Line 9-10 **(b)** Line 5-6

Figure 4.32: Comparing reconstructed signal to post EMD-filtered signal

Even though the amplitude only indicates angle variations, the reconstruction gives an overview of model fit. Comparison to the post-filtered signal in line 9-10 gave a signal-to-noise ratio of 50.4 dB, while line 5-6 gave 60.3 dB, which is far greater than the result for case 2.

Summarized Observations

- Using the voltage angle gives good approximation of the inter-area oscillatory modes
- Voltage angle measurements contain less noise and non-linearities than active power transfer measurements
- Voltage angle is a good indicator of small signal stability

4.3.2 Variable load - Ambient analysis prior to ringdown

Even though the ringdown signal contained little noise, the ambient data shows a clear need for filtering. As seen in Figures 4.33 and 4.34, there is both high-frequency noise and low-frequency components that must be removed.

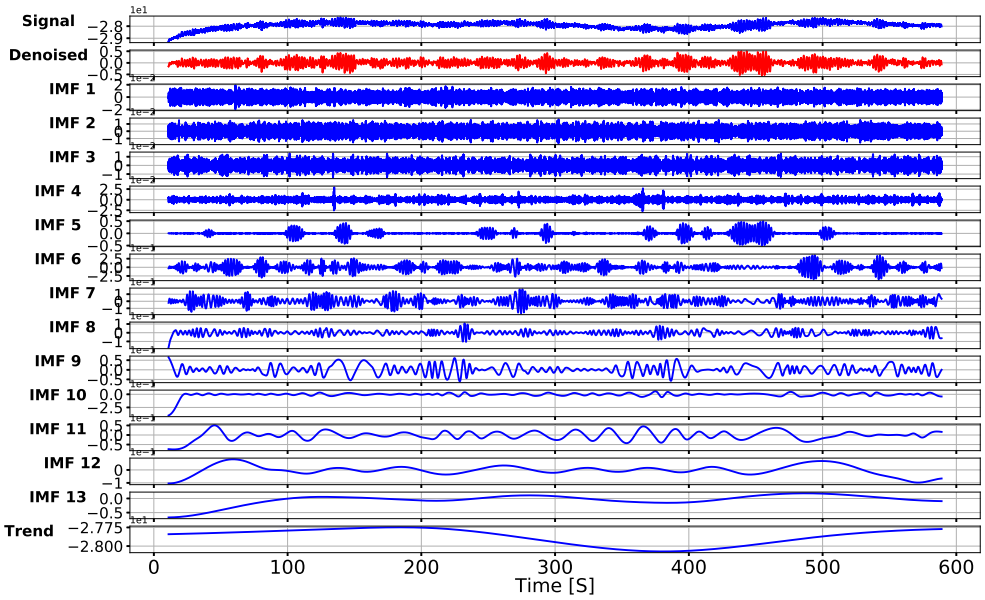

Figure 4.33: IMF plots from EMD-filter results on line 9-10 utilizing IMF 4-9

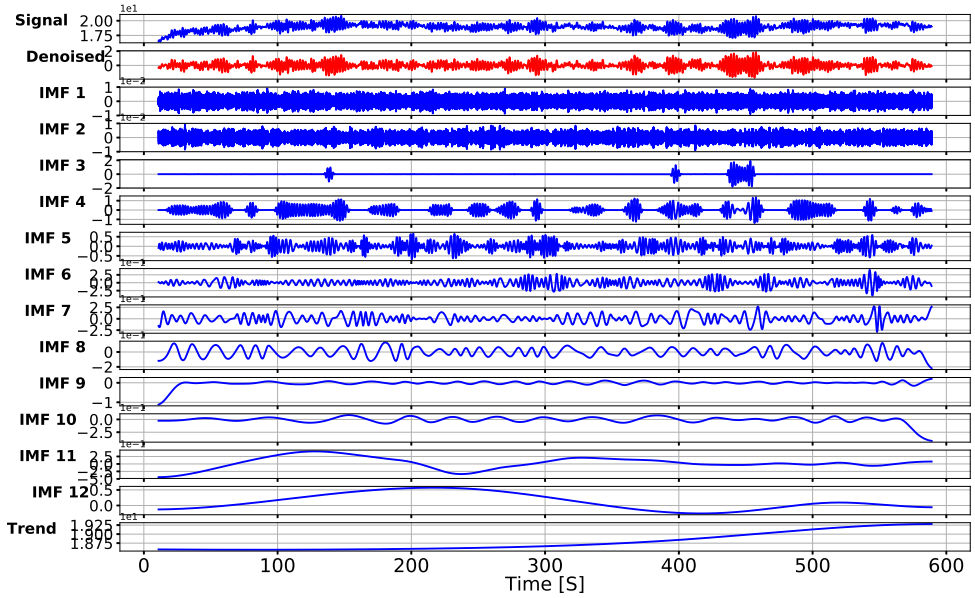

Figure 4.34: IMF plots from EMD-filter results on line 5-6 utilizing IMF 3-8

Test results show that the inter-area mode is present in both lines when tracking modal components. From the analysis of line 5-6, one additional low frequency mode of 0.11 Hz is identified as seen in Figure 4.35.

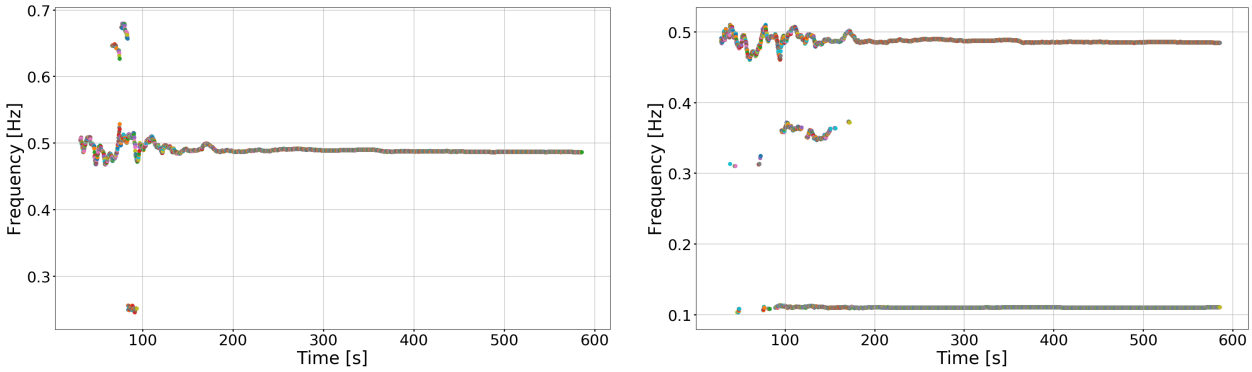

(a) Line 9-10 **(b)** Line 5-6

Figure 4.35: Mode-tracking of identified modes

The damping ratio of the 0.11 Hz mode is 36 %, and appears only in 12 out of 20 model order simulation. Therefore, it is excluded from further study. The inter-area mode is present in all of the 20 model order simulations, with a damping ratio shown in Figure 4.36. The damping ratio is slightly lower in line 9-10 compared with line 5-6, although both are underestimated when compared to the 2.5 % damping estimated by PF.

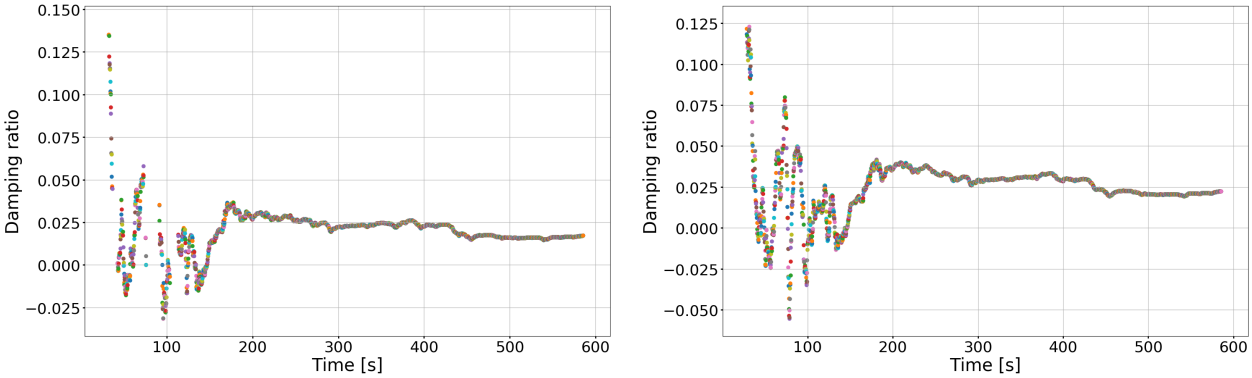

(a) Line 9-10 **(b)** Line 5-6

Figure 4.36: Mode-tracking of damping on inter-area mode in Figure 4.35

The exact result of estimation is shown in Table 4.13, where a comparison with PF confirms that the measurement analysis gives a good estimation of the inter-area mode.

Table 4.13: Modal information at the end of ambient data prior to fault

Results on line 9-10		**Results on line 5-6**	
Freq. [Hz]	η	**Freq. [Hz]**	η
0.486	0.017	0.485	0.022
		0.11	0.36

For a final validation of the identified modes, the signal is analyzed using Welch's method as seen in Figure 4.37. Both measured signals show a clear peak at 0.485 Hz, confirming that the inter-area mode is dominant in the voltage angle measurement.

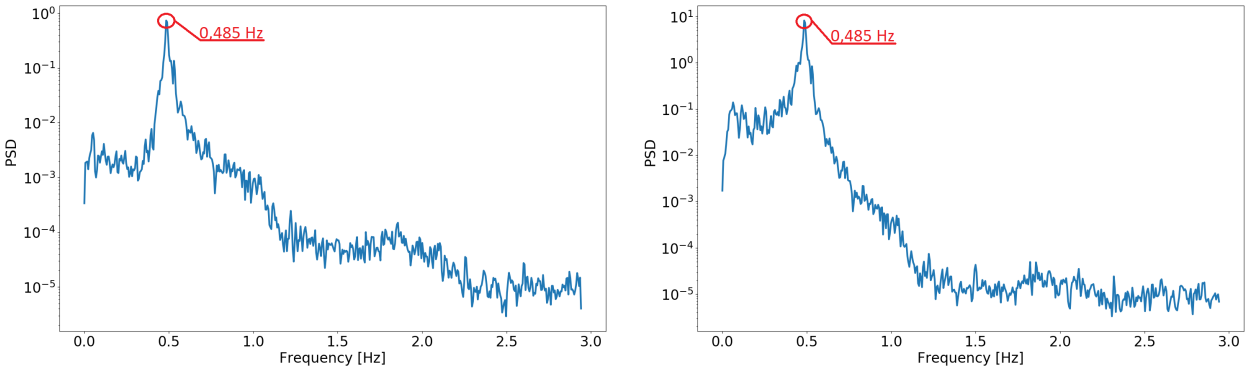

(a) Line 9-10 **(b)** Line 5-6

Figure 4.37: Welch power spectrum of measured signal

Summarized Observations

- Voltage angle measurements give a good indication on the most dominant mode in the signal.
- Analyses show that ambient data gives a perfect estimation of frequency, while it tends to underestimate the damping ratio.
- Power spectrum analysis corroborates the method used by arriving at the same conclusion as in both RRLS and PF.

4.3.3 Variable load - Ambient analysis after ringdown

From section 4.2.3, the analysis of ambient data after the ringdown was inconclusive. This was a result of bad approximation in the reconstructed signal in line 5-6, in addition to the absence of the expected inter-area mode in the same line. The results in this test are of particular interest, as they may corroborate the hypothesis that the use of voltage angle in modal estimation gives a better approximation.

Decomposition of the measured signals are shown in Figures 4.38 and 4.39, where the results of detrending are clearly seen in the denoised signals.

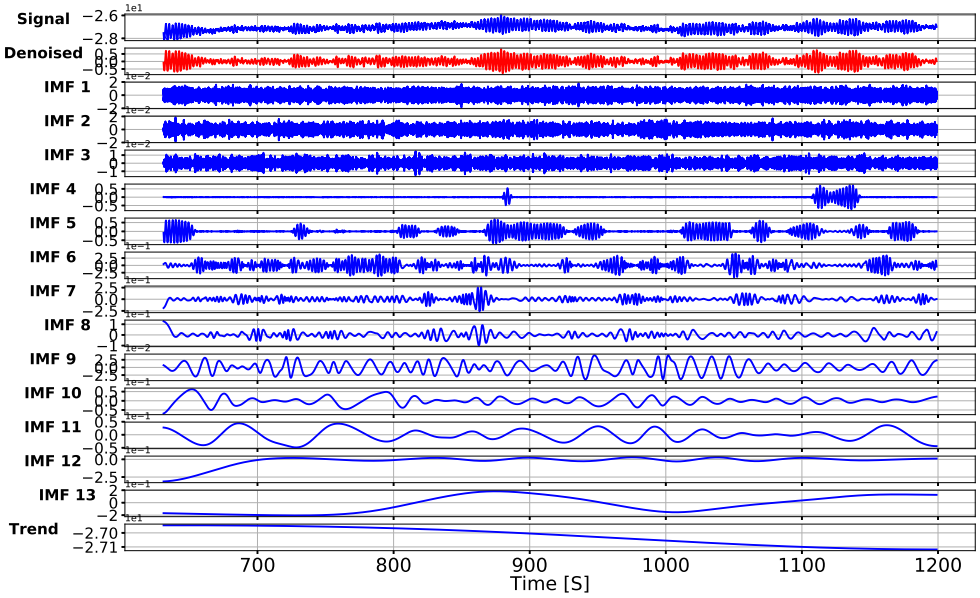

Figure 4.38: IMF plots from EMD-filter results on line 9-10 utilizing IMF 4-9

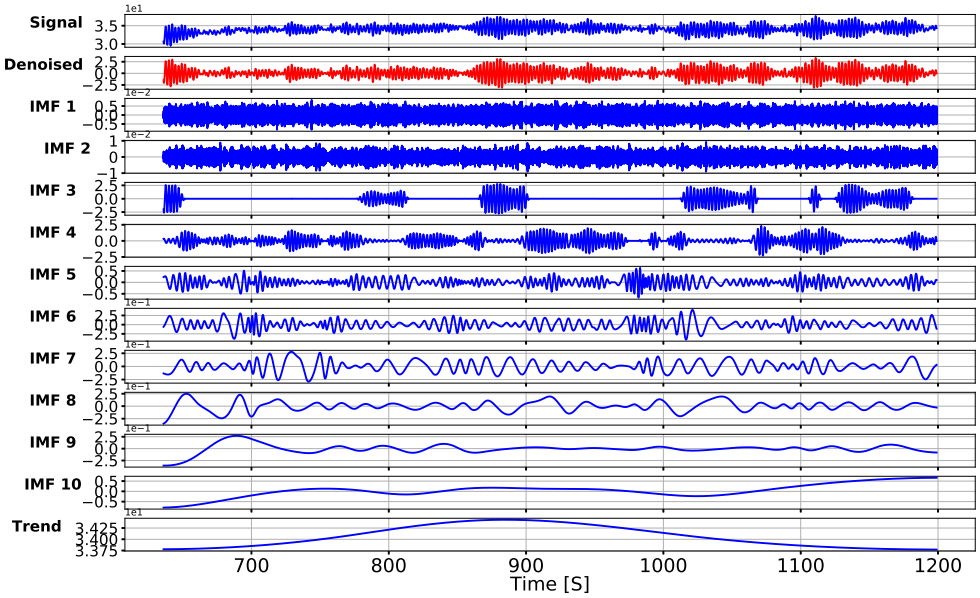

Figure 4.39: IMF plots from EMD-filter results on line 5-6 utilizing IMF 3-6

Analyzing the denoised signal using the RRLS method combined with clustering, results in the identified frequencies shown in Figure 4.40.

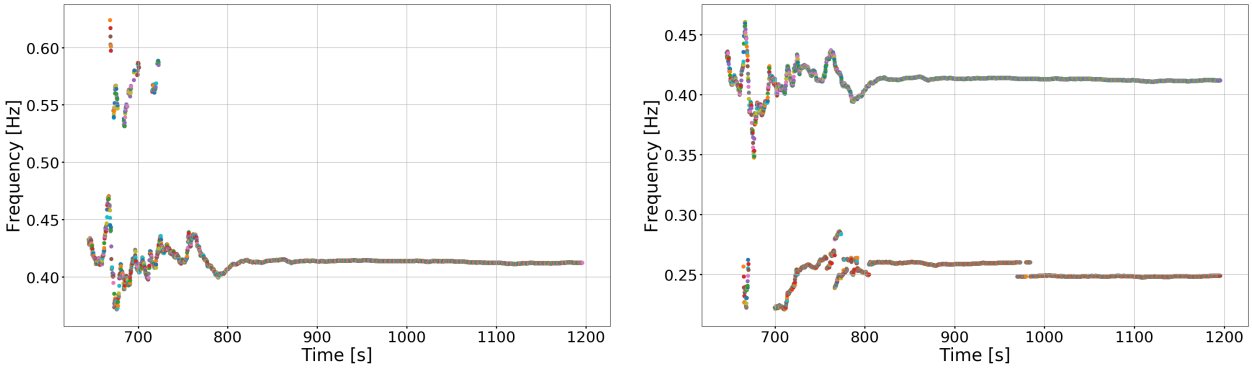

(a) Line 9-10 **(b)** Line 5-6

Figure 4.40: Mode-tracking of identified modes

From the frequency plot, it is clear that there are major differences compared with case 2 in section 4.2.3. Line 9-10 finds one clear frequency converging at 0.412 Hz. In addition, a second mode is initially found, although it is quickly ruled out by the clustering method as convergence approaches. Line 5-6 does in this case find two modes, instead of three for the previous case. Of the two modes, one is the inter-area at 0.412 Hz, not identified in the previous case. This mode shows the same development as the identified mode in line 9-10. The second mode identified is at the frequency of 0.249 Hz, although it is not consistent throughout the measured time period. The damping ratios of the inter-area mode identified are shown in Figure 4.41.

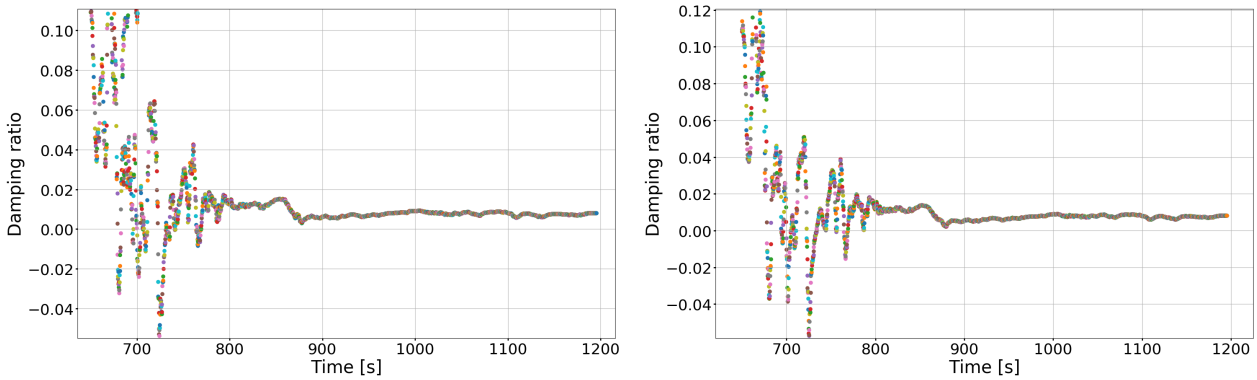

(a) 0.412 Hz mode in line 9-10 **(b)** 0.412 Hz mode in line 5-6

Figure 4.41: Damping of modes in Figure 4.40

Similar to the frequency estimation, damping ratio in the two lines show the same characteristics, both converging at approximately 0.8 %, which is below the critical limit at 5 %. The extracted information of all identified modes are shown in Table 4.14.

Table 4.14: Modal information at end of ambient data post fault

Results on line 9-10		**Results on line 5-6**	
Freq. [Hz]	η	**Freq. [Hz]**	η
0.412	0.008	0.412	0.008
		0.249	0.29

The 0.249 Hz mode, identified in line 5-6, shows a damping of more that 29 %. A damping ratio of this magnitude is too high to be of interest, and the mode is neglected.

The result of modal estimation in both lines give a good approximation of frequency in the 0.412 Hz mode when compared to the modes estimated by PF in Table 4.10. With both lines estimating the frequency at 0.412 Hz and PF identifying it at 0.414 Hz, the estimation error is approximately zero. The damping ratio is however underestimated in both lines. With the voltage angle as a variable, the lines give the same damping ratio of 0.8 %, which is close to the estimate from line 9-10 in case 2. From this, it is observed that estimates based on the voltage angle in all lines give the same result as the estimates based on lines with a single oscillatory mode in the measurement of active power transfer. Remembering that only the dominant, inter-area mode is identified, it may not always be the best solution as local modes are not identified.

Even though the results seem valid, Welch's method is applied as seen in Figure 4.42.

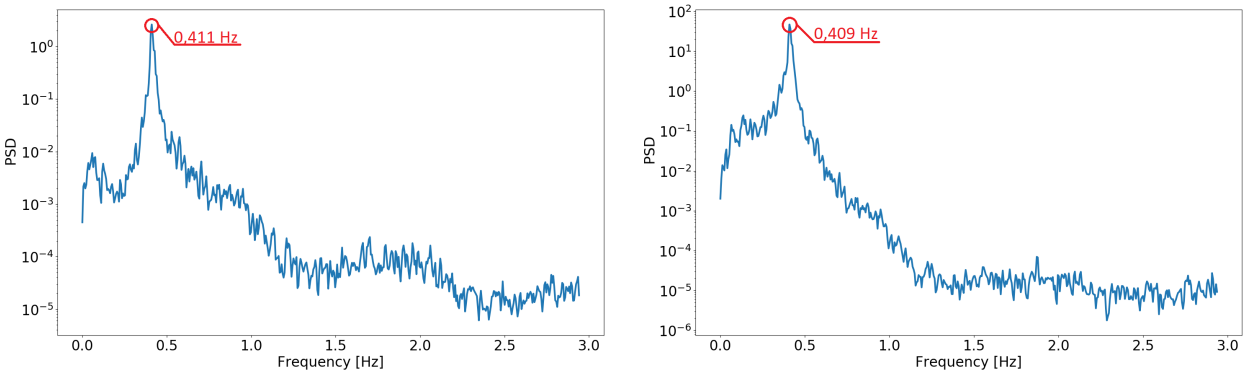

(a) Line 9-10 **(b)** Line 5-6

Figure 4.42: Welch's power spectrum of measured signal

Both signals show one clear peak, although with a small difference between them of 0.001 Hz. As Welch's method only gives an indication of frequencies in a certain range, the exact peak is not always the true frequency. The conclusion is the same nevertheless, with both signals having one clear mode.

Summarized Observations

- Voltage angle results show a similar modal estimation in all measured signals.
- All measured lines find the approximately 0.41 Hz inter-area mode and none of the remaining modes.
- Damping ratio is slightly underestimated in estimations based on voltage angle.

Case 3 summary

A comparison of the ambient and ringdown results shows that the system changes during the fault. The modal content prior to the fault does not match that during ringdown or that of the ambient data after the fault. The results show that the system during ringdown is in a transition state, although closer to that in the ambient signal after. During the ringdown, the modes change from a pre-fault state to a post-fault state. The frequency and damping gives a good indication of the state the system moves towards.

The damping ratios from the ambient data are in general estimated below its actual value. When the signal has a clear, oscillatory tendency, it is expected to appear with a lower damping ratio than it actually has. Since the modal components are under constant excitation, they will appear with a generally lower damping ratio. Although difficult to approximate accurately, it gives a good indication of small signal stability.

5 Testing and validation on PMU data

The advantage of simulated data is that validation methods are often readily available. A disadvantage is that the dynamics may not reflect the measurements from real world PMUs. There are several reasons for this:

- Assumptions of system input (random load variations, etc.)
- Measurement noise
- Unforeseen dynamics in the complex power system

This section contains analysis of different measurements from PMUs in the Nordic grid. Some of them include incidents, like small disturbances to induce ringdowns of various quality, which may or may not represent the true modal characteristics of the system. Others only comprise ambient data, electro-mechanical oscillations mixed with noise, trends and non-linear, slow dynamics. The origin of these dynamics is not known to the authors of this thesis, as no *a priori* knowledge of the signal content is available. Hence the only evaluation alternative is to compare them against each other, and attempt to extract valuable information of the underlying dynamics.

5.1 Case 1 - 10 Hz

The first case involves one hour of power flow measurements before, during and after a large disturbance in the Nordic Grid.

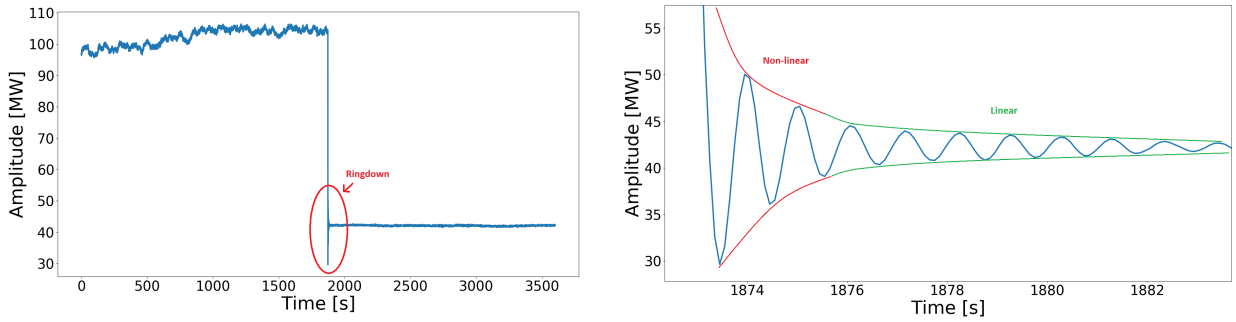

(a) Ringdown and ambient data from the Nordic Grid

(b) Non-linear and linear portions of ringdown

Figure 5.1: Measurements from a large disturbance in the Nordic Grid, with ringdown portion expanded.

The PMU that captured this incident provides only 10 Hz measurements, which has various consequences. No pre-filtering of high frequency noise will be possible, so the purpose of EMD is reduced to removal of trend and low-frequency, non-linear variations (below approximately 0.2 Hz). Downsampling is not performed, as a lot of information is lost with the already low

sampling rate, and 10 Hz is not too high for identification of electro-mechanical modes with neither Prony nor RRLS.

At t = 1872 seconds, the power flow drops to below half of its pre-disturbance state. The following ringdown can, with visual inspection, be determined to have clear, sinusoidal features. However, the first portion of the ringdown contains non-linear characteristics, and is unusable for the linear analysis of Prony. This concept will be demonstrated further in this case study. For now, Prony analysis will be applied to the linear portion, which will give a good indication of the true modal characteristics of the system.

5.1.1 Linear portion of ringdown signal

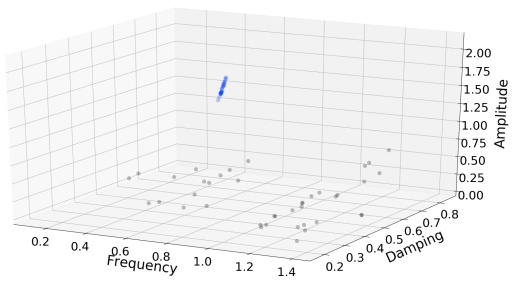

(a) Cluster plot of ringdown

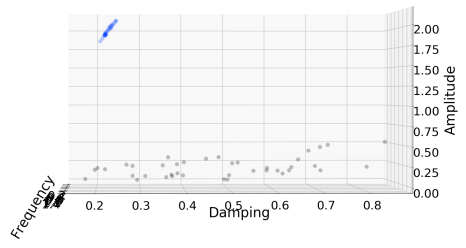

(b) Cluster plot, showing variation in damping estimate

Figure 5.2: Cluster plots of ringdown signal

The (average) results from Figure 5.2 are presented in Table 5.1.

Table 5.1: Ringdown: dominant mode(s)

Freq. [Hz]	Damp. Ratio	Amp.	Phase [rad]	# occurrences
0.970	0.037	2.45	-1.65π	27/27

Figure 5.2 shows that the modes are moving very little for varying model order, which indicates strong influence on signal dynamics. This is supported by 100% occurrences of this mode, i.e. the mode is found for all model orders. Additionally, all trivial modes are of low-amplitude, so the fit should be good as well. This is verified in the reconstruction.

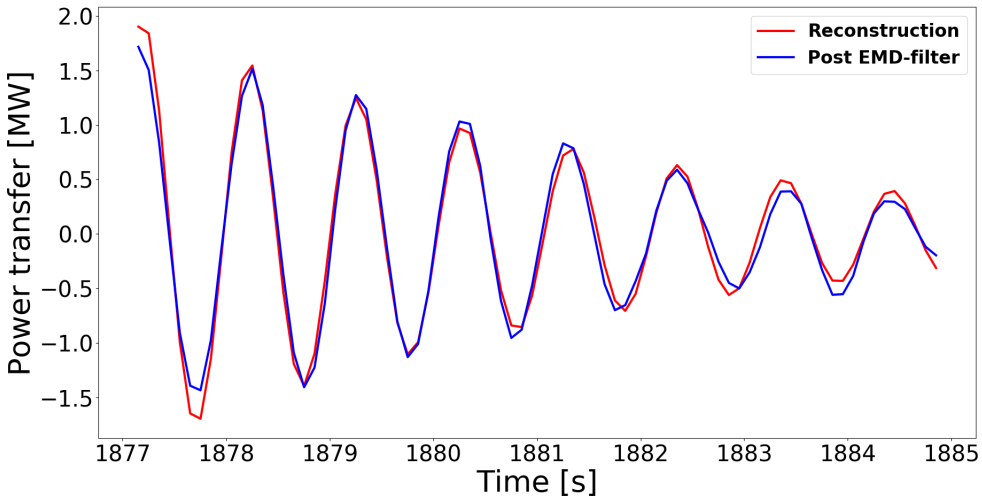

Figure 5.3: Reconstruction of modes, in this case one decaying sine wave

5.1.2 Including non-linear portion in linear ringdown analysis

This section is dedicated to show the importance of choosing the correct signal and time window for Prony analysis. After a large disturbance, small-signal stability is not sufficient for describing the observed phenomena. The relevant field is called large-signal stability, and includes non-linear, sub-transient behaviour. However, it is not trivial to determine where the non-linear effects terminate and linear models are applicable. This highlights one benefit of the applied method: only the modes with clear impact on the signal will be extracted. The cluster plot in Figure 5.4 contains more valuable information - Prony uses trivial modes close in frequency, with high amplitude and damping, for fitting of the sub-transient portion.

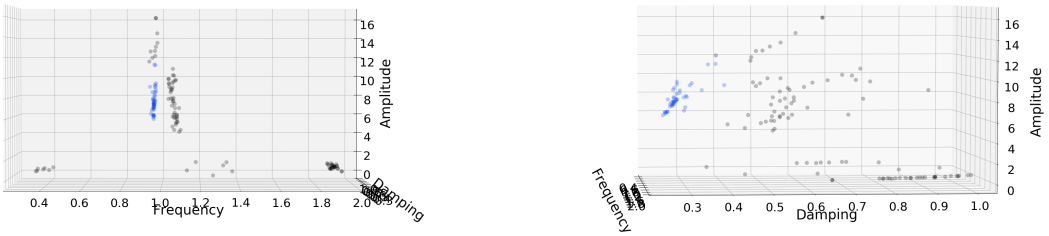

(a) Cluster plot focusing on frequency and amplitude

(b) Cluster plot, showing variation in damping estimate and amplitude

Figure 5.4: Cluster plots of non-linear ringdown signal

The (average) results from Figure 5.2 are presented in Table 5.2.

Table 5.2: Ringdown: dominant mode(s)

Freq. [Hz]	Damp. Ratio	Amp.	Phase [rad]	# occurrences
0.966	0.047	7.36	0.21π	43/49

Comparing Table 5.2 with Table 5.1 shows that the dominant mode is extracted even with the non-linear portion. The damping ratio is off with 1%, which is not unacceptable - bot still not as accurate as it could be. The amplitude and phase have changed greatly, which is expected as the analysis starts at an earlier time. It can be observed that the cluster is slightly more spread out, and the number of occurrences is less than 100 %.

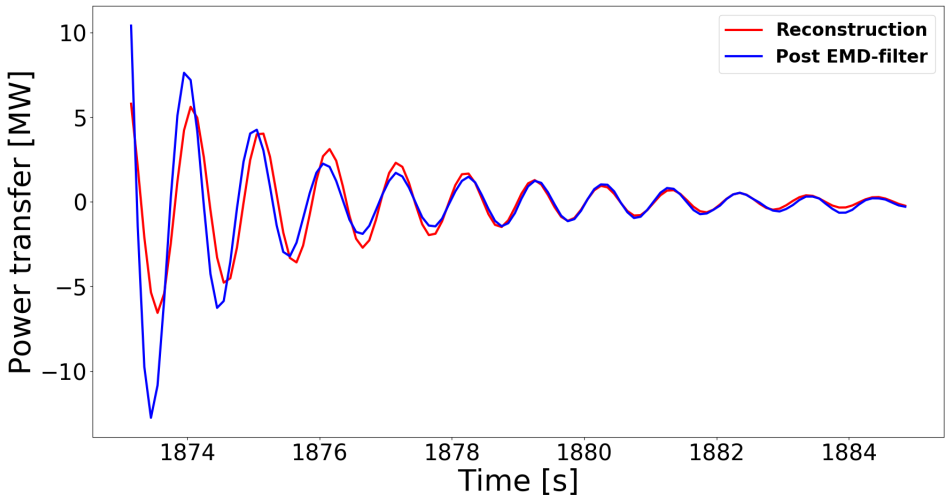

Figure 5.5: Reconstruction of transient behaviour including nonlinear portion

The reconstruction reveals a trade-off between estimating the non-linear and linear portion (in the least-squares sense), and consequently the estimation of the linear characteristics suffers, although not dramatically.

Summarized Observations

- Clear ringdowns are indeed obtainable from a real grid.
- For 10 Hz sampling, EMD-filter acts as a high-pass filter.
- Selecting the appropriate time-window yields decisive results.
- Including non-linear portions will corrupt the estimation, yet Prony may still yield usable results.

5.1.3 Ambient data prior to ringdown

Around half an hour of data is available for ambient analysis before the disturbance. Only one mode was observable in the ringdown portion, and although that was after the disturbance, the ambient analysis should reveal a mode in the same frequency range. As the ringdown response is the impulse response of the system, this is indeed the only mode that should be observable at the location, for the given operating state. Due to limited research in the area, it cannot be directly deduced that this will be the only mode observable in the measured ambient data. Indeed, it will be shown that the ambient data before the disturbance contains additional frequency content in the electro-mechanical range.
As before, the ambient data is pre-filtered with the Empirical Mode Decomposition.

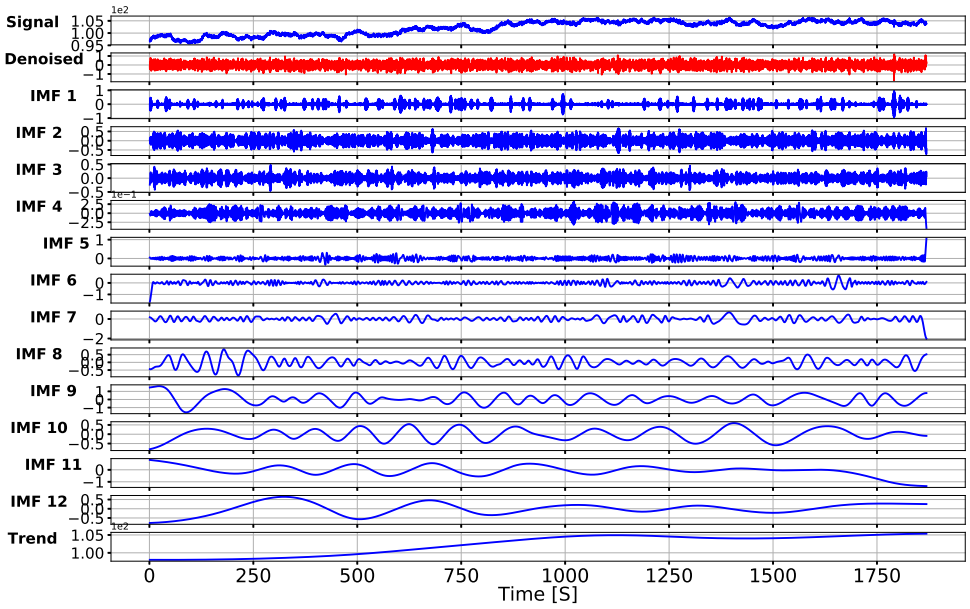

Figure 5.6: IMF plot of EMD result, extracting IMF 1-5

Before proceeding with RRLS, a small consideration of the filtering is presented. As the EMD extracts IMFs from a frequency range, the number of IMFs has a great impact on the resulting frequency spectrum.

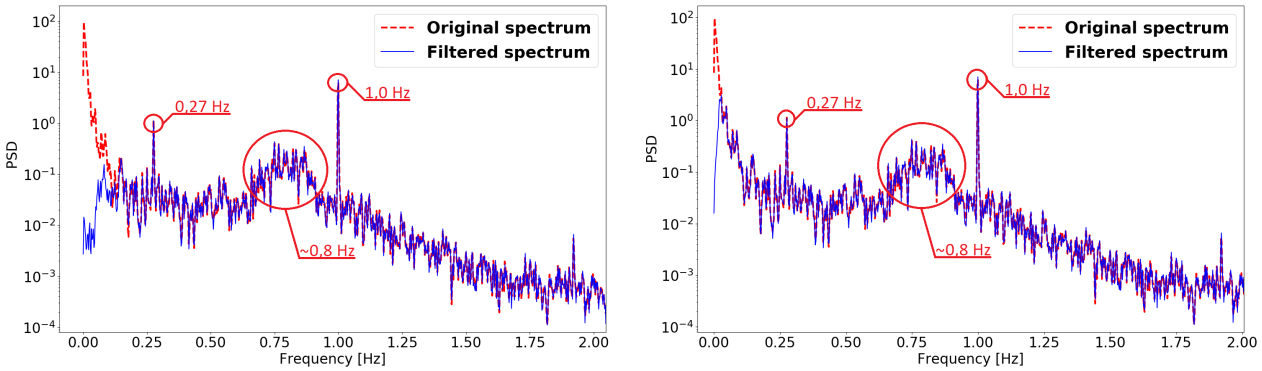

(a) Using IMF 1-5 **(b)** Using IMF 1-7

Figure 5.7: Comparison of Welch's power spectra of measured signal with varying IMF composition

In Figure 5.7, the frequency spectra are shown for the extraction of IMF 1-5 and IMF 1-7. Observe that excluding IMF 6 - 12 and the trend does not alter the frequency range of interest. This goes a long way in verifying EMD as a high-pass filter. Additionally, no changes are made to the high-frequency spectrum, as the first IMF extracted is IMF 1. From both spectra, a clear spike is visible at 1 Hz, and another around 0.25 Hz. A flatter peak can be seen around 0.8 Hz.

Continuing with IMF 1-5, RRLS is applied to the whole data set.

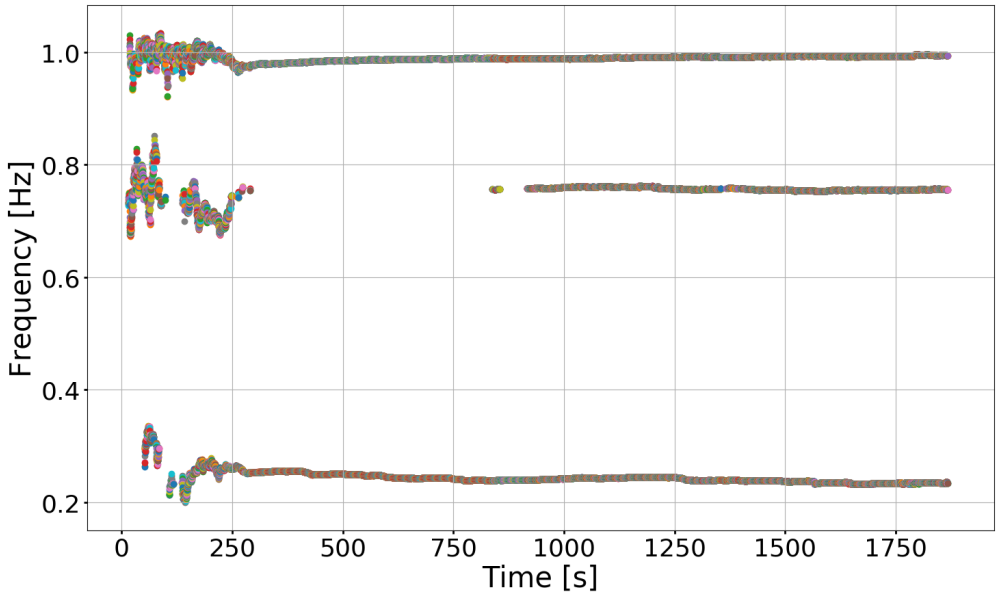

Figure 5.8: Mode-tracking of identified modes in PMU signal

Figure 5.8 shows that RRLS finds all three frequencies, although with different degrees of certainty. This is seen in Figure 5.9, presenting the cluster plot at a timestep around 1700 seconds - the cluster at 1 Hz is much more compact than the other two. The averaged values for this cluster plot are shown in Table 5.3.

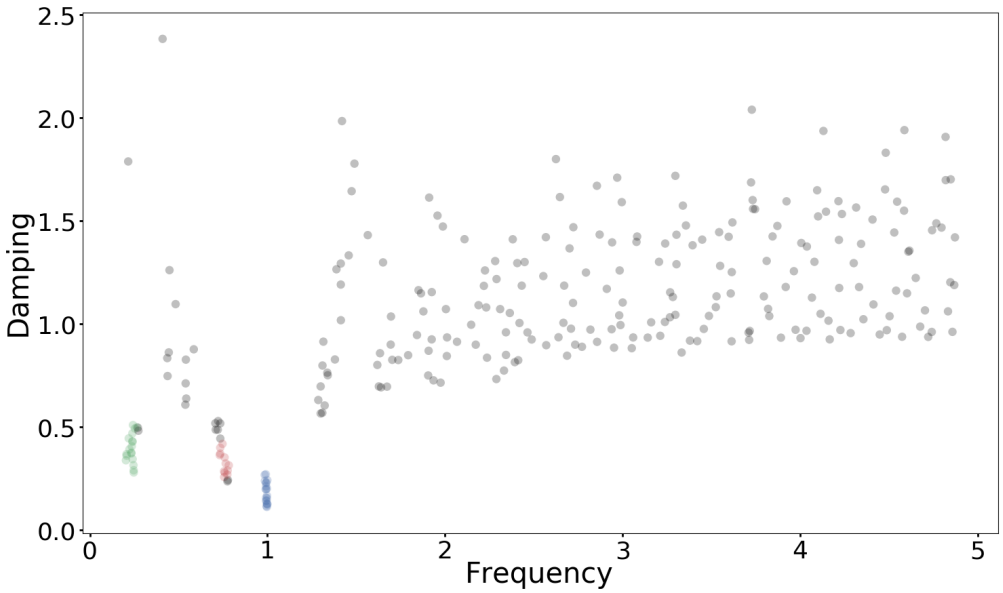

Figure 5.9: Mode-tracking of identified modes in PMU signal

Table 5.3: Modes identified prior to ringdown

Mode	Freq. [Hz]	Damp. Ratio η	# occurrences
1	0.994	0.029	20 / 20
2	0.756	0.068	12 / 20
3	0.235	0.26	18 / 20

The 0.25 Hz mode has a very high damping, which makes it less interesting than the two others.

The 1 Hz mode is identified relatively accurately, considering that the frequency should not be expected to be fixed for the volatile ambient data. RRLS has not identified the 0.75 Hz mode in the middle part. It looks like it should converge around 250 seconds, yet the results are not decisive enough for the clustering algorithm until 800 seconds. The damping plots of the two higher frequencies are shown in Figure 5.10.

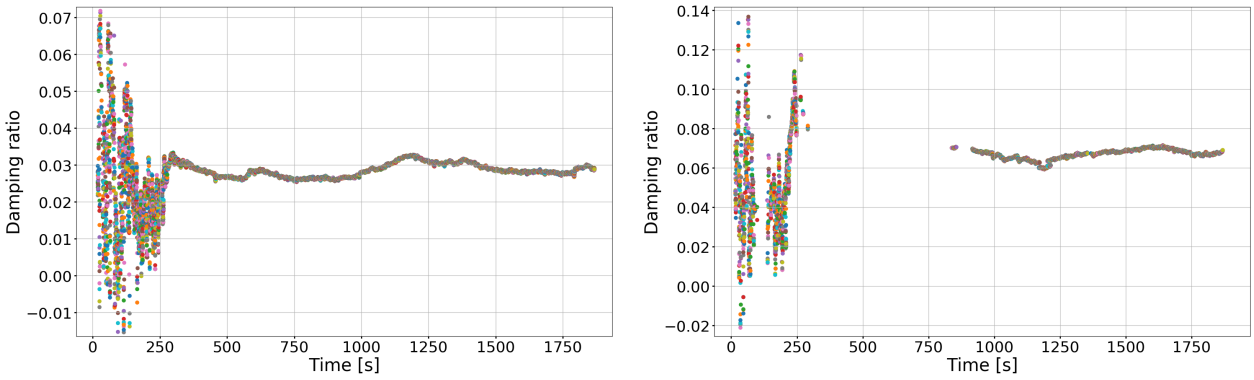

(a) Damping ratio of the 1 Hz mode **(b)** Damping ratio of the 0.75 Hz mode

Figure 5.10: Damping ratio of the two most critical modes

When RRLS finds the 0.75 Hz mode, it determines the damping to be 6%. This is quite low, and could easily be confused for a system mode. If the ambient analyzer identifies low-damped electro-mechanical oscillations that are not related to the system dynamics, false alarms can be tripped. Nonetheless, the low consistency of the mode estimate indicates limited trustworthiness. Further investigation of ambient data and behaviour of load variations could facilitate further improvement of the ambient analyzers.

Summarized Observations

- The 1 Hz mode identified in the ringdown is indisputably distinguishable in the ambient data.
- Additional modes are observed in the ambient data. Their presence in the signal is indicated by both Welch's method and RRLS, which increases their credibility. However, they are probably not related to the system modes, as they are not observable in the ringdown.

5.1.4 Ambient data after ringdown

As the ringdown fades out, the measurements return to their common, ambient state. The same analysis procedure is followed: EMD, Welch and RRLS with Clustering.

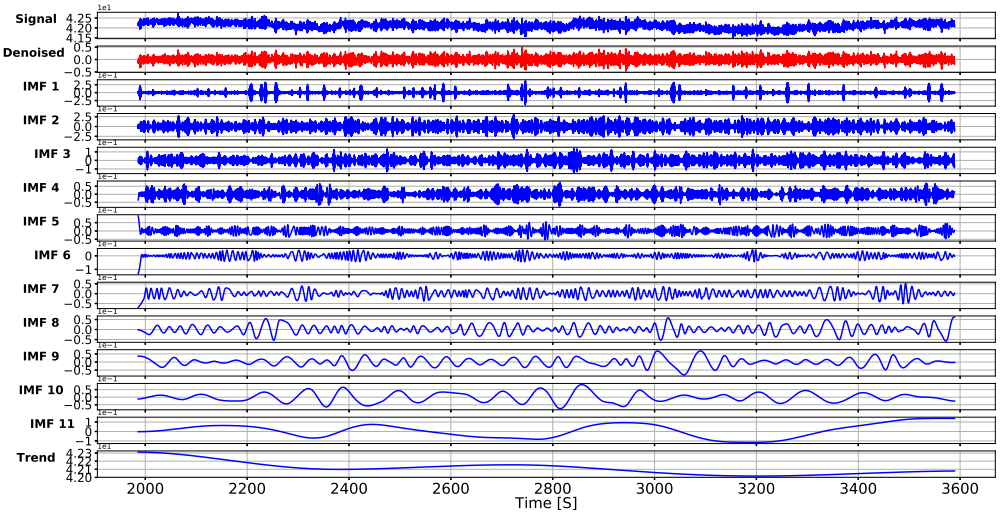

Figure 5.11: IMF plot of EMD result, extracting IMF 1-6

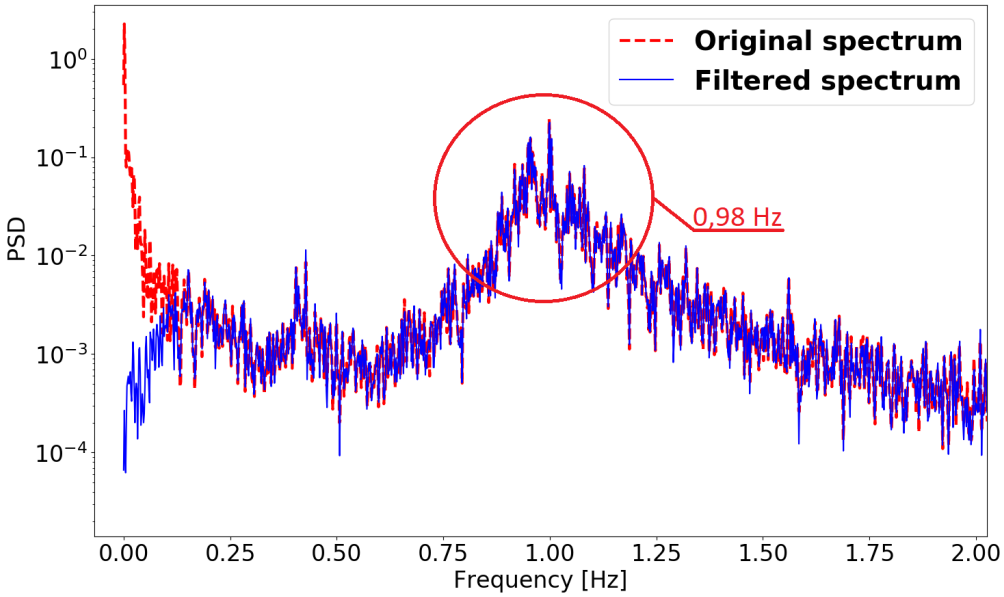

Figure 5.12: Comparison of Welch's power spectrum in measured signal with and without EMD-filtering

The sharp spike at 1 Hz is now gone, and a rounder peak has taken its place. It is still distinguishable, yet not as pure as before, and may indicate that this frequency is somewhat varying. Around 0.4 Hz, there is a smaller bump, but not large enough to be decisive. The following shows the results from RRLS.

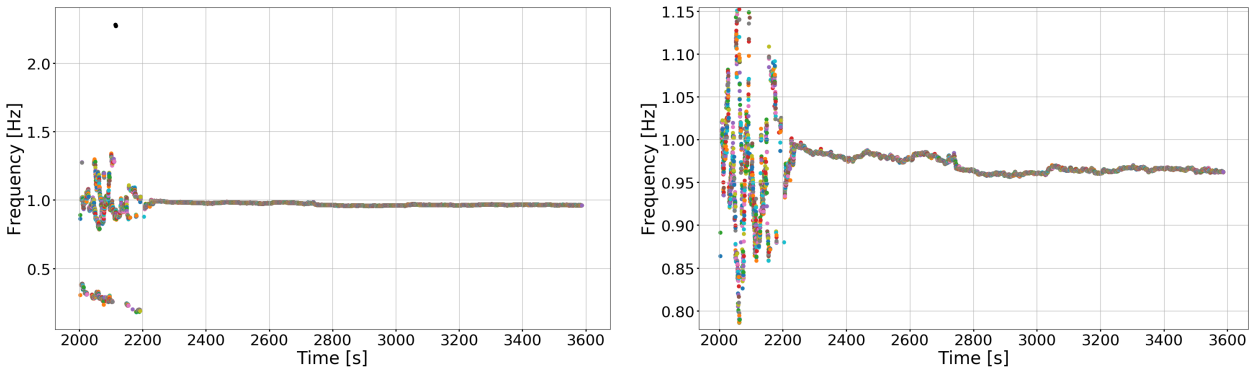

(a) Identified modal components **(b)** Closer inspection of the 1 Hz mode

Figure 5.13: Tracking of frequency of estimated modes

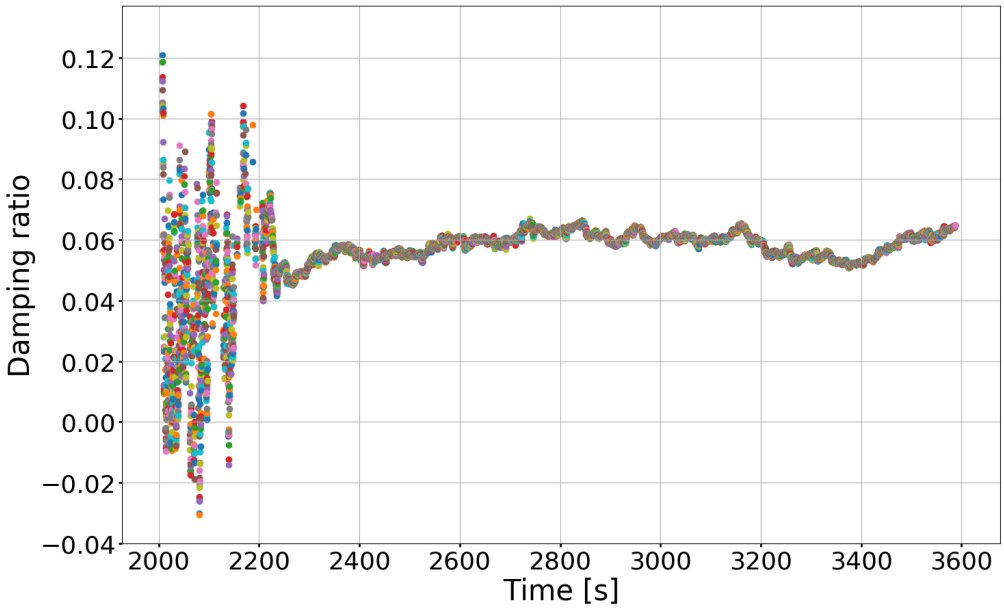

Figure 5.14: Damping of 0.96 Hz mode

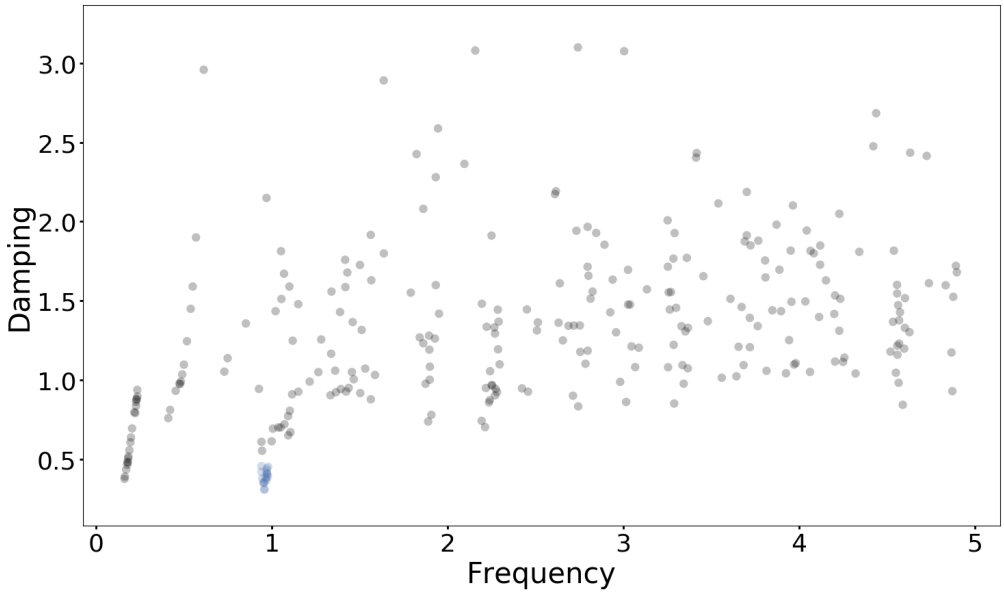

Figure 5.15: Clustering result after convergence

Table 5.4: Modes identified after ringdown

Mode	Freq. [Hz]	Damp. Ratio η	# occurrences
1	0.963	0.062	18 / 20

RRLS successfully identifies the 1 Hz mode in the complete time window. Its damping is actually increased to around 6 %, from the ringdown estimate of 3.7 %. This is a strange phenomenon, as both these values should describe the same system, provided no other changes or control actions have occurred. Unfortunately, no knowledge of the system itself is available, so the evaluation of whether this is due to system changes or limitations of the method is difficult. The forgetting factor μ has a high impact on the results, and bad tuning of this could certainly yield misleading results. The implemented linear increase in μ may be unsuitable since its effect is closer to logarithmic than linear. Time-varying forgetting factor is indeed a complicating matter [18] [38], and the approach with clustering may further complicate the choice of this parameter. However, if the algorithm is unable to identify clusters, this means that the regular RLS approach (i.e. one model order and no clustering) would be very sensitive to the choice of model order.

Summarized Observations

- Only the 1 Hz mode is identified in ambient measurements after the ringdown.
- The damping is higher than in the ringdown. This could be due to control effects, or badly tuned forgetting factor.

Case 1 summary

Real-world signals introduce new challenges, which are not experienced to the same extent in simulated data. Apparently, the ambient data has richer frequency content than observed in the ringdown. The additional signal mode at 0.75 Hz could easily be mistaken for real system dynamics if no transient information was available. All three portions clearly identified the presence of the low-damped 1 Hz mode, which strongly suggests that this is a system electro-mechanical mode with critical damping. The other two could not be identified in the ringdown, and should not be mistaken for system modes. They do however indicate that ambient measurements contain frequencies in the electro-mechanical range that may not originate from system dynamics. Additionally, the issue of forgetting factor could be very important for correct identification of modal information, in particular damping. Further investigation on this issue is advised to reduce the sensitivity of parameter choice.

5.2 Case 2

The signal analyzed in this case is the same that which was shown in Figure 2.1. The same is shown in Figure 5.16, where all ambient data prior to and after the ringdown provided by Statnett is included.

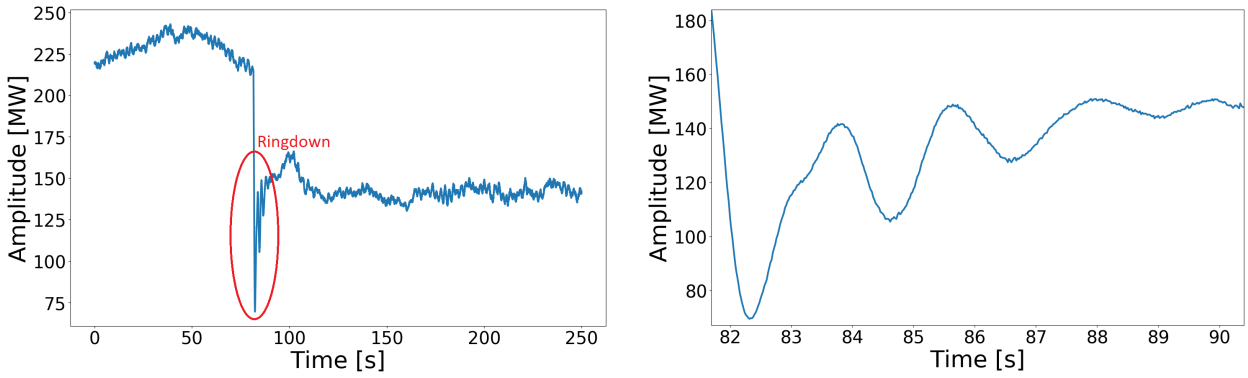

(a) Ringdown and ambient data from the Nordic Grid

(b) Ringdown-portion of signal

Figure 5.16: Measurements from a disturbance in the Nordic Grid, with ringdown portion expanded.

The PMU data from this incident is sampled at 50 Hz, providing the possibility of pre-filtering high frequency noise. The ringdown signal is unfortunately not as distinct as that shown in Section 5.1, although it serves its purpose on aspects in the methods not yet illustrated.

Of important note is the value of data quality. Not only the placement of the PMU, but how it is measured is vital. When analyzing ambient signals, a long enough data stream is important to ensure that convergence is obtained. In the provided data, generation outage occurs after only 81 seconds.

5.2.1 Ringdown analysis

The ringdown portion of the signal is the same that was analyzed in the paper in appendix A.

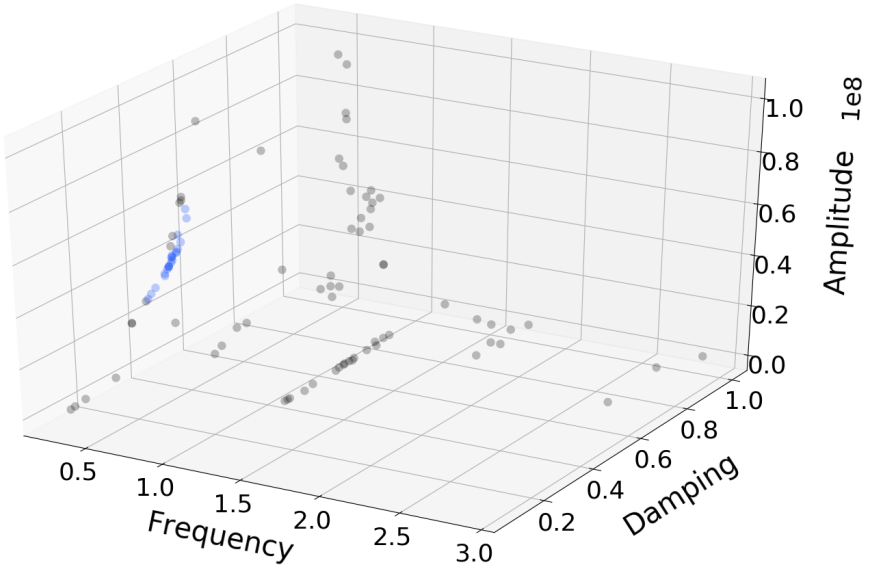

Figure 5.17: Cluster plot of ringdown signal

Based on analysis using PA_O and resulting clustering shown in Figure 5.17, the mode in Table 5.5 is obtained.

Table 5.5: Ringdown: dominant mode(s)

Freq. [Hz]	Damp. Ratio	Amp.	Phase [rad]	# occurrences
0.476	0.116	48.08	0.45π	21/30

The cluster plot in Figure 5.17 shows a signal full of noise and non-linearities, where the identified cluster differs both in damping and amplitude for varying model orders. In addition, the presence of high amplitude noise modes, although well damped, indicates that the signal is affected by non-linearities. For the clear signals tested earlier, the identified mode is present in all model orders. For this case, only 21 of the 30 different model orders tested included the identified mode, indicating that clustering results may be used as an indicator of signal quality.

Reconstruction of the estimated mode indicates that it is the dominating part of the measured signal as seen in Figure 5.18.

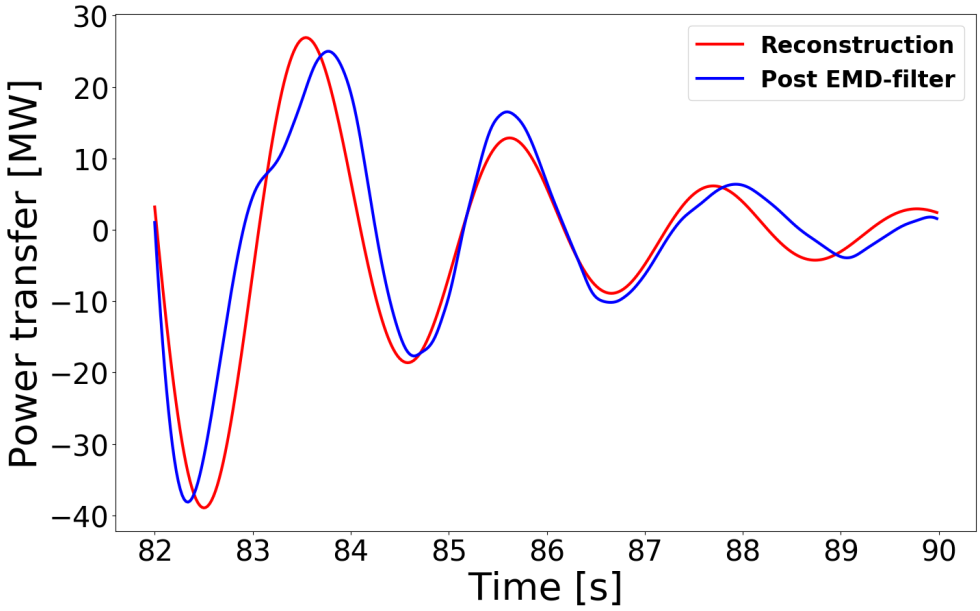

Figure 5.18: Reconstruction of modes, in this case one decaying sine wave

With a signal-to-noise ratio of 14 dB, the reconstructed signal proves the presence of noise, where variable frequency in measured ringdown signal gives an estimation inaccuracy.

Summarized Observations

- Non-linearities affect the ringdown analysis, as several high amplitude and damping trivial modes are generated.
- Number of occurrences of the most dominant mode in the cluster indicates the existence of non-linearities in the signal. If the number of occurrences is low, the oscillations are not just dominated by linear modes.

5.2.2 Ambient data prior to ringdown

With only 81 seconds of data prior to ringdown, the RRLS method implemented will not converge as it is. In order to obtain a credible result, the forgetting factor is kept at 0.9 for a longer period of the measured signal, before gradually increasing to 0.999 midway through the window of analysis. As a result, the estimation outcome is not completely trustworthy, due to the portion of measurements that is forgotten and the fact that only a small part of signal remains to validate the convergence. Using a non-parametric method such as Welch for verification of the estimated modes is no longer as robust, since it is affected by the smaller timewindow.

Figure 5.19 shows pre-filtering using the EMD-technique. With 50 Hz sampling, it is possible to identify and subsequently remove high frequency noise. The resulting denoised signal in red is a combination of IMF 4 through 7.

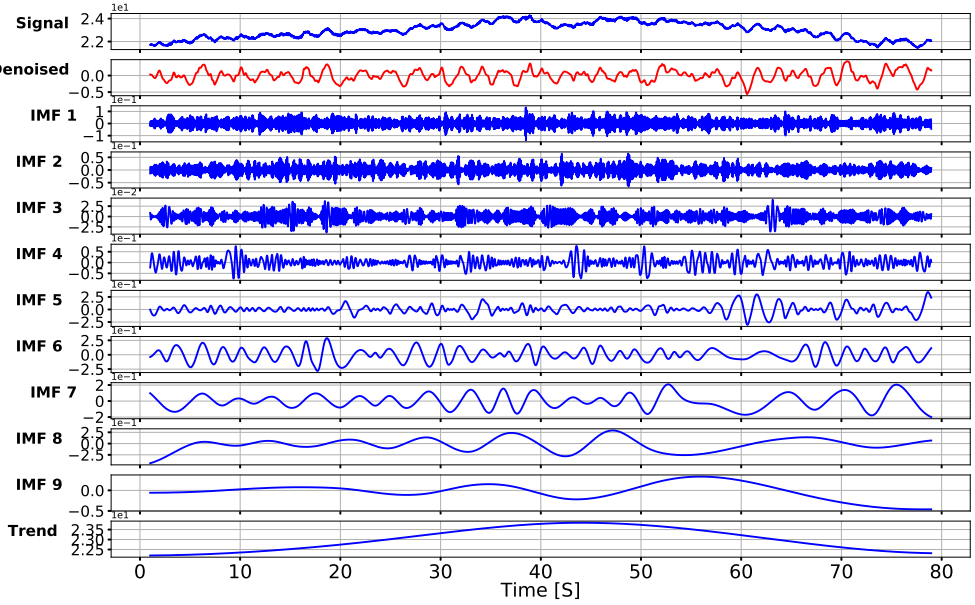

Figure 5.19: IMF plot of EMD result, extracting IMF 4-7

With further analysis depending on the quality of the filtered signal, the stability of filtering is important. A comparison of power spectrum before and after filtering would indicate if the signal is modified, as seen in Figure 5.20.

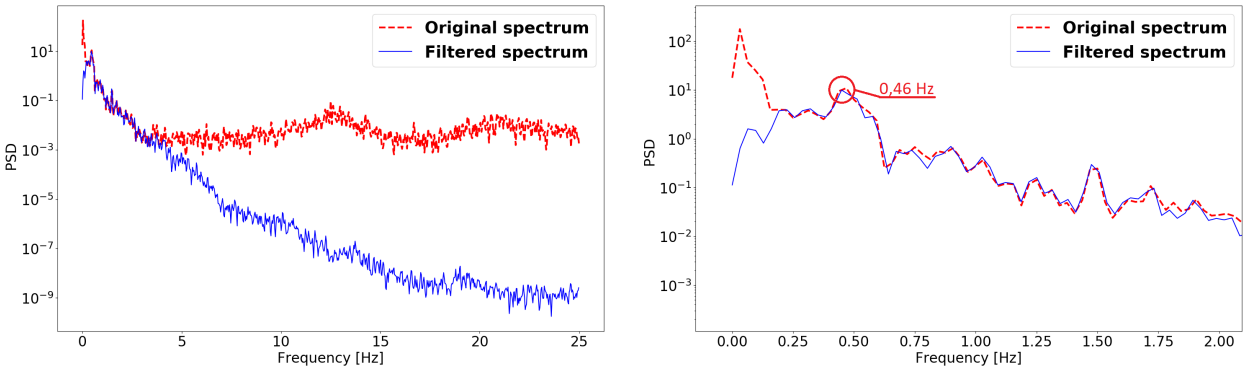

(a) Complete result of spectra **(b)** Spectra in electro-mechanical range

Figure 5.20: Welch's power spectra of measured signal

Figure 5.20a shows the entire resulting spectrum of the pre- and post-filtered signal, both of which are sampled at 50 Hz. As seen, the filtered spectrum indicates effective removal of all frequencies above approximately 4 Hz, with a clear decrease in power. Figure 5.20b gives a better view of the frequencies in the electro-mechanical range, where it can be seen that frequencies below 0.2 Hz have a significantly lower power level. For frequencies in the electro-mechanical range, it can be observed that filtering using EMD maintains the same power level, with only limited adjustments.

The next step is to estimate modal components in the EMD-filtered signal using the RRLS method, the result of which can be seen in Figure 5.21.

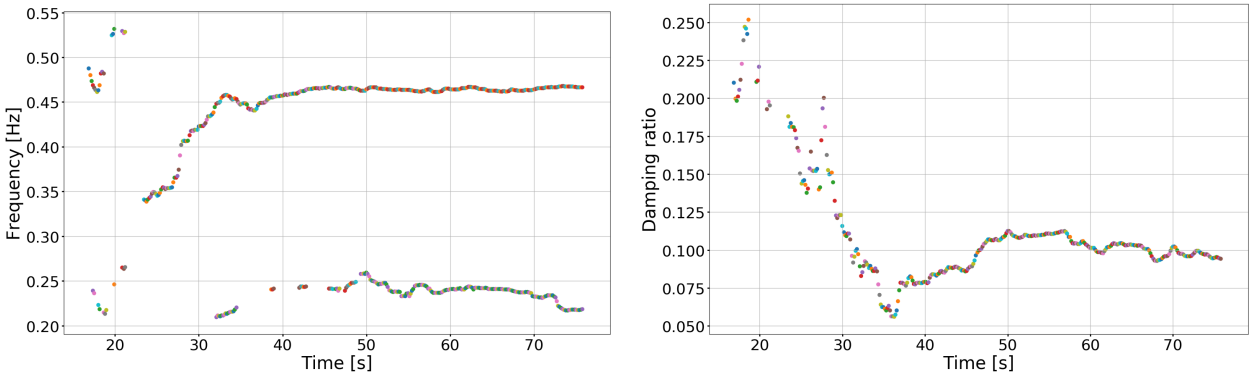

(a) Frequency **(b)** Damping ratio of the 0.467 Hz mode

Figure 5.21: Mode-tracking of identified modes in PMU signal

As seen in Figure 5.21a, one mode indicates convergence at a frequency of 0.467 Hz. The same mode is shown with damping in Figure 5.21b, where it can be noted that convergence is not as assured. With a downward trend on the damping, it gives an indication that convergence has not yet been achieved.

For the second mode with a frequency ending at 0.220 Hz, the damping is of such a magnitude that it is excluded from further analysis, although it can be noted that this mode was not indicated in Welch's power spectrum. Studying the clustering in one of the last timesteps indicates that the resulting modes are the ones actually present as seen in Figure 5.22.

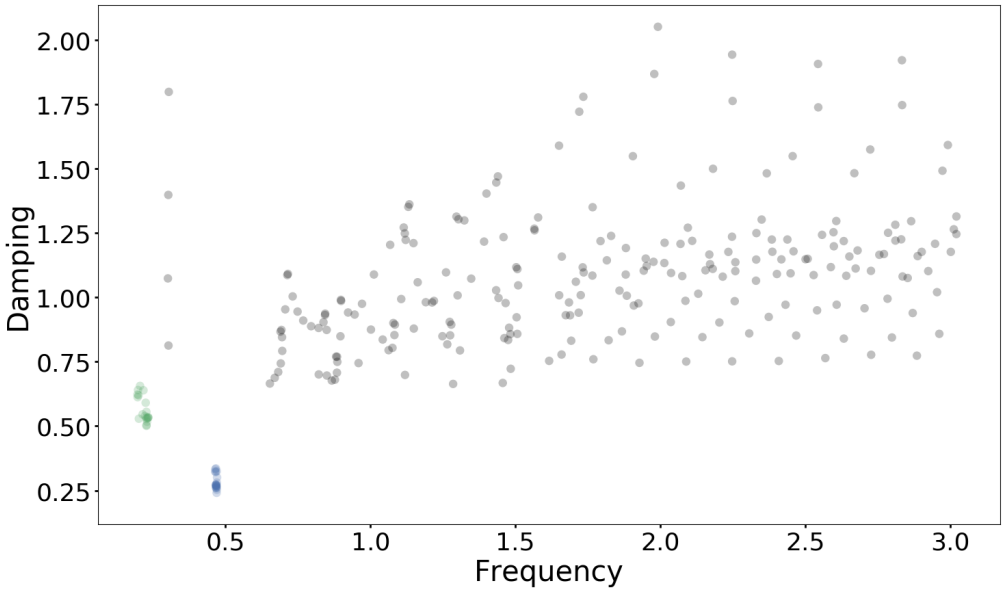

Figure 5.22: Clustering result after convergence

With two distinct clusters, both with occurrences in all of the 20 possible model orders, the number of modal components are clear. However, convergence is questionable, as the clusters are spacious. The extracted modal information is given in Table 5.6.

Table 5.6: Modes identified prior to ringdown

Mode	Freq. [Hz]	Damp. Ratio η	# occurrences
1	0.467	0.095	20 / 20
2	0.220	0.35	20 / 20

With a damping ratio of 9.5 %, the 0.467 Hz mode is well above the critical limit. It can be noted that the result of analysis using Welch's method indicates a mode in the area of 0.46 Hz as seen in Figure 5.20b, thus validating the result. The mode with a frequency estimated at 0.22 Hz, had a corresponding damping ratio equal 35 %.

Summarized Observations

- The timespan of ambient data must be of a length large enough to ensure convergence. In this section, the timespan of just over a minute is too short to give a convincing convergence.
- PMU-data sampled at 50 Hz improves pre-filtering using EMD, as it is possible to identify high-frequency noise at this sampling rate.
- Power spectral density indicates that the EMD-filter technique successfully removes both high frequency noise and low-frequency trend without altering modes in the electro-mechanical range.

5.2.3 Ambient data after ringdown

With two and a half minutes of data after ringdown, the timewindow is almost twice that of the ambient data prior to the event.

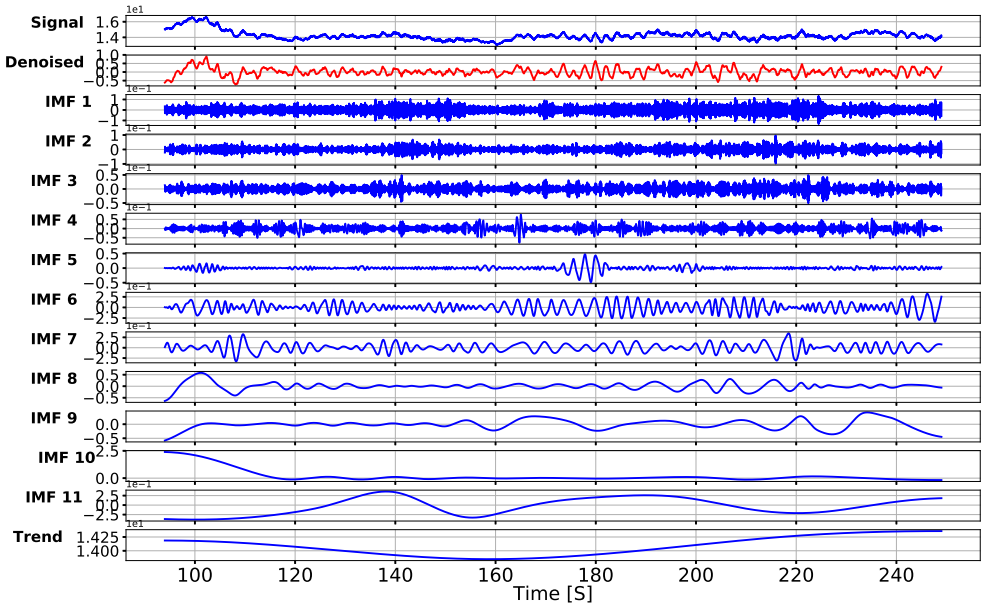

Figure 5.23: IMF plot of EMD result, extracting IMF 4-8

Figure 5.23 shows the Empirical Mode Decomposition, where IMF 4 through 8 are utilized for further analysis. The quality of filtering is tested using Welch's method as seen in Figure 5.24.

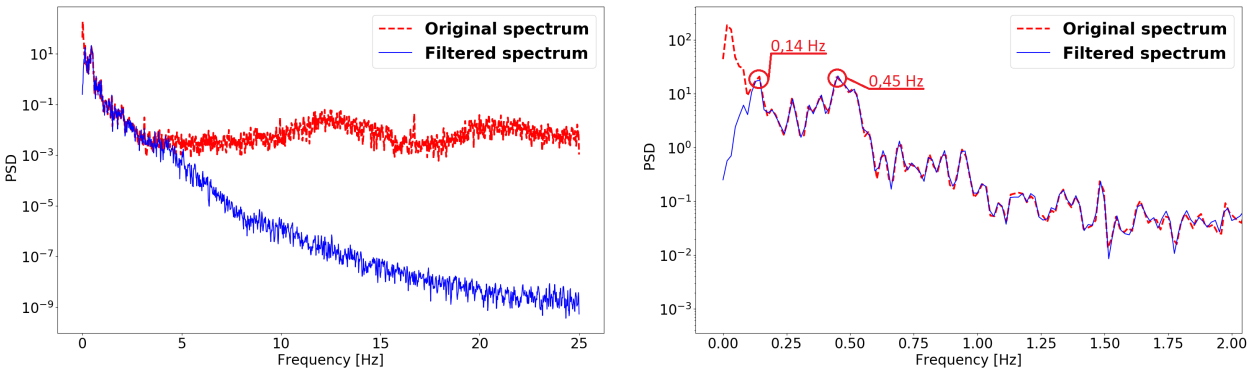

(a) Complete result of spectra **(b)** Spectra in electro-mechanical range

Figure 5.24: Welch's power spectra of measured signal

Similar to the data prior to the ringdown, Figure 5.25a indicates a clear filtering of high frequency noise. With more data to analyze, the spectrum is of higher detail than what was observed in Figure 5.20. This is clear when studying Figure 5.24b, where it can be seen that there has been only limited modifications in the electro-mechanical range. With the cutoff frequency in the lower region at 0.1 Hz, it can be noted that one of the two peaks with the highest power density is located just above with a frequency of 0.14 Hz.

Continuing with IMF 4-8 as validated by the spectrum, RRLS is applied, the result of which is presented in Figure 5.25.

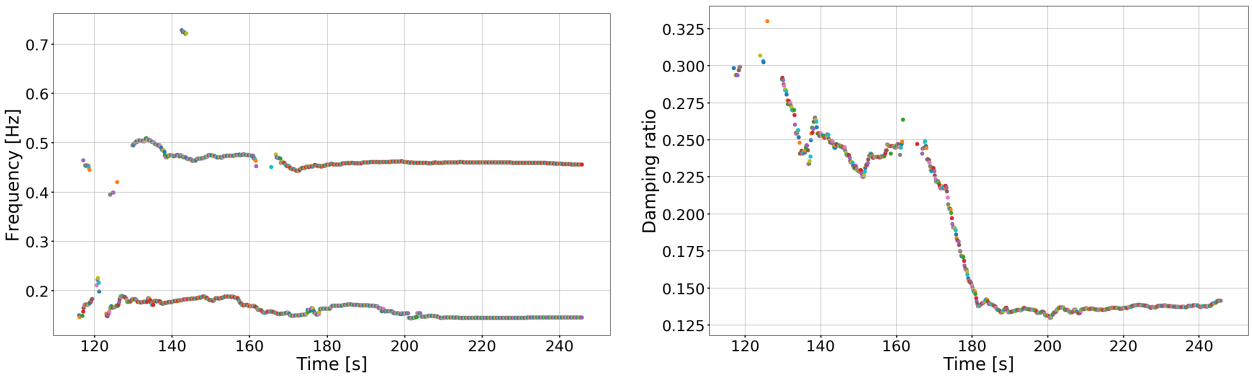

(a) Frequency **(b)** Damping ratio of the 0.455 Hz mode

Figure 5.25: Mode-tracking of identified modes in PMU signal

Figure 5.25a shows the identification of two modes in the signal, both of which appear in the power spectrum in Figure 5.24b. Both modes appear continuously except the highest frequency that contains a few seconds of missing results; however, it can be noted that this is prior to convergence.

The mode with the highest frequency, estimated at 0.455 Hz, is the one with the lowest damping. Figure 5.25b indicates that convergence in this mode is obtained approximately 80 seconds after the fault, where damping ratio stabilizes around 14 %.

The cluster plot in Figure 5.26 shows two clusters clearly separated from the remaining noise.

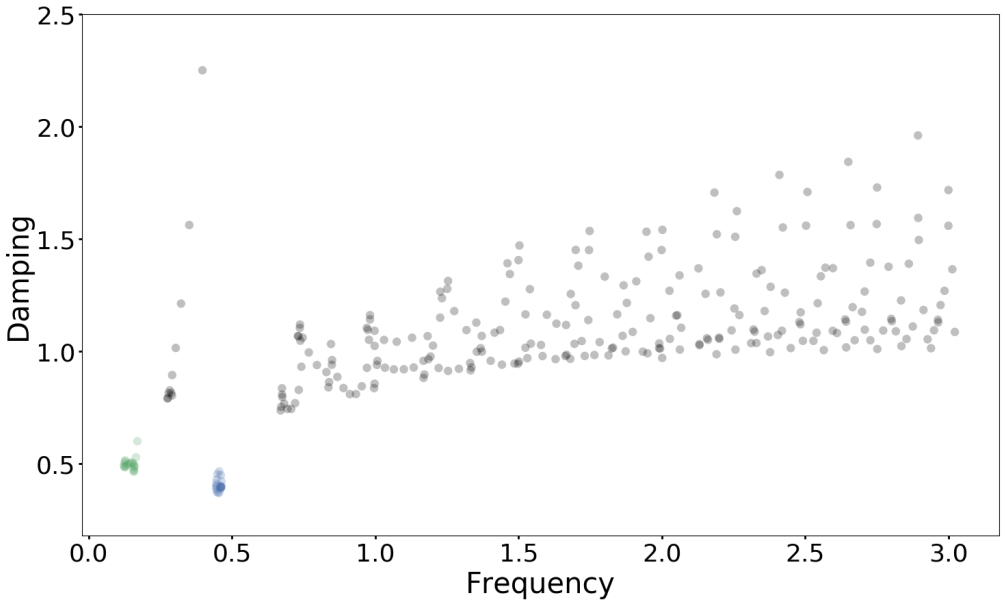

Figure 5.26: Clustering result after convergence

Both clusters identified contain 20 modal components from 20 different model order simulations, giving credibility to the estimate. The extracted modal information is presented in Table 5.7.

Table 5.7: Modes identified after ringdown

Mode	Freq. [Hz]	Damp. Ratio η	# occurrences
1	0.455	0.14	20 / 20
2	0.146	0.48	20 / 20

With a damping ratio at 14 %, the 0.455 Hz mode is well within critical damping limits. For the second mode at 0.146 Hz, the damping ratio is about 48 %.

Summarized Observations

- A longer stream of measurements improves the estimation accuracy of both RRLS and Whelch's method.
- Although highly damped, RRLS estimates two modes accurately compared with results from Welch's method.
- The cluster plot shows two dense clusters, both of which are present for the duration of the measured signal.

Case 2 summary

In this case with loss of generation, the change in frequency is limited when studying the mode with lowest damping ratio. With a variation of 0.02 Hz, the difference may simply be estimation error. The highest frequency estimated is during the ringdown, where the mode is estimated at 0.476 Hz. This is however from a signal that by visual inspection is not completely dominated by linear trends, and the result should be questioned because of the lower number of occurrences in the cluster.

The frequency estimated both prior to and after the ringdown matches those found by the respective analyses using Welch's method, increasing the estimation credibility.

The damping ratio is well within critical limits in both ambient and ringdown. The lowest damping ratio is estimated in the ambient data prior to the fault at 9.5 %, indicating that this area is sufficiently damped.

6 Concluding remarks and further work

A major concern of signal analysis is undoubtedly the data quality and content. Appropriate analysis of PMU measurements for electro-mechanical oscillations requires knowledge of the underlying phenomena. *Performance of any signal analysis method is never better than the quality of the signal itself.* Identifying a suitable area of measurement in the power system where ambient data along with ringdown data contain clear linear oscillations, is far from a trivial issue. Ambient data is particularly difficult, as visual inspection of both frequency and damping is hindered by the continuous, hidden inputs. A toolbox of comparable methods will reduce the impact of any one method's weaknesses, and facilitate better understanding of the measured values. Although the three methods investigated here reinforce each other, they should be accompanied by other methods with different assumptions and strengths.

Prony Analysis has been well established for system identification, yet requires clear ringdowns without significant noise or non-linearities. Much work in this thesis has gone towards improving the accuracy and robustness of PA as a signal analysis tool, while at the same time providing valuable insights into its main characteristics. Its sensitivity regarding model order should not be too high for a suitable ringdown. This trait is exploited so that *if* the sensitivity is high, no erroneous modes are found by the clustering algorithm. Thus PA becomes more user-friendly, which is of great importance for power system operators, who have a need for simple, yet reliable analysis tools.

PA is not the only parametric method sensitive to model order selection. Modal identification on ambient data using Robust Recursive Least Square, is based on the same principles. By exploiting its sensitivity to changing model order, trivial modes may be excluded. Generally, estimation accuracy and validity is a major concern in signal analysis. Through clustering, and subsequently the number of identified modes in each cluster, the weakness of parametric methods in this thesis is transformed to a strength for proper identification.

Clustering has yet another purpose when applying the RRLS method on ambient data. With automated selection of modes in each timestep, a seamless tracking of modes is possible. Hence, there is no need to pre-select the mode of interest, as all modes present will be pursued.

Filter application of Empirical Mode Decomposition has large potential in power system measurements, as the measurements contain non-linear and non-stationary dynamics. The parametric methods of Prony and RRLS have abilities to deal with small distortions in the signal, yet improve significantly if band-pass filtering is performed first. The performance of EMD filtering has been evaluated by the frequency spectrum estimate of Welch's method. Results show the capabilities of EMD in a power system setting, with a clear band-pass filtering of the signal without modifying the frequencies in the electro-mechanical range. Additionally, Welch's method provides a non-parametric frequency spectrum of the signal, which enables another way of identifying dominant modes. As no method is perfect, mutual verification contributes to increased legitimacy of the resulting estimate.

Concluding remarks

- The applied methods establish a signal analysis toolbox for power system identification in Smart Grids. Appropriate combination of the tools enables analysis of a variety of power system measurements.
- A comprehensive study of several techniques is presented in this thesis. Although their application is narrowed down to power system identification, most of the shown characteristics also hold true in the general field of signal analysis.
- EMD is successfully implemented and evaluated as a band-pass filter.
- Clustering automatically and accurately identify true, dominant modes in a signal for both Prony and RRLS.

Further work

Although the study has described successfully new applications of described techniques, continuous improvement is prudent. The last comments describe the open doors and possibilities the authors of this thesis have identified.

- Thorough investigation of ambient dynamics could pave way for dedicated analysis tools.
- A major concern is the acquisition of suitable PMU measurements. The location of the equipment, as well as the output variable, is important for correct identification. Optimal placement of PMUs for dynamic stability assessment should be subject to more investigation.
- The possibility for recursive EMD, or otherwise applying it in a real-time scenario could be of great value for certain applications. RRLS is tailored for near real-time purposes like mode-metering, and would benefit from a real-time filtering technique.
- The impact of forgetting factor on convergence and accuracy of RRLS should be investigated. Manual tuning is a hindrance for online applications, and a barrier for interested parties without significant experience with the method. A robust and simple solution would improve its user-friendliness significantly.
- Signal analysis leans on much empirical knowledge, and is a field with huge amount of data processing. Machine learning techniques like clustering will aid in uncovering patterns that are obscure to the human mind. Clustering has successfully proven its capabilities through improvements of both RRLS and PA; surely the methodology is applicable in a multitude of areas.

References

[1] Z. Huang *et al.*, "Mango – modal analysis for grid operation: A method for damping improvement through operating point adjustment," tech. rep., Pacific Northwest National Laboratory (U.S.), October 2010.

[2] J. Condren and T. W. Gedra, "Expected-security-cost optimal power flow with small-signal stability constraints," *IEEE Transactions on Power Systems*, vol. 21, no. 4, pp. 1736–1743, 2006.

[3] J. Machowski, "Power system dynamics : Stability and control," 2008.

[4] J. Hauer, "Initial results in prony analysis of power system response signals," *IEEE Transactions on Power Systems*, vol. 5, no. 1, 1990.

[5] F. Castaniè, *Spectral Analysis: Parametric and Non-Parametric Digital Methods*. London, UK: ISTE, January 2010.

[6] N. Zhou, J. W. Pierre, D. J. Trudnowski, and R. T. Guttromson, "Robust rls methods for online estimation of power system electromechanical modes," *IEEE Transactions on Power Systems*, vol. 22, no. 3, pp. 1240–1249, 2007.

[7] A. R. Messina, *Inter-area oscillations in power systems : a nonlinear and nonstationary perspective*. Power Electronics and Power Systems, New York: Springer, 2009.

[8] J. Thambirajah, E. Barocio, and N. Thornhill, "Comparative review of methods for stability monitoring in electrical power systems and vibrating structures," *IET Generation, Transmission and Distribution*, vol. 4, pp. 1086–1086, January 2010.

[9] C.-T. Chen, *Linear system theory and design*. Oxford series in electrical and computer engineering, New York: Oxford University Press, 3rd ed. ed., 1999.

[10] T. H. Park, "Linear time-invariant systems," in *Introduction To Digital Signal Processing*, pp. 122–144, World Scientific Publishing Co. Pte. Ltd., 2010.

[11] J. Machowski, J. W. Bialek, and J. R. Bumby, *Power system dynamics : stability and control*. Chichester: Wiley, 2nd ed. ed., 2008.

[12] D. Lynch, "Numerical partial differential equations for environmental scientists and engineers: A first practical course," in *Numerical Partial Differential Equations for Environmental Scientists and Engineers*, ch. 2.1, Springer US, April 2005.

[13] G. Prony, "Essai experimental–,-," *J. de l'Ecole Polytechnique*, 1795.

[14] N. Zhou, F. Zhenyu Huang, J. Tuffner, J. Pierre, and J. Shuangshuang Jin, "Automatic implementation of prony analysis for electromechanical mode identification from phasor measurements," pp. 1–8, IEEE Publishing, July 2010.

[15] G. Strang, *Introduction to linear algebra*. Wellesley, Mass: Wellesley-Cambridge Press, 4th ed. ed., 2009.

[16] B. Lathi, *Signal processing and linear systems*, ch. 9. Carmichael, Calif: Berkeley Cambridge Press, 1998.

[17] J. Hauer, "Application of prony analysis to the determination of modal content and equivalent models for measured power system response," *IEEE Transactions on Power Systems*, vol. 6, no. 3, 1991.

[18] B. Kovačević, M. Milosavljević, and M. D. Veinović, "Robust recursive ar speech analysis," *Signal Processing*, vol. 44, no. 2, pp. 125–138, 1995.

[19] H. L. Van Trees, *Detection, estimation, and modulation theory : Pt. 4 : Optimum array processing*, vol. Pt. 4. New York: Wiley, 2002.

[20] P. Welch, "The use of fast fourier transform for the estimation of power spectra: a method based on time averaging over short, modified periodograms," *IEEE Transactions on audio and electroacoustics*, vol. 15, no. 2, pp. 70–73, 1967.

[21] E. Jones, T. Oliphant, P. Peterson, *et al.*, "SciPy: Open source scientific tools for Python," 2001–. [Online; accessed ¡today¿].

[22] R. Kumaresan and Y. Feng, "Fir prefiltering improves prony's method," *IEEE Transactions on Signal Processing*, vol. 39, no. 3, pp. 736–741, 1991.

[23] J. Sanchez-Gasca and D. Trudnowski, "Identification of electromechanical modes in power systems," *IEEE Task Force Report, Special Publication TP462*, 2012.

[24] G. Rilling, P. Flandrin, P. Goncalves, *et al.*, "On empirical mode decomposition and its algorithms," in *IEEE-EURASIP workshop on nonlinear signal and image processing*, vol. 3, pp. 8–11, NSIP-03, Grado (I), 2003.

[25] P. Flandrin, G. Rilling, and P. Goncalves, "Empirical mode decomposition as a filter bank," *IEEE signal processing letters*, vol. 11, no. 2, pp. 112–114, 2004.

[26] J. Deshpande, "Pyhht tutorials." `http://pyhht.readthedocs.io/en/latest/tutorials.html`, 2015.

[27] O. B. Fosso and M. Molinas, "Method for mode mixing separation in empirical mode decomposition," September 2017.

[28] M. Ester, H.-P. Kriegel, J. Sander, X. Xu, *et al.*, "A density-based algorithm for discovering clusters in large spatial databases with noise.," in *Kdd*, vol. 96, pp. 226–231, 1996.

[29] J. Erman, M. Arlitt, and A. Mahanti, "Traffic classification using clustering algorithms," in *Proceedings of the 2006 SIGCOMM workshop on Mining network data*, pp. 281–286, ACM, 2006.

[30] D. H. Johnson, "Signal-to-noise ratio," *Scholarpedia*, vol. 1, no. 12, p. 2088, 2006.

[31] C. E. Shannon, "Communication in the presence of noise," *Proceedings of the IRE*, vol. 37, no. 1, pp. 10–21, 1949.

[32] B. S. Everitt, "Nyquist frequency," 2002.

[33] J. D. Broesch, *Digital signal processing demystified*. Engineering mentor series, Solana Beach, Calif.: HighText publications, 1997.

[34] G. D'Antona, *Digital Signal Processing for Measurement Systems : Theory and Applications*. Information technology–transmission, processing, and storage Digital signal processing for measurement systems, Springer US, 2006.

[35] J. W. Ning Zhou, D. Pierre, and D. Trudnowski, "A stepwise regression method for estimating dominant electromechanical modes," *Power Systems, IEEE Transactions on*, vol. 27, pp. 1051–1059, May 2012.

[36] *Inter-area Oscillations in Power Systems: A Nonlinear and Nonstationary Perspective*. Power Electronics and Power Systems, Boston, MA: Springer US, 2009.

[37] P. Kundur, *Power system stability and control*. The EPRI power system engineering series, New York: McGraw-Hill, 1994.

[38] C. Paleologu, J. Benesty, and S. Ciochina, "A robust variable forgetting factor recursive least-squares algorithm for system identification," *IEEE Signal Processing Letters*, vol. 15, pp. 597–600, 2008.

A Appendix - Paper to be published

Prony's method as a tool for power system identification in Smart Grids

Sjur Føyen
Dept. of Electric Power Eng.
NTNU
Trondheim, Norway
sjur.foyen@gmail.com

Mads-Emil Kvammen
Dept. of Electric Power Eng.
NTNU
Trondheim, Norway
mekvammen@gmail.com

Olav Bjarte Fosso
Dept. of Electric Power Eng.
NTNU
Trondheim, Norway
olav.fosso@ntnu.no

***Abstract*—This paper investigates the theory, intuition and performance of two known implementations of Prony's method. Such methods are useful for identifying the individual modes of a system without constructing a component-based model. In the Smart Grid, Prony Analysis has been widely used on post-disturbance ring-down measurements, which have been increasingly available with the extensive deployment of PMU's. Both methods decompose the signal into decaying sinusoidals, and estimate the frequency, damping, amplitude and phase of each modal component. The first method is based on the original Prony's method, whilst the second method is based on the thought that the system can be viewed as a digital synthesis problem where the system has the properties of an infinite impulse response filter. Both methods employ EMD-based pre-filtering. Additionally, a cluster based approach is proposed for circumventing the issue of determining model order, so that the true modes of the estimation can be distinguished from the trivial modes.**

***Index Terms*—Prony Analysis, model order, modal analysis, signal processing, linear prediction model, linear time-invariant systems, clustering, empirical mode decomposition**

I. Introduction

Prony's method with it's variations are ways for extracting modal information from a signal. The signal is modeled as a sum of damped, complex exponentials - or equivalently - decaying sinusoidals. The goal is to determine the frequency, damping, phase and amplitude of these components. The first description of such a method is not new, in fact, it was first discovered by Gaspard de Prony in the 18th' century [1]. Several of the involved process tasks are demanding, like rooting a high order polynomial and performing linear least-square estimation, although with present computing power these have become trivial matters. Prony Analysis (PA) for power system ringdown analysis was initiated in 1990 by J.F. Hauer [2]. Since then, significant research has been made in order to tackle low-damped small-signal oscillations in the power system. High frequency measurement equipment like Phasor Measurement Units, have been instrumental to the implementation of real-time observation and control of the Smart Grid. Huang *et al.* [3] gives a thorough presentation of the motivation for measurement-based mode tracking and control, and presents a tool for aiding operating personnel.

Different versions of Prony have recently been implemented and used for practical, industrial purposes in the power system sector, as seen in [4] and [5]. Prony's method can be classified as a linear modal estimation technique, and is used on ringdown signals where the modal components are observable. There are other methods in this category, as the Matrix Pencil method and the Eigensystem Realization Algorithm (ERA) [6]. In industry as well as academia, non-linear methods for modal estimation are emerging. The Variable Projection method is one example of this [6].

The motivation for this paper is to address some of the major issues with Prony analysis as a measurement-based modal estimation technique. Empirical mode decomposition (EMD) is used as a robust pre-filtering technique to remove high frequency noise. Clustering methods for all modes found by running Prony for multiple model orders, are used to avoid the need for specifying this in advance. The latter reduces the need for *a priori* knowledge of the signal, and more importantly, increases the trustworthiness of the results.

As most documentation available rely on heavy experience from signal analysis theory, this paper aims at providing a pedagogical introduction to the underlying concepts of each method. They will be described and demonstrated as general signal analysis tools, yet the paper is partly influenced by the Smart Grid perspective. The first method is here referred to as **Original Prony** (abbreviated PA_O), as it is the same theory as initially used by Gaspard de Prony. The second is named **Prony Filter** (PA_F), for it is implemented from the perspective of digital filter theory [7]. However, both arrive at the same end-point, the modal decomposition information of the signal. Note that both methods are implemented as off-line, block-processing methods. This is to reduce the comprehensiveness of the theory. For real-time applications, the reader is referred to the improved recursive Prony algorithm proposed in [8].

Three steps are made for testing the two methods. The first is to create synthetic signals, so that the desired outcome is known. Secondly, time-domain simulations are

done for a small power system model, where the desired information is partially known through linearization of the component-based model. The final step is to test with PMU data from real world Smart Grid event.

II. Theory

A. Discretization

Although there are different ways of conducting a Prony analysis, they all rely on important concepts in the field of signal analysis. In order to fully understand any implementation of Prony, it is essential to be familiar with these concepts. The starting point is to determine the desired model as a Linear Time-Invariant (LTI) system. Such a system can be characterised entirely by a single function called the system's impulse response. LTI systems are subject to several mathematical concepts laid out in [9]. An example of a time-continuous LTI model is given below.

$$c_2\frac{\delta^2 y(t)}{\delta t^2}+c_1\frac{\delta y(t)}{\delta t}=d_2\frac{\delta^2 x(t)}{\delta t^2}+d_1\frac{\delta x(t)}{\delta t}+d_0 x(t) \quad (1)$$

where $y(t)$ = response (output), $x(t)$ = excitation (input) and c, d = constant coefficients.

This describes the system as a time-continuous model. However, the measurement values are obtained as samples at discrete time points. Thus, the model must be described with finite differences, that is, with discrete equations. This conversion is of course not necessary if the physical phenomena actually is discrete. However, as many models are time-continuous, this theory serves as a connection between the time-continuous model, and the sinusoid information obtained through the discrete analysis of Prony.

$$\begin{aligned} y(t) &= y[n] \\ \frac{\delta^p y(t)}{\delta t^p} &= \frac{\nabla^p y[n]}{h^p}+O(h) \end{aligned} \quad (2)$$

where O(h) is leading error of order h and

$$\frac{\nabla^p y[n]}{h^p} \propto y[n]-y[n-1]-\ldots-y[n-p]$$

where (2) shows the relationship between derivatives and backward finite differences [10]. Rewriting (1) as an approximated discrete system yields:

$$a_0 y[n]+a_1 y[n-1]+a_2 y[n-2]=b_0 x[n]+b_1 x[n-1]+b_2 x[n-2] \quad (3)$$

where a and b are coefficients different from - but related to - c and d in (1).

Rearranging, and generalizing to p previous values for y, and q previous values for x gives the general difference equation shown in (4).

The estimation of a_i and b_i is the desired information for deriving the modal decomposition of the signal. From this point on, the derivation of the two methods will differ.

$$y[n]=-\sum_{i=1}^{p} a_i y[n-i]+\sum_{i=0}^{q} b_i x[n-i] \quad (4)$$

B. Original Prony

PA_O assumes zero input to the system, which eliminates the b_i-terms. This difference equation represents a Linear Prediction Model (LPM). Having N number of samples, and choosing a model order p, the LPM can be extended to (5) by stating that the difference equation should be satisfied for the previous $(N-p)$ measurements:

$$\underbrace{-\begin{bmatrix} y[N-1] \\ y[N-2] \\ \vdots \\ y[p] \end{bmatrix}}_{=\mathbf{b}} = \underbrace{\begin{bmatrix} y[N-2] & y[N-3] & \cdots & y[N-p-1] \\ y[N-3] & y[N-4] & \cdots & y[N-p-2] \\ \vdots & \vdots & \ddots & \vdots \\ y[p-1] & y[p-2] & \cdots & y[0] \end{bmatrix}}_{=\mathbf{A}} \cdot \begin{bmatrix} a_1 \\ \vdots \\ a_p \end{bmatrix} \quad (5)$$

This is an over-determined system for $N > 2p$, with $(N-p)$ rows and p columns. For solving this system, the linear least-square approximation method is used, yielding an estimation of the **a**-coefficients that will describe a model close to the measured values. This method is intuitively described in [11, Ch. 4.3].

The next step is to connect these predictor coefficients to the modal decomposition. This is done through the Z-transform. It is shown in [12] that they form the characteristic equation in (6):

$$1+a_1 z^{-1}+\ldots+a_p z^{-p}=0 \quad (6)$$

The polynomial is factorized in order to obtain the roots of the polynomial (e.g. by using the freely available numpy.roots in python).

These roots are closely linked to the eigenvalues of the modal decomposition in the following manner:

$$\lambda_n = f_{samp}\ln\zeta_n \quad (7)$$

Where f_{samp} is the sampling frequency of the input signal and ζ_n is the corresponding polynomial root. From the eigenvalues, the frequencies f and damping ratios η are found:

$$f_n=\frac{|Im(\lambda_n)|}{2\cdot\pi} \qquad \eta_n=\frac{Re(\lambda_n)}{|\lambda_n|} \quad (8)$$

The amplitude and phase of the modal components are estimated by another least-squares approximation. Extending equation (9) to all measurement values, results in equation (10), as stated in [13].

C. Prony filter

In this Prony variation, the perspective is slightly different. The system is assumed to be a Linear Time-Invariant system (LTI-system) with the properties of an Infinite Impulse Response filter (IIR-filter) [14, chap. 10].

$$y[k] = \sum_{i=1}^{p} C_i \zeta_i^k, \quad k = 0, 1, ..., N-1 \tag{9}$$

Where $C_i = \frac{1}{2} A_i e^{\pm j\phi_i}$

$$\begin{bmatrix} y[0] \\ y[1] \\ \vdots \\ y[N-1] \end{bmatrix} = \begin{bmatrix} \zeta_1^0 & \cdots & \zeta_p^0 \\ \zeta_1^1 & \cdots & \zeta_p^1 \\ \vdots & \ddots & \vdots \\ \zeta_1^{N-1} & \cdots & \zeta_p^{N-1} \end{bmatrix} \cdot \underbrace{\begin{bmatrix} C_1 \\ C_2 \\ \vdots \\ C_p \end{bmatrix}}_{=\mathbf{C}} \tag{10}$$

Modelling the system as an IIR-filter means that an impulse is assumed to excite the system at time $t = t_0$ through the system transfer function, which results in a time-response that is possible to measure. This can be viewed as a digital synthesis problem, which means that the desired information is an approximated transfer function that models the system response as close as possible.

By utilizing the Z-transform and its timeshift operator on the difference equation in (4), the transfer function of the system can be obtained.

$$\begin{aligned} Z\{y[n]\} &= -a_1 Y(z) z^{-1} - \ldots - a_p Y(z) z^{-p} + b_0 X(z) + \ldots + b_q X(z) z^{-q} \\ &\Downarrow \\ Y(z) &= -Y(z)\left(a_1 z^{-1} + \ldots + a_p z^{-p}\right) + X(z)\left(b_0 z^0 + \ldots + b_q z^{-q}\right) \\ &\Downarrow \\ Y(z)\left(1 + a_1 z^{-1} + \ldots + a_p z^{-p}\right) &= X(z)\left(b_0 + \ldots + b_q z^{-q}\right) \\ &\Downarrow \\ \frac{Y(z)}{X(z)} &= H(z) = \frac{b_0 + b_1 z^{-1} + \ldots + b_q z^{-q}}{1 + a_1 z^{-1} + \ldots + a_p z^{-p}} \end{aligned} \tag{11}$$

The main difference in the two methods can be seen already. PA_O assumes all input to be zero - eliminating the terms with **b**-coefficients from the difference equation. In PA_F all input is zero, *except* $x[0]$ which is equal to 1, resulting in q zeros in the transfer function. An important assumption in PA_F is that the resulting IIR filter is causal. This is ensured if the order of the denominator p is greater that the order of the nominator q [14, p. 145], and that the signal prior to $t = t[0]$ is assumed to be zero. To ensure this, and to avoid unnecessary computations without much improvement of the result, the q-order is set to $p-1$.

It can be noted that the coefficients are strictly real numbers. From the general difference equation, inserting $x[0] = 1$ and remembering that b_n equals zero for $n > q$, the equation system shown in equation (12) can be obtained.

Firstly, the least square solution for the **a**-coefficients in equation (12) is found for $n = q+1$ to $n = N$, similar to equation (5). Note that given the same p-order, PA_F utilizes $p-q-1$ more equations than PA_O for determining the **a**-coefficients.

$$\begin{aligned} n = 0&: \; b_0 - y[0] = 0 \\ n = 1&: \; b_1 - y[1] - a_1 y[0] = 0 \\ &\vdots \\ n = q&: \; b_q - y[q] - a_1 y[q-1] - \ldots - a_q y[0] = 0 \\ n = q+1&: \; -y[q+1] - a_1 y[q] - \ldots - a_{q+1} y[0] = 0 \\ &\vdots \\ n = p&: \; -y[p] - a_1 y[p-1] - \ldots - a_p y[0] = 0 \\ &\vdots \\ n = N&: \; -y[N] - a_1 y[N-1] - \ldots - a_p y[N-p] = 0 \end{aligned} \tag{12}$$

The next step is to solve for the **b**-coefficients by using equation (12) for $n = 0$ to $n = q$. There is no need for least-square approximation as this system has only one unique solution.

The eigenvalues, and thus frequency and damping, can be found from the roots of the denominator (poles) in equation (11) (similar to PA_O). The very same roots are used in a Laurent series expansion of the transfer function, to find the amplitude and phase of the modal components.

$$H(z) = \frac{R_1}{z^{-1} + \zeta_1} + \ldots + \frac{R_p}{z^{-1} + \zeta_p} \tag{13}$$

Where R_n is the residue connected to the pole ζ_n for n from 1 to p. It is important to remember that the poles appear in complex conjugate pairs in this calculation. The residue is given as a complex value where the amplitude and phase can be found from the absolute value and angle respectively. To find the modes and thus frequency and damping, the poles need to be scaled as shown in equation (7). Lastly, the frequency and damping is found using equation (8).

D. EMD

There exists a variety of solutions to improve PAs robustness under noisy conditions. Kumaresan and Feng [15] propose two different pre-filtering methods to improve PA, one based on a predefined FIR filter and one defining the pre-filter iteratively from the measured data. Pre-filtering using the EMD-technique is also proposed in [16].

In this paper, Empirical Mode Decomposition (EMD) is used as a band pass filter, removing high frequency noise and the signal trend. EMD is a method for nonlinear, non-stationary signal processing that decomposes the signal into a set of Intrinsic Mode Functions (IMFs) [17]. The conditions for an IMF are that its mean value is zero, and that the number of extremas equals the number of zero-crossings (or at most differs by one). The stepwise process to identify IMFs in a measured signal $y(t)$ is:

1) Start with signal y(t) as input
2) Identify extremas
3) Calculate the upper and lower envelope of the signal (e_{up}, e_{down})

4) Find the mean value ($m(t)$) of the upper and lower envelope
5) Extract the difference from the signal: $d(t) = y(t)$ - $m(t)$
6) Repeat step 2-5 with $d(t)$ as input, until it satisfies the conditions of an IMF
7) Set $d(t)$ as an IMF, and subtract it from the input signal. Repeat the process with the residue $r(t)$ as input signal ($r(t) = y(t)$ - $d(t)$)
8) Continue until there are no more extrema present in signal

The EMD output extracts modal components starting with the highest frequency and ending with the residual "trend" of the signal. The hierarchy in the decomposed modes gives the EMD characteristics similar to that of a dyadic filter bank [18]. The average frequency of each IMF, gives a rough criterion for choosing which IMF to include in the filtered signal. By merging the IMFs with an average frequency in the electro-mechanical range (oscillating frequency from 0.2 to 2 Hz), the high frequency components and the signal trend (given by the residual) is excluded, and a filter has been implemented.

One challenge when using the EMD, is that modes with closely spaced frequencies may be mixed together. This makes the basic version of EMD more challenging for identification of electro-mechanical modes unless special strategies are used for intermittent or closely-spaced tones as described in [19]. For high frequency filtering on the other hand, its characteristics are well suited, as it elegantly extracts high frequency components without altering the remaining signal components.

In this paper, the EMD implemented is based on the work by Deshpande [20].

E. Cluster

To solve the problem of identifying the number of modes present in a signal, and thus solve the challenge of model order selection, this paper proposes to run PA in a range of model orders. By performing PA with every model order between a lower and a higher limit, the idea is that the true modes and their shapes will remain close to constant. True modes are those that are responsible for actual linear behaviour in the system. Subsequently, the trivial modes (identified by their frequency, damping and amplitude) will change significantly. Trivial modes are those that fit the noise and nonlinear behaviour.

A lower limit of $p = 10$ and an upper limit of $p = N/2$ is chosen for the model order range to ensure a good basis for clustering. The lower limit is defined as 10 to mitigate simulations where the number of observable modes is larger than the model order.

The clustering method used in this paper is a density-based algorithm named "Density-based spatial clustering of applications with noise" (DBSCAN). This method was first proposed by Ester *et al.* [21], to make clustering more versatile. Density-based algorithms are not limited to finding spherical clusters of a predefined size. It can on the other hand, by considering the density of an area, find clusters of arbitrary shapes. It works as an unsupervised learning mechanism, labelling data in clusters and assigning the rest as noise [22].

The DBSCAN algorithm depends on two input parameters: epsilon (ϵ) and minimum cluster size (minClu). By firstly assuming that none of the input-data belongs to a cluster, DBSCAN chooses one of the unassigned objects as a starting point p. From this point all objects within a distance of ϵ is considered as a neighbour. If the point p is found to be a core point [21], it finds all objects in its area using ϵ and minClu. All these objects are then assigned to the same cluster. If p is not considered as a core object, and is not present in another cluster, it is labelled as noise. The clustering is completed once every object is either assigned to a cluster or labelled as noise.

In this paper, the input data for DBSCAN is three-dimensional. Frequency, damping and amplitude of all identified modes from all model order simulations of PA are utilised. For weighting purposes, the algorithm is altered so that only a small deviation in frequency is allowed. For amplitude and damping, some deviation is accepted in each cluster.

III. Remarks on implementation

The modes of interest in this paper, lies in the electro-mechanical range. In accordance with the Nyquist-Shannon sampling theorem [23], the sampling frequency must be at least 4 Hz to contain information of the modes at 2 Hz. In this paper the sampling frequency is set to 6 Hz, well above the minimum limit, to avoid loss of modal information. For data sampled at higher frequencies, approximately 6 Hz is achieved through downsampling. The sampling theorem applies to the high frequency noise as well. When the sampling frequency is below twice the noise frequency, information is lost and signal aliasing occurs [24]. To assure that this problem is handled, the signal is filtered for high frequency noise by using the EMD-technique, without altering the components in the electromechanical range.

For higher model orders, many of the modes found by PA have insignificant amplitudes, or very high damping ratios. These are filtered out before feeding the clustering algorithm with the modes, as they do not influence the signal dynamics. Choosing a hard limit on mode amplitude (1/30 relative to highest amplitude), and excluding modes with damping ratio above 50%, is a brute way of post-filtering the results. A more sophisticated evaluation method is presented by Zhou, Pier and Trudnowski [25]. However, the hard limit is sufficient for this method, with the purpose of removing the obvious trivial modes. The clustering algorithm is responsible for classifying the rest.

A. Proposed method

- Pre-Filtering using EMD

  - Identify signal IMFs
  - Extract IMFs in the electro-mechanical range
  - Rebuild signal without high frequency noise and signal trend
- Downsample signal to 6 Hz
- Define range of model orders to be investigated
- Do PA for all p orders in defined range
- Cluster the resulting modes

B. Steps of PA

PA_O :

- Build LPM in (5)
- Estimate **a**-coefficients using least-squares
- Find roots of characteristic polynomial in (6)
- Calculate eigenvalues from roots with (7)
- Establish equation system shown in (10)
- Solve the equation system for residual **C**

PA_F :

- Define q as $p-1$
- Build equation system in (12)
- Obtain least-square solution for **a**-coefficients
- Utilise q first equations to obtain **b**-coefficients
- Insert **a**- and **b**-coefficients into transfer function in (11)
- Calculate Laurent series expansion of transfer function with (13)
- Calculate eigenvalues from roots of denominator
- Find residual from denominator

Common for both methods :

- Calculate frequency and damping from eigenvalue
- Calculate amplitude and phase from residual
- Post-filter of insignificant modes

IV. Testing

A. Synthetic signal

First, the two methods will be demonstrated for synthetic signals. 3-dimensional plots are used to demonstrate the clustering method, as well as how the results of the Prony analysis vary with the model order.

$$\begin{aligned} y(t) = {} & 16cos(2\pi * 1.55 + 1.5\pi)e^{-0.25t} \\ & + 30cos(2\pi * 0.28 + 0.5\pi)e^{-0.04t} \\ & + 20cos(2\pi * 0.75 + 0.2\pi)e^{-0.3t} \end{aligned} \tag{14}$$

The synthetic signal tested is shown in equation (14), and contains three modes with a damping ratio (η) of 0.026, 0.023 and 0.064 respectively.

The three coloured dots in Figure 1 are actually clusters, each consisting of 55 data points obtained from PA_O, equalling the number of runs with different model orders. These results are only shown to demonstrate that the modal decomposition will be determined exactly for all model orders in the defined range, given a pure sinusoidal signal like this. Averaging each cluster, yields the modal components of equation (14) to a precision of 8 decimals. The results are similar for PA_F.

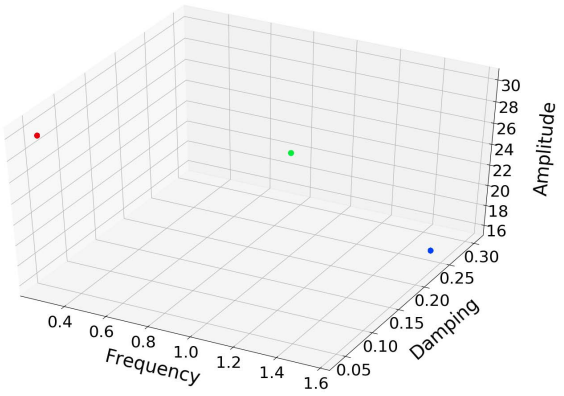

Fig. 1: Clustering of pure, synthetic signal

Introducing noise to the signal will degrade the performance of Prony, as experienced by previous authors [25]. Given the same synthetic signal, embedded in 20 dB white Gaussian noise, the performance of the EMD-filter Prony can be evaluated.

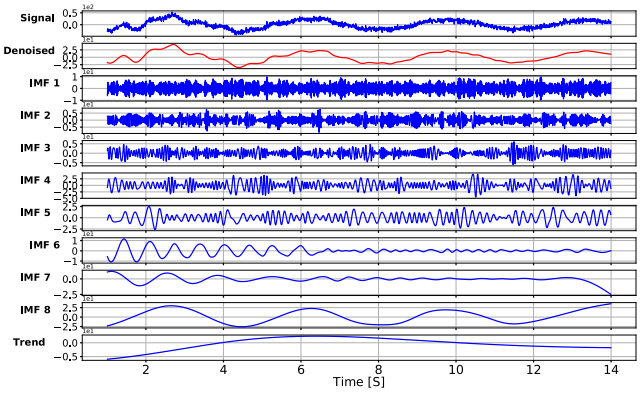

Fig. 2: Decomposing noisy signal using EMD

Summation of IMF 6 - IMF 8, yields the red, filtered signal in Figure 2. Clustering and averaging yields the modal components shown in Table I. The signal is reconstructed using only these modes in Figure 3b, which yields a signal-to-noise ratio (SNR) of approximately 43.5 dB for both methods when comparing with the EMD-filtered signal.

As seen in Table I, the frequency and damping ratio has minor deviations (less than 1/100) compared to the original signal. Amplitude and phase deviates slightly more, but are still close to original when comparing with the noise that was added to the system. When comparing the two methods, it is observed that the differences are negligible.

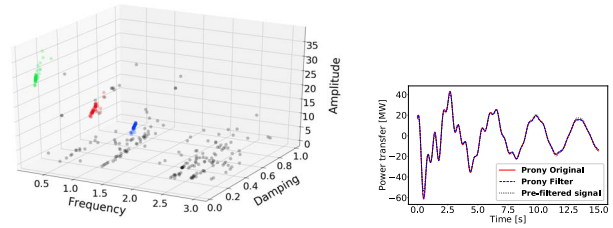

(a) Clustering of noisy, synthetic signal **(b)** Reconstruction

Fig. 3: Analysis of PMU-data

TABLE I: Consistent modes for multiple model orders

PA_O				PA_F			
Freq. [Hz]	η	**Amp.**	**Phase [rad]**	**Freq. [Hz]**	η	**Amp.**	**Phase [rad]**
0,755	0,069	21,96	$0{,}18\pi$	0,756	0,069	21,64	$0{,}18\pi$
0,278	0,026	31,42	$0{,}52\pi$	0,278	0,030	31,48	$0{,}53\pi$
1,548	0,027	16,92	$1{,}52\pi$	1,548	0,027	16,82	$1{,}52\pi$

B. Power Factory simulation

The next step is to test on measurements from a Power Factory (PF) model. The model used is the *Kundur Two Area Model* [26, p. 813] showed in Figure 4 .

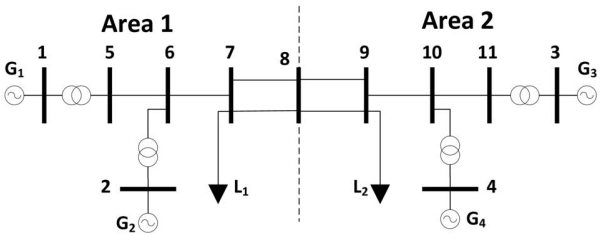

Fig. 4: Kundur Two Area System

To simulate a larger fault and create oscillations, the line between bus 6 and 7 are disconnected and reconnected 0.05 s later. Power flow measurements between bus 5 and 6, and bus 10 and 11, are then analyzed to identify modes.

Using the built-in modal analysis tool in PF, the frequency and damping of the modal components present in the system are found. It must be kept in mind that it will find all modes, and not just those that are excited by a given fault. The oscillatory modes identified by PF are:

TABLE II: Modes identified by PF

Mode	**Freq. [Hz]**	**Damp. Ratio** η
1	0,475	0,024
2	0,700	0,052
3	0,989	0,110

PF calculates the modal components present based on steady-state snapshot of the power system. In this test, variable load was added in order to better simulate the real world grid. Ambient noise was simulated as Gaussian white noise, similar to the synthetic signal. Furthermore, the ambient noise included an increase in the mean of the load 5 seconds into the time window of analysis. The result of this can be seen in Figure 5. The signal-to-noise ratio of the signal with variable load compared to the constant load signal, is approximately 10 dB for both lines. It can be noted that adding the ambient noise reduces the damping of the signal, as well as shifting the signal slightly. This continuous change in the system, makes the comparison of the modal estimation to the PF modes in Table II less trivial, as the modes change in each time-step. The assumption is then, as it was for the synthetic signal, that linear behaviour dominates the ringdown signal.

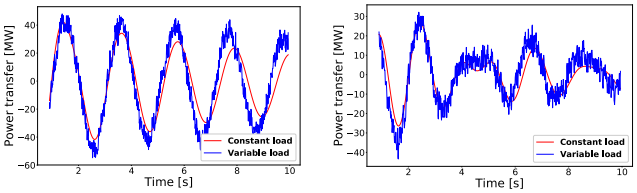

(a) Line 10-11 **(b)** Line 5-6

Fig. 5: Comparing measured signal for same fault with and without load variation

Running both PA_O and PA_F on the constant load signal, resulted in both methods identifying all three modes in the measurements from line 5-6 and line 10-11. Reconstructing and comparing to the measured signals, resulted in a signal-to-noise ratio of 50 dB and 63 dB for line 5-6 and line 10-11 respectively. The results were close to identical in PA_O and PA_F. It was also noted that for line 5-6, the 0.475 Hz mode and 0.700 Hz mode in Table II were both observable, while it was barely possible to distinguish the 0.989 Hz mode. For line 10-11, only the 0.475 Hz mode was distinguishable with a large magnitude, while the other two were small (just above 1/30 of the magnitude). With a close to 180° phase shift between the two areas, the 0.475 Hz mode is identified as a clear inter-area mode.

Figure 6a shows the ringdown signal with ambient noise. By using the EMD-method as a filter to remove high frequency components and the trend, the signal shown in Figure 6b is obtained.

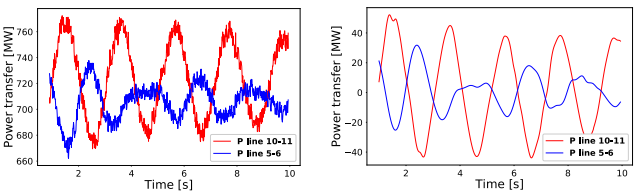

(a) Measurements before EMD-filtering **(b)** Measurements after EMD-filtering

Fig. 6: Measured signal

It can be observed that the EMD-filter removes most of the noise in the signal. Applying PA_O and PA_F combined

with clustering, gives the modal estimation shown in Table III and IV.

TABLE III: Modes identified from measurements on line 5-6

PA_O				PA_F			
Fre. [Hz]	η	**Amp.**	**Phase [rad]**	**Fre. [Hz]**	η	**Amp.**	**Phase [rad]**
0,489	0,034	20,900	$0{,}50\pi$	0,489	0,036	20,961	$0{,}53\pi$
0,710	0,048	16,153	$0{,}02\pi$	0,710	0,047	15,374	$0{,}02\pi$

TABLE IV: Mode identified from measurements on line 10-11

PA_O				PA_F			
Freq. [Hz]	η	**Amp.**	**Phase [rad]**	**Freq. [Hz]**	η	**Amp.**	**Phase [rad]**
0,486	0,014	47,946	$-0{,}52\pi$	0,486	0,015	47,999	$-0{,}52\pi$

The results are as expected not identical to Table II. The ambient noise has altered both frequency and damping, compared with results from PF as seen in Figure 5. From the measurements on the line between bus 5 and 6, only two of the modes are found. This was as expected, since these two were the most observable in the signal, while the last one barely was present. Similarly, only the most observable mode from the noise free test was found in line 10-11.

One important note is that the mode with the smallest damping ratio found by PF, still is the most critical mode with ambient noise included. With a phase-shift close to 180°, the mode oscillates between the two areas. The 0.700 Hz mode on the other hand, was barely present in Area 2 in the noise free signals and can be labelled as a local mode in Area 1. By plotting the estimated modes together with the signal after filtering, the estimation accuracy can be evaluated as seen in Figure 7.

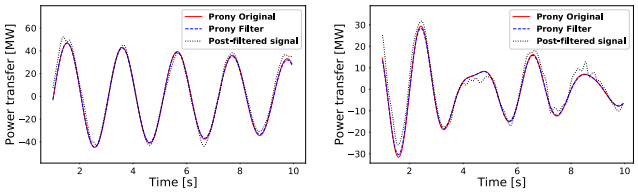

(a) Line 10-11 **(b)** Line 5-6

Fig. 7: Comparing measured signal after EMD-filtering with identified modes

The curve fit seen in Figure 7a and 7b shows that the modal components dominating the signal has been identified. PA_O and PA_F perform similarly, both estimations yielding SNR of 35 dB for Figure 7a and 22 dB for Figure 7b.

C. PMU-data

In this section, PMU-data from the nordic grid is analyzed. The PMU-measurements contain information of a production outage, with resulting oscillations in the grid. Identification of this oscillation is vital for stable operation in a smartgrid. Figure 8 shows the PMU-measurement, with the ringdown portion magnified.

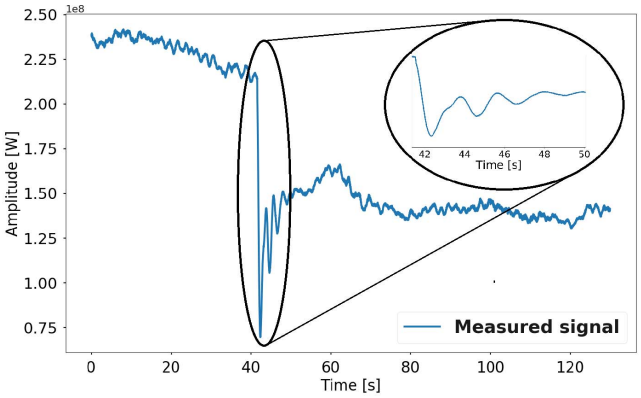

Fig. 8: PMU-data example

Even though the ringdown part of the signal is large compared to the ambient noise, the latter must be removed to avoid aliasing and improve the performance of PA. Figure 9 shows the decomposed signal. Summation of IMF 4 and IMF 5, yields the denoised signal for further analysis.

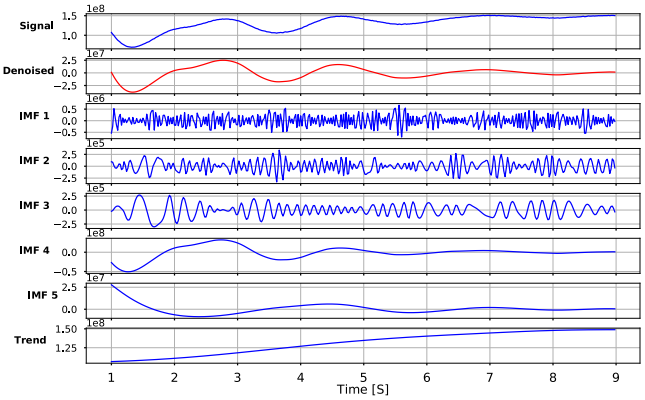

Fig. 9: Decomposing PMU-data into IMFs

Running both PA methods for 30 different model orders gives the modal plot shown in Figure 10a. The identified cluster contains data from 21 of the 30 simulations of PA_O. For PA_F 20 out of 30 simulations were connected to the identified cluster. The remaining data-points were labelled as trivial modes.

Figure 10b shows the comparison of the identified modes in Table V with the filtered PMU-measurement, where both methods had a signal-to-noise ratio of 14 dB after reconstruction. The results in Table V show small differences between the two methods. In addition, the mode identified has a damping ratio well within the limit of what is acceptable.

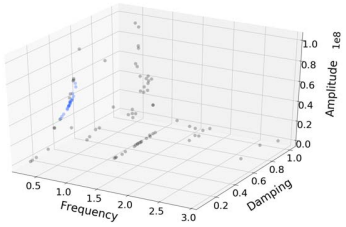

(a) Cluster identification using PA_O

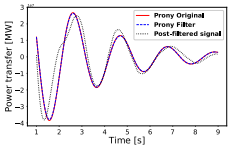

(b) Identified mode compared with original signal after EMD-filtering

Fig. 10: Analysis of PMU-data

TABLE V: Identified mode

PA_O				PA_F			
Freq. [Hz]	η	**Amp.**	**Phase [rad]**	**Freq. [Hz]**	η	**Amp.**	**Phase [rad]**
0,476	0,116	48,08	$0{,}45\pi$	0,477	0,117	47,91	$0{,}44\pi$

D. Computational burden

From Table VI it can be observed that the most demanding routine is PA_F, spending close to or more than twice the time of PA_O in all tests. The EMD spends in general less time than PA, although it must be kept in mind that the Prony method's are run for 30 or more different model orders. The clustering algorithm spends a negligible amount of time. These tests were run using Intel Core i7 8650U.

TABLE VI: Computation time in seconds

	Synthetic signal	**PF**	**PMU**
Time window	15	12	10
EMD filter	0,235	0,193	0,089
PA_O	0,514	0,255	0,117
PA_F	0,903	0,369	0,292
Clustering	0,003	0,002	0,001

V. Conclusion

The intuition of Prony Analysis, along with it's main drawbacks, have been addressed in this paper. Pre-filtering of signal noise and trend is elegantly performed by the EMD technique, and improves performance of PA in noisy conditions. Performing PA for multiple model orders, indicates the consistency of true modes, and fluctuations of trivial modes. This phenomena is exploited by the clustering method, enabling correct identification of true modal components. This method is versatile, as demonstrated by testing for both Prony methods. Improvements to PA, like recursive implementation for real-time observation and control, can be incorporated into the clustering method. Comparing PA_O and PA_F reveals only small differences in performance, except for the extra computation time required in PA_F.

Acknowledgment

The authors would like to thank Prof. Kjetil Uhlen of NTNU for providing PMU-data and Dinh Thuc Duong of NTNU for sharing his experience with PA in the power system.

References

[1] G. Prony, "Essai experimental–,-," *J. de l'Ecole Polytechnique*, 1795.
[2] J. Hauer, "Initial results in prony analysis of power system response signals," *IEEE Transactions on Power Systems*, vol. 5, no. 1, 1990.
[3] Z. Huang, N. Zhou, F. K. Tuffner, Y. Chen, D. J. Trudnowski, R. Diao, J. C. Fuller, W. A. Mittelstadt, J. F. Hauer, and J. E. Dagle, "Mango – modal analysis for grid operation: A method for damping improvement through operating point adjustment," October 2010.
[4] A. R. Borden, B. C. Lesieutre, and J. Gronquist, "Power system modal analysis tool developed for industry use," in *North American Power Symposium (NAPS), 2013*, pp. 1–6, IEEE, 2013.
[5] W. J. S. I. Subcommittee, "Oscillation detection and analysis applications in wecc." https://www.wecc.biz/Reliability/WECC%20JSIS%20Oscillation%20Detection%20and%20Analysis%20Applications%20-%202013-06-12-APPROVED.pdf, Nov. 2012.
[6] A. R. Borden and B. C. Lesieutre, "Variable projection method for power system modal identification," *Power Systems, IEEE Transactions on*, vol. 29, pp. 2613–2620, November 2014.
[7] R. Barbosa, J. Tenreiro Machado, and M. Silva, "Time domain design of fractional differintegrators using least-squares," *Signal Processing*, vol. 86, pp. 2567–2581, October 2006.
[8] N. Zhou, Z. Huang, F. Tuffner, S. Jin, J. Lin, and M. Hauer, "Final project report oscillation detection and analysis," *CIEE report.[online]. Available: https:// uc-ciee.org/ downloads/ ODA_Final_Report.pdf*, 2010.
[9] T. H. Park, "Linear time-invariant systems," in *Introduction To Digital Signal Processing*, pp. 122–144, World Scientific Publishing Co. Pte. Ltd., 2010.
[10] D. Lynch, "Numerical partial differential equations for environmental scientists and engineers," ch. 2.1, Springer US, April 2005.
[11] G. Strang, "Introduction to linear algebra," 2009.
[12] B. Lathi, *Signal processing and linear systems*, ch. 11. Carmichael, Calif: Berkeley Cambridge Press, 1998.
[13] J. Hauer, "Application of prony analysis to the determination of modal content and equivalent models for measured power system response," *IEEE Transactions on Power Systems*, vol. 6, no. 3, 1991.
[14] J. D. Broesch, "Digital signal processing demystified," 2000.
[15] R. Kumaresan and Y. Feng, "Fir prefiltering improves prony's method," *IEEE Transactions on Signal Processing*, vol. 39, no. 3, pp. 736–741, 1991.
[16] J. Sanchez-Gasca and D. Trudnowski, "Identification of electromechanical modes in power systems," *IEEE Task Force Report, Special Publication TP462*, 2012.
[17] G. Rilling, P. Flandrin, P. Goncalves, *et al.*, "On empirical mode decomposition and its algorithms," in *IEEE-EURASIP workshop on nonlinear signal and image processing*, vol. 3, pp. 8–11, NSIP-03, Grado (I), 2003.
[18] P. Flandrin, G. Rilling, and P. Goncalves, "Empirical mode decomposition as a filter bank," *IEEE signal processing letters*, vol. 11, no. 2, pp. 112–114, 2004.
[19] O. B. Fosso and M. Molinas, "Method for mode mixing separation in empirical mode decomposition," September 2017.
[20] J. Deshpande, "Pyhht tutorials." http://pyhht.readthedocs.io/en/latest/tutorials.html, 2015.
[21] M. Ester, H.-P. Kriegel, J. Sander, X. Xu, *et al.*, "A density-based algorithm for discovering clusters in large spatial databases with noise.," in *Kdd*, vol. 96, pp. 226–231, 1996.
[22] J. Erman, M. Arlitt, and A. Mahanti, "Traffic classification using clustering algorithms," in *Proceedings of the 2006 SIGCOMM workshop on Mining network data*, pp. 281–286, ACM, 2006.
[23] C. E. Shannon, "Communication in the presence of noise," *Proceedings of the IRE*, vol. 37, no. 1, pp. 10–21, 1949.
[24] G. D'Antona, "Digital signal processing for measurement systems : Theory and applications," 2006.
[25] J. W. Ning Zhou, D. Pierre, and D. Trudnowski, "A stepwise regression method for estimating dominant electromechanical modes," *Power Systems, IEEE Transactions on*, vol. 27, pp. 1051–1059, May 2012.
[26] P. Kundur, "Power system stability and control," 1994.

B Appendix - Poster for SPEEDAM 2018

Prony's method as a tool for power system identification in Smart Grids

NTNU

Sjur Føyen, Mads-Emil Kvammen, and Olav B. Fosso

Department of Electric Power Engineering,
Norwegian University of Science and Technology
Trondheim, Norway

Motivation

Dynamic stability is a major concern for power system operators, and may prove to be increasingly challenging with less inertia and more power electronic converters in the Smart Grid. If this issue is neglected, the risk of large area **blackouts** increases.

One example is from the US in 1996: unstable oscillations forced a complete system breakdown where 7.5 million customers lost their power supply for periods ranging from minutes to 6 hours. The following figure demonstrates how this breakup was visible from power flow measurements, and the indications that could be used to avoid the disaster.

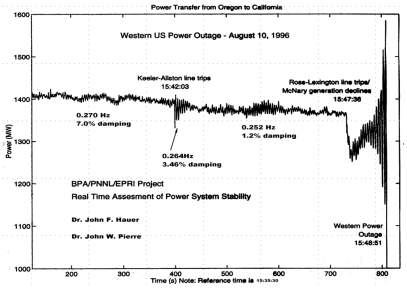

Figure 1: WECC breakdown [1]

However, operators today are good at keeping the system well within stability limits, by including substantial margins in calculation of **power transfer constraints**. The challenge is mainly to **reduce investment** costs as much as possible, by operating the system close to the limits while still maintaining stability. Increased awareness and real-time monitoring of system damping will aid in pushing this limit and move towards a **Smarter Grid**.

Objective

Small-signal stability has for a long time been assessed by component-based models, i.e. classical eigenvalue analysis of a linearized power system. Prony's method attempts to evaluate the same small-signal stability, by fitting post-disturbance (ringdown) measurements to a sum of damped sinusoids.

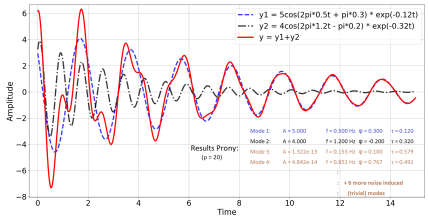

Figure 2: Demonstration of Prony Analysis

Correct estimation of the modal content of a multi-modal sine wave is a trivial matter, as long as the signal does not exhibit non-linear, non-stationary and/or noisy features. However, power system measurements are often just that. The task is to obtain the **linear characteristics** in a somewhat distorted signal.

Proposed method

First, a time-window of analysis containing a proper ringdown must be identified. PMU data from a production outage incident in the Nordic Grid is shown below, with the **ringdown** portion enlarged.

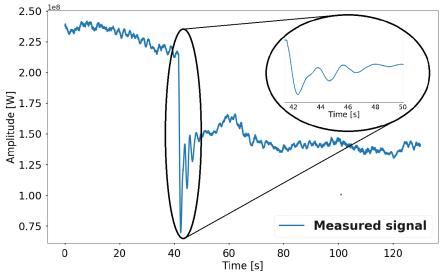

Figure 3: PMU signal with ringdown enlarged

Then, the signal must be properly **band-passed filtered** to extract the approximate frequency band of interest, electro-mechanical modes in the range of 0.2-2 Hz. This is achieved with the Empirical Mode Decomposition (EMD), and as the time-window is short, it effectively does two things: low-pass filtering and trend removal.

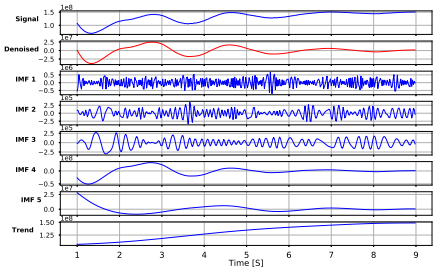

Figure 4: Empirical Mode Decomposition

Now Prony Analysis (*PA*) can be applied. Two known implementations are investigated: Original Prony (PA_O) and Prony Filter (PA_F). For both, the choice of model order is often crucial to validity and accuracy of results. This issue is circumvented by running *PA* for multiple model orders, and clustering all the estimated modes. The **true** (dominating, supposedly responsible for system dynamics) modes remain relatively constant, and are thus distinguished from the **trivial** (originates from noise and non-linear behaviour) modes that change significantly.

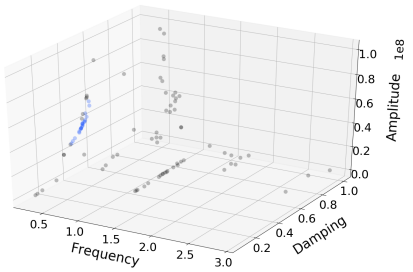

Figure 5: Cluster identification using *PA*

The resulting clusters are averaged to find the approximate frequency, damping, phase and amplitude estimates. If no clusters are found, it is a strong indicator that the signal does not exhibit dominant, linear characteristics; thus the signal should not be used for evaluating the small-signal stability of the originating system.

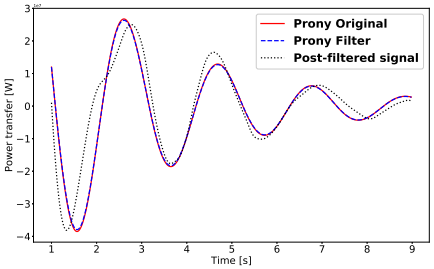

Figure 6: Identified mode compared with original signal after EMD-filtering

Reconstruction of identified mode demonstrates how *PA* captures the linear characteristics, although the signal is partially influenced by non-linearities.

Conclusion

- EMD elegantly performs low-pass filtering and trend removal
- By performing *PA* for multiple model orders, true and trivial modes can be separated through clustering
- Clustering increases the trustworthiness of the resulting modes
- Clustering is versatile and can be incorporated in recursive, real-time PA
- Comparing PA_O and PA_F reveals only small differences in performance, except for the extra computation time required by PA_F

References

[1] Z. Huang *et al.*, "Mango – modal analysis for grid operation: A method for damping improvement through operating point adjustment," tech. rep., Pacific Northwest National Laboratory (U.S.), October 2010.